
Scaling Assessment for the Design of the OSU APEX-1000 Test Facility

Manuscript Completed: May 12, 2003

Prepared For

**U.S. Department of Energy
Germantown, Maryland**

Scaling Assessment for the Design of the OSU APEX-1000 Test Facility

Manuscript Completed: May 12, 2003

Prepared by

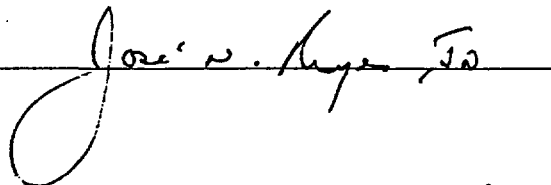
José N. Reyes, Jr.
Qiao Wu
John B. King, Jr.

Department of Nuclear Engineering
Oregon State University
116 Radiation Center
Corvallis, OR 97331-5902

Prepared For

U.S. Department of Energy
Germantown, Maryland

OSU Program Manager:



Westinghouse Reviewer:



COPYRIGHT NOTICE

This document bears an Oregon State University copyright notice. The NRC is permitted to make the number of copies of the information contained in these reports which are necessary for its internal use in connection with generic and plant-specific reviews and approvals as well as the issuance, denial, amendment, transfer, renewal, modification, suspension, revocation, or violation of a license, permit, order, or regulation subject to the requirements of 10 CFR 2.790 regarding restrictions on public disclosure to the extent such information has been identified as proprietary by Westinghouse, copyright protection notwithstanding. With respect to the non-proprietary versions of these reports, the NRC is permitted to make the number of copies beyond these necessary for its internal use which are necessary in order to have one copy available for public viewing in the appropriate docket files in the public document room in Washington, DC and in local public document rooms as may be required by NRC regulations if the number of copies submitted is insufficient for this purpose. Copies made by the NRC must include the copyright notice in all instances and the proprietary notice if the original was identified as proprietary.

ABSTRACT

This document presents the scaling analysis performed to guide the OSU APEX-1000 test facility modifications. The basis for the majority of this work is the original AP600 Scaling Analysis, WCAP-14270, that was performed in support of the design of the existing Advanced Plant Experiment (APEX) at Oregon State University. The analyses presented herein demonstrate that all of the scaling criteria developed for the AP600 program are applicable to the AP1000. Furthermore, this analysis, in conjunction with the AP1000 design information, has been used to identify and guide the design modifications needed to make APEX suitable for AP1000 testing. This scaling analysis provides the basis for the following test facility modifications: core decay power, the CMT and Pressurizer volumes, the ADS-4, IRWST, PRHR, and CMT line resistances, the IRWST and containment flood-up elevations, the ADS-4 flow area, the Pressurizer Surge line diameter, the Upper Core plate and Upper Support Plate flow areas and the Upper Plenum structures.

TABLE OF CONTENTS

Section	Title	Page
Abstract		v
List of Tables.....		ix
List of Figures		xi
1.0	INTRODUCTION.....	1-1
1.1	Comparison of the AP600 and AP1000 Design Parameters	1-2
1.2	Modifications to the APEX Test Facility.....	1-4
1.3	Rationale for APEX Modifications	1-4
1.4	Applicability of the AP600 Scaling Analysis	1-6
1.5	Scope of the Current Scaling Assessment.....	1-8
2.0	HIERARCHICAL TWO-TIERED SCALING (H2TS) METHODOLOGY	2-1
2.1	Time Ratios	2-3
2.2	Process Ranking Using Characteristic Time Ratios.....	2-4
2.3	Scaling Criteria Development	2-5
2.4	Evaluation of Scale Distortion	2-5
3.0	SCALING ANALYSES FOR THE APEX-1000 MODIFICATIONS	3-1
3.1	Core Decay Power and Flow Area Scaling Analysis	3-3
	3.1.1 Maximum Core Power	3-3
	3.1.2 Core Flow Area.....	3-3
	3.1.3 Decay Power Algorithm.....	3-3
3.2	IRWST, CMT, Sump and Pressurizer Geometric Scaling Analysis	3-6
3.3	ADS-4, IRWST, CMT, PRHR and Sump Recirculation Line Scaling	3-7
4.0	PRESSURIZER SURGE LINE SCALING ANALYSIS.....	4-1
5.0	REACTOR COOLANT SYSTEM DEPRESSURIZATION SCALING ANALYSIS.....	5-1
5.1	Reference Pressure for LOCA Transients.....	5-2
5.2	Governing Equations for RCS Two-Phase Fluid Depressurization	5-3
5.3	Top-Down Reactor Coolant System Depressurization Scaling Analysis.....	5-5
	5.3.1 Similarity of Pressure Trajectories in Dimensionless Phase Space	5-7
5.4	Bottom-Up Scaling Depressurization Scaling Analysis.....	5-8
	5.4.1 Self-Similarity of Fluid Properties in Phase Equilibria (P_{sat} Scaling)	5-8
	5.4.2 Equations of State for Saturated Pressure and Temperature (T_{sat} Scaling)	5-12
	5.4.3 Dilation Property Group for Saturated Liquid-Vapor Blowdowns	5-15
	5.4.4 Critical Flow Models.....	5-18

TABLE OF CONTENTS (cont.)

Section	Title	Page
5.5	RCS depressurization and Inventory Scaling Criteria.....	5-20
5.5.1	Saturated Vapor Break Flow Areas.....	5-22
5.5.2	Saturated Liquid Break Flow Areas.....	5-22
5.5.3	ADS Valve Flow Area Scaling Ratios.....	5-23
5.5.4	DVI Mass Flow Rate Scaling Ratio.....	5-24
5.5.5	Net Power Scaling Ratio.....	5-24
5.6	Initial Conditions and Flow Areas.....	5-24
5.7	Summary and Conclusions.....	5-27
6.0	SCALING ANALYSIS OF THE FULL PRESSURE ADS 4 BLOWDOWN TO IRWST INJECTION TRANSITION PERIOD.....	6-1
6.1	Description of the ADS-4 Blowdown to IRWST Injection Thermal Hydraulic Phenomena.....	6-1
6.2	Top-Down RCS Depressurization and Mass Inventory Scaling Analysis (Pressure Similitude).....	6-2
6.3	Bottom-Up Scaling Analysis.....	6-6
6.3.1	Flashing and Liquid Boil-off Rate.....	6-6
6.3.2	IRWST Full Height Liquid Head and Injection Flow Rate.....	6-7
6.3.3	Core Fluid Mixture Level Swell.....	6-7
6.3.4	Initial Conditions for the Full Pressure ADS-4 Blowdown Tests.....	6-10
7.0	UPPER PLENUM ENTRAINMENT SCALING ANALYSIS.....	7-1
7.1	Top-Down Scaling Analysis.....	7-2
7.1.1	Dimensionless Liquid Mass Balance.....	7-3
7.1.2	Preserving the Upper Plenum Draining Rate During Integral System Testing...7-5	7-5
7.2	Bottom-up Scaling Analysis.....	7-6
7.2.1	Pool Entrainment.....	7-6
7.2.2	Upper Plenum Liquid Entrainment Rate Scaling Criteria.....	7-14
7.2.3	Scaling Criterion for Lateral De-entrainment.....	7-16
7.2.4	Scaling Criterion for the Upper Core Plate.....	7-18
7.2.5	Scaling Criterion for the Upper Support Plate.....	7-19
7.2.6	Design of APEX Upper Plenum Guide Tube Bundle, Upper Core Plate and Upper Support Plate.....	7-19
7.2.7	Assessment of Pool Entrainment Limiting Conditions.....	7-23
7.3	Evaluation of Scale Distortion.....	7-25
7.3.1	Impact of Reduced Flow Area in the Upper Core Plate.....	7-26
8.0	SUMMARY AND CONCLUSIONS.....	8-1
9.0	REFERENCES.....	9-1

LIST OF TABLES

Table	Title	Page
Table 1	Important NSSS Design Changes	1-2
Table 2	Changes to Passive Safety System Design Features	1-3
Table 3	Proposed Modifications to the APEX Test Facility	1-4
Table 4	APEX-1000 Primary Loop Scaling Ratios from WCAP-142701	3-1
Table 5	APEX-1000 Passive Safety System Scaling Ratios from WCAP-142701	3-2
Table 6	Results of IRWST, CMT, Sump and Pressurizer Geometry Scaling	3-6
Table 7	IRWST and Sump Recirculation Line Resistance Values (ft/gpm ²)	3-9
Table 8	MT and PRHR Line Resistance Line Values (ft/gpm ²)	3-10
Table 9	DS-4 Line Resistance Values(ft/gpm ²)	3-10
Table 10	Results of Pressurizer Surge Line Scaling Analysis	4-3
Table 11	APEX-1000 LOCA Initial Conditions	5-24
Table 12	Summary of APEX-1000 ADS 1-4 Valve Flow Areas for LOCA	5-25
Table 13	Summary of APEX-1000 ADS 1-2 Valve Flow Areas for Inadvertent Opening of ADS.....	5-26
Table 14	APEX-1000 Break and Steam Generator PORV Sizes.....	5-26
Table 15	Time Constants and II Groups for APEX Pressure Scaled LOCAs.....	5-27
Table 16	Comparison of APEX and AP1000 Core Averaged Void Fractions.....	6-9
Table 17	Proposed Initial Conditions for a Full Pressure ADS-4 Blowdown Test in APEX-1000.....	6-11
Table 18	Comparison of the APEX and AP1000 Upper Plenum Geometries	7-22
Table 19	Ratio of P Groups for Near Surface and Momentum Controlled Upper Plenum Entrainment	7-26

LIST OF FIGURES

Figure	Title	Page
Figure 1	General Scaling Methodology for the APEX Test Facility (AP600 Program, WCAP-14270).....	1-7
Figure 2	Flow Diagram for the Hierarchical, Two-Tiered Scaling Analysis (NUREG/CR5809).....	2-2
Figure 3	Comparison of the APEX-1000 Decay Power Algorithm and the Ideally Scaled AP1000 Decay Power Curve.....	3-4
Figure 4	Comparison of the APEX-1000 Integrated Decay Power to the Ideally Scaled AP1000 Decay Power	3-5
Figure 5	Flow Chart of the Primary Side Depressurization Scaling Analysis.....	5-1
Figure 6	Primary and Secondary Side Pressures During a Typical 2-Inch Break LOCA in APEX	5-2
Figure 7	Scaling Relationship Between AP1000 and APEX Saturation Pressure.....	5-8
Figure 8	Power Law for Pv_{fg}/h_{fg} as a Function of Pressure	5-10
Figure 9	Power Law for s_f as a Function of Pressure	5-10
Figure 10	Power Law for v_g as a Function of Pressure	5-11
Figure 11	Power Law for v_{fg} as a Function of Pressure.....	5-11
Figure 12	Comparison of Equation (77) to Steam Tables	5-12
Figure 13	Scaling Relationship Between AP1000 and APEX Saturation Temperature.....	5-14
Figure 14	Plot of Dimensionless Mixture Specific Energy as a Function of Dimensionless Pressure	5-16
Figure 15	Critical Mass Flux for Saturated Liquid Breaks as Predicted by the Henry-Fauske Model ($x_{Brk} = 0.03$).....	5-20
Figure 16	Description of the Transition from ADS-4 Blowdown to the Onset of IRWST Injection	6-2
Figure 17	Scaling Analysis Flow Chart for the Full Pressure ADS-4 Blowdown Experiments	6-3
Figure 18	Comparison of AP1000 and APEX Axial Void Fraction Profiles for an Average Subchannel.....	6-10
Figure 19	Upper Plenum Scaling Analysis Flow Chart.....	7-1
Figure 20	Upper Plenum Control Volume Located Below the Hot Legs.....	7-2
Figure 21	APEX Upper Core Plate Geometry.....	7-20
Figure 22	APEX Upper Plenum Guide Tube Pitch and Diameter	7-21
Figure 23	APEX Upper Support Plate Flow Hole Locations	7-21
Figure 24	Assessment of AP1000 and APEX Upper Plenum Pool Entrainment Regimes for a 2.8% Core Decay Power at Atmospheric Pressure	7-23

1.0 INTRODUCTION

Advanced reactors are being designed to utilize passive safety systems to provide core cooling following loss-of-coolant accidents. These passive systems do not rely on safety grade pumps or AC power. They rely on natural driving forces such as gravity, compressed gas, and natural circulation to provide core cooling for an indefinite period of time after an accident. The AP600 is an advanced nuclear plant that uses passive safety systems that have received Design Certification from the U.S. Nuclear Regulatory Commission. The performance of the AP600 passive safety systems was assessed using validated safety analysis computer codes. An extensive AP600 test program was conducted to provide the data required to develop and verify the computer code models needed to confidently predict the AP600 passive safety system behavior. The AP600 test program included separate-effects tests that modeled individual components and/or phenomenon. It also included integral systems tests that modeled the integrated performance of the passive safety systems.

As part of the AP600 Design Certification, the APEX Test Facility was constructed at Oregon State University. The APEX facility is a low-pressure, 1/4-height integral systems test facility that can model the long-term core cooling phenomenon associated with an advanced passive plant using passive safety systems. Extensive scaling studies were performed so that the AP600 thermal-hydraulic phenomena of interest would be accurately modeled in APEX. The APEX facility operates at 1/2 time scale and at a reduced pressure and temperature scale. Using the scaled parameters, a test in the APEX facility occurs twice as fast as a transient in the actual design. A typical test is performed by bringing the facility into a steady-state operational mode. Several valves have been installed into the facility at strategic points to simulate a break in the cooling system. After steady-state is reached, a specific break valve is opened to simulate an accident. All of the safety systems (except the passive containment cooling system) and plant logic in the AP600 design have been built into the APEX facility. Over 750 instruments monitor the plant response to the simulated accident event. A total of 28 integral system tests were successfully performed for Westinghouse and DOE in support of the AP600 plant certification effort. In addition, a total of 47 confirmatory tests were successfully performed for the NRC.

This document presents the scaling analysis that was formed to guide the OSU APEX-1000 test facility modifications. The basis for the majority of this work is the original AP600 Scaling Analysis, WCAP-14270, that was performed in support of the design of the existing Advanced Plant Experiment (APEX) at Oregon State University.¹ The analyses presented herein provides the scaling criteria that need to be implemented to model the AP1000 design changes in the APEX test facility. This analysis, in conjunction with the AP1000 design information, has been used to identify and guide the design modifications needed to make APEX suitable for AP1000 testing.

1.1 Comparison of the AP600 and AP1000 Design Parameters

Westinghouse has recently issued its *AP1000 Plant Parameters Report*.² Table 1 provides a summary comparison of the key design parameters of the AP1000 with those of the AP600.

Parameter	AP600	AP1000
Reactor Core Power, MWt	1933	3400
Hot Leg Temperature, °F	600	610
Number of Fuel Assemblies	145	157
Active Fuel Length, ft	12	14
Average Linear Power, kW/ft	4.10	5.707
Average Heat Flux, Btu/(hr-ft ²)	142,869	198,933
Steam Generator Heat Transfer Area per unit, ft ²	75,180	123,538
Reactor Coolant Pump Flow, gpm	51,000	78,750
Pressurizer Volume, ft ³	1,600	2,100

The most significant change is the increased core power. The reactor vessel volume remains unchanged. The steam generator tube surface area, the pressurizer volume and the reactor coolant pump flow have all increased to accommodate the increased core power. A comparison summarizing the changes to the passive safety system design is provided in Table 2. Several changes have been made. The volume of the CMTs and the IRWST has been increased. The flow capacity for the IRWST, ADS-4 and PRHR has been increased by reducing the resistance in each line. The PRHR surface area has also increased. The details of the AP1000 design are provided in the Westinghouse Plant Parameters document.²

Table 2 Changes to Passive Safety System Design Features			
	AP600	AP1000	Comment
IRWST Volume, ft ³ Water Level, ft Line Resistance, % Design Flow Rate, %	70,798 28.0 100% 100%	75,300 28.79 32% 184%	The IRWST level has been increased in the AP1000 by using more accurate level instruments. This permits a high operating level.
Core Makeup Tanks Number Volume, ft ³ Line Resistance, % Design Flow Rate, %	2 2000 100% 100%	2 2512 64% 124%	Core makeup tank (CMT) volume and flow rate is increased to provide additional safety injection flow. CMT elevations are maintained at the AP600 level. The duration of CMT injection is maintained similar to AP600.
Accumulators Number Volume, ft ³ Pressure, psig	2 2000 700	2 2000 700	The accumulators are the same as AP600. Accumulator sizing is based on LBLOCA performance and is determined largely on reactor vessels volume.
Automatic Depressurization Stages 1-3 Location, Configuration, Vent Area, %	Top PZR 6 paths 100 %	Top PZR 6 paths 100 %	The first three stages of ADS are the same as AP600. Their sizing basis is to reduce pressure to permit adequate injection from the accumulators and to permit transition to 4 th stage ADS.
Automatic Depressurization Stage 4 Location, Configuration, Line size, Nominal Vent Area, % Line Resistance Capacity	Hot Leg 4 paths 10-inch 100% 100% 100%	Hot Legs 4 paths 14-inch 176% 28% 189%	The ADS 4 th stage vent area is increased more than the ratio of the core power. The 4 th stage ADS venting is the most important design feature to allow for stable IRWST/sump injection during long term core cooling.
Passive RHR Heat Exchanger Type Surface Area, % Design Flow Rate, % Design Heat Transfer, %	C-Tube 100% 100% 100%	C-Tube 122% 174% 172%	The AP1000 PRHR HX retains the AP600 configuration. The heat transfer surface area is increased by extending the length of the heat exchanger. The inlet and outlet piping has been increased resulting in higher flow rates.
Containment Diameter, ft Overall Height, ft Design Pressure, psig Net Free Volume, ft ³	130 189.83 45 173 x10 ⁶	130 215.33 59 2.07 x10 ⁶	The AP1000 containment volume and design pressure are increased to accommodate higher mass and energy releases.
Passive Containment Cooling System Water Storage Tank Volume (Top of Overflow), gallons	580,000	800,000	The PCS water storage tank was increased to accommodate higher flow rates. The PCS flow rates have been increased based on the increased in core power.

1.2 Modifications to the APEX Test Facility

Based on a review of the design changes listed in Tables 1 and 2, and their detailed description in the AP1000 Plant Parameters document², the set of modifications listed in Table 3 were proposed for APEX to best simulate AP1000 thermal hydraulic behavior.

Component	Modification to APEX
Reactor Power	Increase core power by 67%. (Maximum of 1 MW)
Pressurizer	Increase Pressurizer volume. Reduce Pressurizer Surge Line Diameter.
Steam Generator Heat Transfer Area	No change required for testing.
Reactor Coolant Pump Flow	No change required for testing.
Core Makeup Tanks	Increase Core Makeup Tank (CMT) volumes by 25%. Reduce line resistance to 64% of original value.
Accumulators	None. No changes to original design.
IRWST	Increase IRWST liquid level.
Automatic Depressurization Stages 1-3	None. No changes to original design.
Automatic Depressurization Stage 4	Increase ADS-4 flow area by 76%. Reduce line resistance to 28% of original value.
Passive Residual Heat Removal (PRHR) Heat Exchanger	Increase PRHR flow capacity by 74% by reducing line resistance. No change in surface area/tube number required for testing.
Containment Sump Flood-Up Elevation	Change flood-up elevation in primary sump tank.
Passive Containment Cooling System	Not part of APEX Testing Program.

1.3 Rationale for APEX Modifications

This sections presents the rationale for the proposed modifications. An increase in the reactor core power is needed to preserve the proper power to volume scaling ratio. This is a key feature of the original scaling analysis and is essential to simulating decay heat behavior, loop natural circulation and primary system depressurization rates. The APEX power increase is limited to 1 MW without having to replace the power distribution system. This power represents ~ 2.8% decay power for the AP1000 on a scaled basis. An increase in pressurizer volume is essential because it is a major source of liquid to the core during primary system blowdowns. The reduction in pressurizer surge line diameter was identified as a need by the NRC at the conclusion of the AP600 research program.³ This modification is needed to assure

properly scaled pressurizer draining behavior during primary system blowdowns and properly scaled surge line pressure drop behavior during ADS 1-3 operation.

Increases to the APEX steam generator tube volume and heat transfer area were not deemed necessary for several reasons. First, their tube volume is small compared to the remainder of the primary system. Second, they are oversized for the decay power operations involved in testing. That is, they have much more surface area than needed to remove core heat. One impact of not increasing the steam generator surface area will be an increase in the core fluid temperature rise. This is well within the design constraints of the existing facility. The increased number of tubes, however, significantly reduces the primary loop pressure drop because of the increased number of parallel flow paths in the steam generator. As a result, the APEX facility will not be able to match the scaled primary loop natural circulation flow rates that arise early in the SBLOCA transients. However, all of the passive safety system and sump re-circulation natural circulation flows can be properly scaled.

An increase in reactor coolant pump flow capacity was not necessary because the pumps are tripped at the start of each transient. Their primary contribution during testing is their resistance which will be preserved.

The core makeup tank volumes will be increased because they are an essential part of the passive safety system response. ADS actuation is dependent on the CMT liquid volume. The CMT line resistance shall also be reduced to simulate the scaled CMT draining rates. CMT volume and flow rate are critical to the transition from ADS 4 blowdown to IRWST injection. Full pressure ADS-4 blowdown transition tests are being considered.

The IRWST injection flow rate has a significant impact on core cooling. Therefore the IRWST lines will be modified to increase their flow capacity to match the AP1000 design on a scaled basis. The onset of IRWST injection is dependent on the liquid level height in the tank. The APEX IRWST minimum liquid volume will be preserved to match the design change. However, the scaled liquid height and the IRWST liquid volume cannot be exactly preserved simultaneously. The containment sump flood-up curb height will be adjusted accordingly.

The fourth stage valves of the Automatic Depressurization System (ADS-4) assure that the primary system pressure will be reduced below the IRWST liquid level head so that injection can begin. The increased flow area is needed to properly simulate the AP1000 ADS-4 operation. In addition, the resistance of each ADS-4 line will be decreased accordingly to properly match the pressure drop behavior under non-choked flow conditions.

Increases to the PRHR heat exchanger tube volume and surface area were not deemed necessary for the experiment. As with the steam generator, the PRHR tube volume is small compared to the primary loop volume. Furthermore, it is oversized for the decay power operations involved in testing. That is, they have much more surface area than needed to remove core heat. The impact of not increasing the PRHR will be an increase in the core fluid temperature rise. This is well within the design constraints of the existing facility. Properly scaled natural circulation flow rates are assured by adjusting the PRHR loop resistance.

The ADS 1-3 valves and the accumulators remain the same as the original AP600 design. Therefore these components will not be modified for the AP1000 testing program.

1.4 Applicability of the AP600 Scaling Analysis

The original scaling analysis performed in support of the design of the APEX Test Facility for AP600 certification is documented in WCAP-14270. The comprehensive report represents the first successful application of the Hierarchical Two-Tiered Scaling (H2TS) methodology for the design and construction of an experimental test facility. The report was issued by Westinghouse in January 1995.¹ The objective of the scaling study was to obtain the physical dimensions of a test facility that would simulate the flow and heat transfer behavior of importance to the AP600 passive safety system operation. The report includes all of the scaling criteria that was needed to define the geometry and operating conditions of the reduced scale APEX test facility.

Figure 1 shows the General Scaling Methodology used to design the APEX Test facility for the AP600 test program. First, the general objectives of the test program were stated. The general objective was to assess the passive safety system operation for Loss-of-Coolant-Accidents (LOCA). A SBLOCA Phenomena Identification and Ranking Table (PIRT) was then developed to identify the important thermal hydraulic phenomena that should be preserved in the test facility. The next step was to perform a scaling analysis for each of the AP600 operational modes during the LOCA. Four key modes of operation were identified; Natural Circulation, System Depressurization, Venting/Draining/ Injection, and Recirculation. The analyses resulted in a set of dimensionless groups and similarity criteria that had to be preserved in the test facility. These similarity criteria were derived from the governing equations of mass, momentum and energy conservation for the system, subsystems and components for each of the four operating modes. The similarity criteria were used to obtain the scaling ratios needed to design the test facility geometry and operating conditions.

As shown in Figure 1, the scaling ratios were developed for a specific set of experiment objectives, that produce a specific set of system responses (i.e., operation modes and thermal hydraulic phenomenon) within a specific plant geometry. A review of the scaling ratios reveals that they are also directly applicable to the design of the APEX-1000 test facility for the following reasons.

First, the experiment objectives of the APEX-1000 test program are a subset of the AP600 experiment objectives. Therefore, the same operation modes and thermal hydraulic phenomena will be produced.

Westinghouse recently issued an AP1000 Phenomena Identification and Ranking Tables (PIRT) and Scaling Assessment, which reviews the original scaling analysis effort and assesses the applicability of the original AP600 test program to the AP1000 design.⁴ Westinghouse concluded that the AP1000 PIRT was the same as the AP600 PIRT with the exception of the potential higher importance of hot leg entrainment during the post-ADS-4 actuation phases of the small break LOCA. Therefore, entrainment scaling of the post ADS-4 actuation phase was of particular interest to the present study.

Second, the AP1000 design is geometrically similar to the AP600 design. This means that there is a one to one correspondence of primary loop components; arranged in the same sequence and that all of the important AP1000 geometric scales, (i.e., cross-sectional flow areas, volumes, lengths) can be related to the AP600 design by constant scaling factors.

In conclusion, the general scaling methodology remains the same therefore the scaling ratios obtained in the original scaling analysis, with a few exceptions, can be directly applied to the design of an APEX-1000 test facility. The following section describes the scope of the scaling assessment for the APEX-1000 test facility.

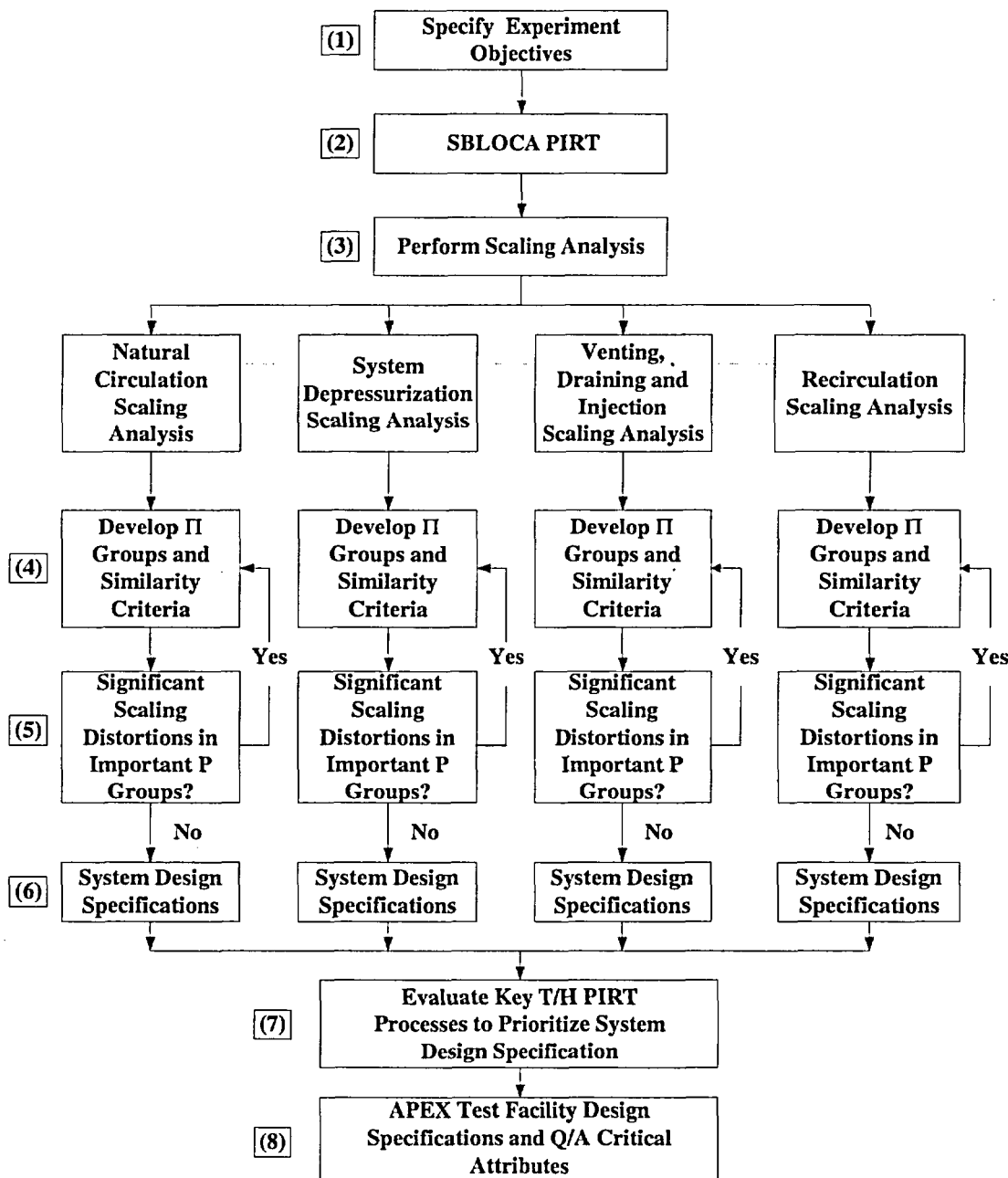


Figure 1 General Scaling Methodology for the APEX Test Facility (AP600 Program, WCAP-14270)¹

1.5 Scope of the Current Scaling Assessment

The following analyses have been included in the OSU APEX-1000 Scaling Report to guide the design of the APEX test facility modifications presented in Table 3:

- Core Decay Power Scaling Analysis
- IRWST, CMT and Pressurizer Liquid Volume and Height Scaling Analysis
- IRWST, CMT, PRHR and Sump Recirculation Line Scaling
- Pressurizer Surge Line Scaling Analysis
- RCS Depressurization Scaling Analysis
- ADS-4 Blowdown Scaling Analysis
- Upper Plenum Pool Entrainment Scaling Analysis

The core decay power analysis was needed to develop the revised decay power algorithm for the tests. The original power scaling ratios were used in the decay power scaling analysis. The IRWST, CMT and Pressurizer volume scaling analysis were straightforward and implemented the original volume scaling ratios. Similarly, the original line resistance scaling ratios were used to scale the IRWST, CMT, PRHR and Sump recirculation line pressure drops. The pressurizer surge line scaling analysis represents a change to the original scaling analysis. That is, it is intended to provide a better representation of the pressurizer draining process. The pressurizer surge line scaling analysis resulted in a new diameter scaling ratio for the pressurizer surge line. The ADS-4 blowdown scaling analysis represents an improved depressurization scaling analysis technique based on the energy equation. Of particular interest to this study is the transition from ADS-4 blowdown to IRWST injection. The upper plenum pool entrainment scaling analysis is intended to provide a better simulation of the upper plenum entrainment and de-entrainment processes. This analysis also includes an upper core plate flow area scaling analysis to better simulate counter-current flooding in the upper core plate.

2.0 HIERARCHICAL TWO-TIERED SCALING (H2TS) METHODOLOGY

The Hierarchical Two-Tiered Scaling (H2TS) method was used to develop the similarity criteria necessary to scale the APEX-1000 systems and processes of importance to a SBLOCA transient. The H2TS method was developed by the USNRC and is fully described in Appendix D of NUREG/CR-5809⁵. This is the same method that was used to develop the similarity criteria for the original APEX facility.

Figure 2 is taken from NUREG/CR-5809. It presents the four basic elements of the H2TS analysis method. The first element consists of subdividing the plant into a hierarchy of systems. Each system was subdivided into interacting subsystems which were further subdivided into interacting modules which were further subdivided into interacting constituents (materials) which were further subdivided into interacting phases (liquid, vapor or solid). Each phase could be characterized by one or more geometrical configurations and each geometrical configuration could be described by three field equations (mass, energy and momentum conservation equations). Each field equation could be characterized by several processes.

After identifying and subdividing the system of interest, the next step was to identify the scaling level at which the similarity criteria should be developed. This was determined by examining the phenomena being considered. For example, if the phenomenon being considered involved mass, momentum or energy transport between materials such as water and solid particles, then the scaling analysis was performed at the constituent level. If the phenomenon of interest involved mass, momentum or energy transport between vapor and liquid, then the scaling analysis was performed at the phase level. Therefore identifying the scaling level depended on the phenomenon being addressed.

Thermal hydraulic phenomena involving integral reactor coolant system interactions, such as primary system depressurization or loop natural circulation, were examined at the "system" level. Thermal hydraulic phenomena, such as steam generator heat transfer, were examined at the "subsystem" level. Specific interactions between the steam-liquid mixture and the stainless steel structure were examined at the "constituent" level.

Chapter 3 presents the scaling analyses that were performed for the different APEX-1000 test facility modifications. It identifies the thermal hydraulic phenomena of interest, the system level (i.e., control volume) at which the analysis was performed, the geometrical configuration, the applicable balance equations and the processes important to the thermal hydraulic phenomena of interest.

The H2TS method required performing a "Top-Down" (system) scaling analysis. The top-down scaling analysis examined the synergistic effects on the system caused by complex interactions between the constituents which are deemed important by the PIRT. Its purpose was to use the conservation equations at a given scaling level to obtain characteristic time ratios and similarity criteria. It also identified the important processes to be addressed in the bottom-up scaling analysis.

The H2TS method also required performing a "Bottom-Up" (process) scaling analysis. This analysis developed similarity criteria for specific processes such as flow pattern transitions and flow dependent heat transfer. The focus of the bottom-up scaling analysis was to develop similarity criteria to scale individual processes of importance to system behavior as identified by the PIRT.

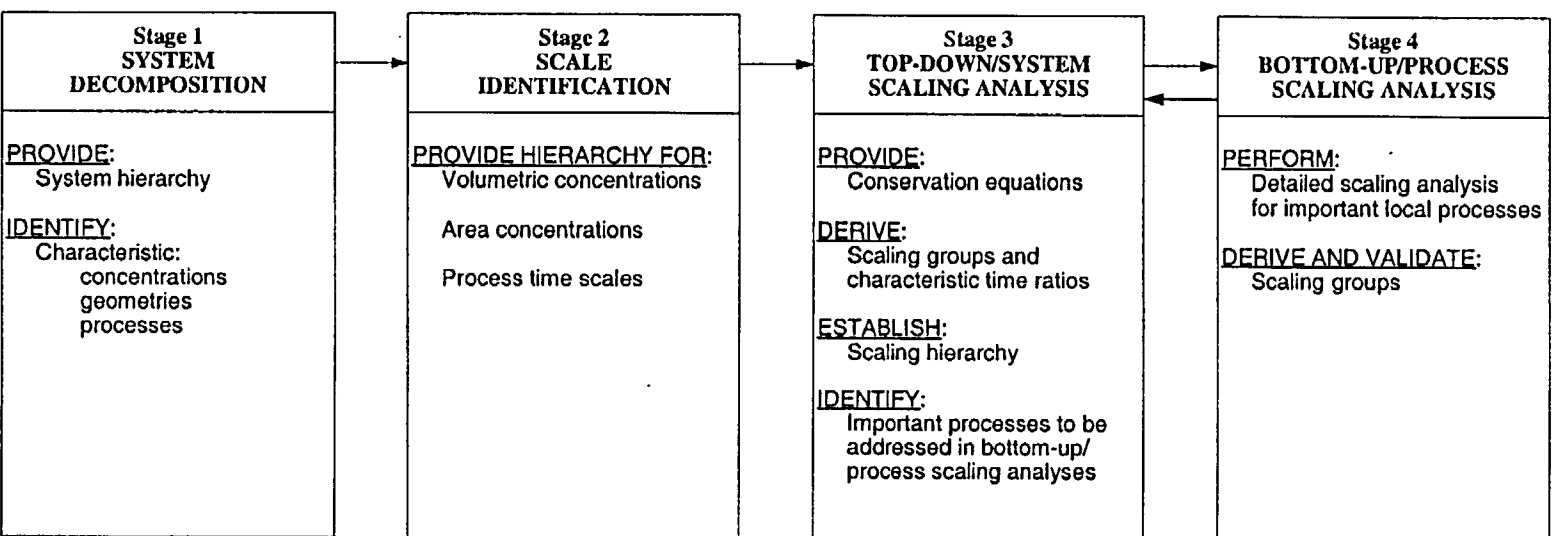


Figure 2 Flow Diagram for the Hierarchical, Two-Tiered Scaling Analysis (NUREG/CR5809)⁶

2.1 Time Ratios

The basic objective of the H2TS method was to develop sets of characteristic time ratios for the transfer processes of interest. This was done by writing the control volume balance equations for each constituent "k" as follows:

$$\frac{dV_k \psi_k}{dt} = \Delta[Q_k \psi_k] \pm \Sigma (j_{kn} A_{kn}) + S_k \quad (1)$$

where

$$\Delta[Q_k \psi_k] = [Q_k \psi_k]_{in} - [Q_k \psi_k]_{out} \quad (2)$$

In equation (1) the ψ_k term represents the conserved property; $\psi_k = \rho, \rho u$ or $\rho \varepsilon$ (mass, momentum or energy per unit volume), V_k is the control volume, Q_k is the volumetric flow rate, j_{kn} is the flux of property ψ_k transferred from constituent "k" to "n" across the transfer area A_{kn} . Hence, $\Delta[Q_k \psi_k]$ represents the usual mass, momentum, or energy convection terms, and $\Sigma j_{kn} A_{kn}$ represents transport process terms such as condensation and S_k represents the distributed sources, such as decay power or body forces acting internal to the control volume.

$$V_k^+ = \frac{V_k}{V_{k,0}}, \psi_k^+ = \frac{\psi_k}{\psi_{k,0}}, Q_k^+ = \frac{Q_k}{Q_{k,0}}, j_{kn}^+ = \frac{j_{kn}}{j_{kn,0}}, A_{kn}^+ = \frac{A_{kn}}{A_{kn,0}}, S_k^+ = \frac{S_k}{S_{k,0}} \quad (3)$$

Equation (1) can be put in dimensionless form by specifying the following dimensionless groups in terms of the constant initial and boundary conditions:

Substituting these groups into equation (1) yields:

$$V_{k,0} \psi_{k,0} \frac{dV_k^+ \psi_k^+}{dt} = Q_{k,0} \psi_{k,0} \Delta[Q_k^+ \psi_k^+] \pm \Sigma (j_{kn,0} A_{kn,0}) j_{kn}^+ A_{kn}^+ + S_{k,0} S_k^+ \quad (4)$$

Dividing both sides of this equation by $Q_{k,0} \psi_{k,0}$ yields:

$$\tau_k \frac{dV_k^+ \psi_k^+}{dt} = \Delta[Q_k^+ \psi_k^+] \pm \Sigma \Pi_{kn} j_{kn}^+ A_{kn}^+ + \Pi_{sk} S_k^+ \quad (5)$$

where the residence time of constituent "k" is

$$\tau_k = \frac{V_{k,0}}{Q_{k,0}} \quad (6)$$

and the characteristic time ratio for a transfer process between constituents “k” and “n” is given by:

$$\Pi_{kn} = \frac{j_{kn,0} A_{kn,0}}{Q_{k,0} \Psi_{k,0}} \quad (7)$$

The characteristic time ratio for the distributed source term within the control volume is given by:

$$\Pi_{sk} = \frac{S_{k,0}}{Q_{k,0} \Psi_{k,0}} \quad (8)$$

Because each transfer process has a characteristic time ratio, it is possible to rank the importance of each process by comparing the time ratios. If a specific transfer process is to have the same effect in the prototype and the model, then the characteristic time ratios must be preserved.

2.2 Process Ranking Using Characteristic Time Ratios

Let us define $M[(P_{i,j}), (P_{i+1,j}), \dots, (P_{N_i, N_j})]$ as the set of time ratios that characterize all of the individual processes that occur during the evolution of a transient. The subscripts i, j, N_i, N_j identify the specific process, the hierarchical level, the total number of specific processes and the total number of hierarchical levels respectively.

Because of differences in geometrical scale and fluid properties, it is impossible to exactly duplicate the “time ratio set” for the full-scale prototype, M_p , in a reduced scale model. That is, exact similitude for all processes cannot be preserved; therefore:

$$M_p \neq M_m \quad (9)$$

The subscript, p , refers to the full-scale prototype and the subscript, m , refers to the reduced scale model.

It is possible to design a reduced scale test facility that preserves the similitude of a subset of time ratios $T[\Pi_{i,j}]$, that characterize the processes of greatest importance to the transient. This optimizes the model design to investigate the important processes while distorting the less important processes.

To determine which processes govern the overall evolution of a transient, numerical estimates of the characteristic time ratios for the prototype and the model must be obtained for each hierarchical level of interest. Physically, each characteristic time ratio, Π_i , is composed of a specific frequency, ω_i , which is an attribute of the specific process, and the residence time constant, τ_{cv} , for the control volume. That is:

$$\Pi_i = \omega_i \tau_{cv} \quad (10)$$

The specific frequency defines the mass, momentum or energy transfer rate for a particular process. The residence time defines the total time available for the transfer process to occur within the control volume. A numerical value of:

$$\Pi_I < 1 \quad (11)$$

means that only a small amount of the conserved property would be transferred in the limited time available for the specific process to evolve. As a result, the specific process would not be important to the overall transient. Numerical values of:

$$\Pi_I \geq 1 \quad (12)$$

means that the specific process evolves at a high enough rate to permit significant amounts of the conserved property to be transferred during the time period, τ_{cv} . Such processes would be important to the overall transient behavior.

2.3 Scaling Criteria Development

The scaling analysis results in a set of characteristic time ratios (dimensionless Π groups) and similarity criteria for each mode of operation. Because it is impossible to identically satisfy all of the similarity criteria simultaneously, the set only includes those criteria which must be satisfied in order to scale the most important phenomena identified by the PIRT.

Scaling criteria were developed by requiring that the characteristic time ratios for a subset of specific processes in the prototype (usually those of greatest importance) are matched in the model at each hierarchical level. That is,

$$T \{ \Pi_i \}_m = T \{ \Pi_i \}_p \quad (13)$$

These criteria were satisfied by adjusting the physical geometry, fluid properties and operating conditions of the model; thus optimizing the model design for the specific process of interest.

2.4 Evaluation of Scale Distortion

The scaling criteria were evaluated to determine if the scale model geometry, boundary conditions or operating conditions would introduce significant scaling distortions. Distortions were also evaluated relative to other modes of operation.

The effect of a distortion in the model for a specific process can be quantified as follows:

$$DF = \frac{[\Pi_i]_p - [\Pi_i]_m}{[\Pi_i]_p} \quad (14)$$

The distortion factor, DF, physically represents the fractional difference in the amount of conserved property transferred through the evolution of a specific process in the prototype to the amount of

conserved property transferred through the same process in the model during their respective residence times. A distortion factor of zero would indicate that the model ideally simulates the specific process. A distortion factor of +0.05 would indicate that the specific process in the model transfers 5 percent less of the conserved property (on a scaled basis) than the same process in the prototype. The distortion factor can also be written as:

$$DF = 1 - [\omega_i]_R [\tau_{cv}]_R \quad (15)$$

or

$$DF = 1 - [\Pi_i]_R \quad (16)$$

The degree to which a specific transfer process could impact a particular transient can be determined by comparing the *maximum* characteristic time ratio for each of the transfer processes that arise during the transient.

Upon satisfying the important scaling criteria, the component geometries and operating conditions were specified for the APEX-1000 test facility.

3.0 SCALING ANALYSES FOR THE APEX-1000 MODIFICATIONS

This chapter presents the scaling analyses performed to obtain the component geometries and system operating conditions for the APEX-1000 test facility. Tables 4 and 5 present the scaling ratios that were derived in WCAP-14270 and used for the design of the APEX-1000 test facility modifications.

Table 4 APEX-1000 Primary Loop Scaling Ratios from WCAP-14270¹	
Parameter	Desired Scaling Ratio
Core	
Length Ratio	
Flow Area Ratio	
Fluid Velocity Ratio	
Power Ratio	
Fluid Residence Time Ratio	
Mass Flow Ratio	
Volume Ratio	
Power/Volume Ratio	
Hot and Cold Legs	
Length Ratio	
Diameter Ratio	
Flow Area Ratio	
Volume Ratio	
Fluid Velocity Ratio	
Fluid Residence Time Ratio	
Mass Flow Ratio	
Pressurizer	
Volume Ratio	
Liquid Height Ratio	

a,b,c

Table 5 APEX-1000 Passive Safety System Scaling Ratios from WCAP-14270¹	
Parameter	Desired Scaling Ratio
CMT	
Length Ratio	
Flow Area Ratio	
Draining Mass Flow Rate Ratio	
Volume Ratio	
Accumulator	
Volume Ratio	
Mass Flow Ratio	
IRWST	
Length Ratio	
Flow Area Ratio	
Draining Mass Flow Rate Ratio	
Volume Ratio	
Lower Containment Sumps	
Length Ratio	
Flow Area Ratio	
Draining Mass Flow Rate Ratio	
Volume Ratio	

a,b,c

The horizontal hot leg and cold leg scaling ratios were established based on preserving flow regime transitions in the legs.

The 1:2 time scaling requirement has been imposed on all of the system components and operations. The scaling ratios presented in Tables 4 and 5 have been applied in the following sections to obtain the revised APEX component geometries as needed to match the new AP1000 design.

3.1 Core Decay Power and Flow Area Scaling Analysis

One of the key changes to the AP1000 is the increase in core thermal power from 1933 MW thermal to 3400 MW thermal. Three modifications were made to the APEX test facility as a result of the power change:

- A higher power core was installed
- The core flow area was adjusted, and
- The decay power algorithm was modified.

3.1.1 Maximum Core Power

Based on the power scaling ratio given in Table 4, the new core power needed in APEX to match a 3% decay power in the AP1000 was:

$$q_{\text{APEX}} = \left[\quad \right]^{a,b,c} \tag{17}$$

This resulted in a desired power in APEX of 1.06 MW thermal. A new 48 rod bundle core with a []^{a,b,c} MW thermal power was installed. This represents a []^{a,b,c} decay power.

3.1.2 Core Flow Area

Based on the core flow area ratio given in Table 4, the new core flow area needed in APEX to properly match the scaled core flow area in AP1000 was:

$$a_{\text{core,APEX}} = \left[\quad \right]^{a,b,c} \tag{18}$$

The AP1000 effective core flow area is []^{a,b,c}. Using the scaling ratio in equation (18), the desired APEX-1000 core flow area is []^{a,b,c}. Using 48 heaters, each having a []^{a,b,c} in diameter results in an actual core flow area of []^{a,b,c}.

3.1.3 Decay Power Algorithm

Establishing the initial conditions for ADS-4 operation and long term cooling requires that the total energy input into the system, to the point of reaching the transition pressure be properly scaled. The integrated core power ratio is written as follows:

$$E_{\text{core,R}} = \frac{\int_0^{t_m} q_{\text{core,m}} dt_m}{\int_0^{t_p} q_{\text{core,p}} dt_p} \tag{19}$$

where t_m is the time it takes in APEX-1000 to reach the ADS-4 opening pressure and t_p is the time it takes in AP1000 to reach the ADS-4 opening pressure. Since the ideal core power scaling ratio given in Table 4 is $[\quad]^{a,b,c}$ and the ideal time scaling ratio is 1:2, the integrated core power ratio should be $[\quad]^{a,b,c}$.

The 1979 Decay Heat Standard for Light Water Reactors was used to model the decay power curve for the AP1000.⁷ Figure 3 shows the decay power algorithm for the APEX-1000 test facility. The power algorithm is designed to match the ideally scaled AP1000 decay power after ~160 seconds. Similarly, as shown in Figure 4, the total integrated decay power matches after 160 seconds.



Figure 3 Comparison of the APEX-1000 Decay Power Algorithm and the Ideally Scaled AP1000 Decay Power Curve

a,b,c



Figure 4 Comparison of the APEX-1000 Integrated Decay Power to the Ideally Scaled AP1000 Decay Power

3.2 IRWST, CMT, Sump and Pressurizer Geometric Scaling Analysis

Table 6 presents the results of applying the scaling ratios of Table 5 to the AP1000 IRWST, CMT, Sump and Pressurizer.

Table 6 Results of IRWST, CMT, Sump and Pressurizer Geometry Scaling										
Parameter	Scaling Ratio	AP1000*	APEX Ideal	APEX Actual	Units	AP1000*	APEX Ideal	APEX Actual	Units	a,b,c
IRWST Liquid Volume (min.)										
IRWST Liquid Level (min.)										
IRWST Liquid Surface Area										
IRWST Level Setpoint for Sump Recirculation										
IRWST Liquid Head on DVI										
CMT Volume										
CMT Internal Diameter										
CMT Internal Height										
CMT Volume for ADS-1 Actuation										
CMT Volume for ADS-4 Actuation										
Sump Liquid Volume Below DVI Elevation										
Difference Between DVI and Sump Flood-up Elevations**										
Sum Liquid Surface Area										
Pressurizer Volume										
Pressurizer Liquid Volume										
Pressurizer Inside Diameter										

* AP1000 Plant Parameters Document²

** Assumes break occurs in loop compartment

3.3 ADS-4, IRWST, CMT, PRHR and Sump Recirculation Line Scaling

A detailed analysis of the pressure drops in the passive safety system balance and injection lines was provided in Chapter 7 of WCAP-14270.¹ The pressure drop for a section of pipe having a constant diameter is given by the following equation:

$$\Delta P = \frac{1}{2} \left(\frac{fl}{D} + K \right) \rho v^2 \quad (20)$$

where f is the Darcy friction factor, l/D is the piping length to diameter ratio, K is the form loss coefficient due to fittings and bends, and v is the fluid velocity in the section of pipe. For single-phase, non-choked, fluid flow with fluid property similitude, the ratio of the model to the prototype can be written as:

$$\Delta P_R = F_{T,R} v_R^2 \quad (21)$$

In this equation, $F_{T,R}$ is the ratio of the total friction and form loss coefficients. To preserve the line pressure drops, it is required that the pressure drop ratio, ΔP_R , be 0.25 and that the velocity ratio, v_R , be 0.5. Substituting these scaling ratios into the equation above yields the following requirement:

$$F_{T,R} = 1 \quad (22)$$

For the piping under consideration, the form loss coefficients, K , dominate. That is, the presence of valves, elbows and other fittings make the value of K much larger than the value of fl/D . In light of this fact, the line resistance can be adjusted using a flow orifice.

The AP1000 line resistance data, R (ft/gpm²), is expressed in terms of head loss over the square of volumetric flow rate. That is, the line resistance is expressed in terms of measured quantities as follows:

$$R = \frac{g_c \Delta P}{g \rho Q^2} \quad (23)$$

The resistance is related to the friction and form loss factors as follows:

$$R = \frac{1}{2} \left(\frac{fl}{D} + K \right) \frac{1}{a^2} \quad (24)$$

where "a" is the flow area of the pipe. Therefore, the units of line resistance are often expressed as 1/ft⁴. The flow area scaling ratio is given as 1:48. Therefore the line resistance scaling ratio for single-phase fluid under non-choked flow conditions is given as:

$$R_R = 48^2 = 2304 \quad (25)$$

Table 7 lists the range of line resistance values required for the IRWST and Sump Recirculation lines in the APEX-1000 test facility. Table 8 presents similar values for the CMT and PRHR lines.

The ADS-4/Hot Leg Nozzle diameter and resistance was scaled as with previous lines. However, the two ADS-4 branch lines that comprise a single ADS-4 train on a hot leg require a different scaling approach because the intent is to model two ADS-4 branch lines with a single line in the APEX-1000 test facility. That is, the flow area of one APEX ADS-4 branch line must equal the scaled flow area of two AP1000 branch lines:

$$a_{\text{APEX}} = \frac{2a_{\text{AP1000}}}{48} \quad (26)$$

In terms of a diameter scaling ratio, the ratio of a single ADS-4 branch line diameter in APEX to a single ADS-4 branch line in the AP1000 is:

$$D_{\text{ADS,R}} = \frac{1}{\sqrt{24}} \quad (27)$$

Table 9 presents the ADS-4 line diameters and resistance assuming that two AP1000 ADS-4 branch lines are modeled with a single branch line in APEX.

IRWST to Sump Tee	API1000				IDEAL APEX				a,b,c
	I.D. (in)	Min	Nom	Max	I.D. (in)	Min	Nom	Max	
Line A									
Line B									
Sump Tee to MOV Isol Valve									
Line A									
Line B									
Mow so Valve to Check Squib Valve									
Line A									
Line B									
Check/Squib Valves Parallel Paths									
Line A									
Line B									
Check/Squib Valves to DVI Injection Line Tee									
Line A									
Line B									
IRWST Injection Line to DVI Nozzle									
Line A									
Line B									
Sump Recirculation Path to IRWST Injection Line Tee									
Line A									
Line B									
IRWST Drain to Containment									
Line A									
Line B									

CMT	API1000				IDEAL APEX			
	I.D. (in)	Min	Nom	Max	I.D. (in)	Min	Nom	Max
Cold Leg Balance Line								
CMT to ACC Tee								
ACC to DVI								
PRHR								
RCS HL to ADS-4 Reducer								
ADS-4 Reducer to PRHR Reducer								
PRHR Reducer to PRHR HX Inlet								
PRHR HX Inlet								
PRHR HX Tube								
PRHR HX Outlet								
PRHR HX Outlet to SG								

a,b,c

ADS-4	API1000				IDEAL APEX			
	I.D. (in)	Min	Nom	Max	I.D. (in)	Min	Nom	Max
ADS-4/Hot Leg Nozzle								
ADS-4 Branch Line								
ADS-4-1 (50%)								
ADS-4-1 100%								
ADS-4-2 (50%)								
ADS-4-2 (100%)								

a,b,c

4.0 PRESSURIZER SURGE LINE SCALING ANALYSIS

This section represents a change to the original pressurizer (PZR) surge line scaling analysis presented in WCAP-14270. The original PZR surge line scaling analysis focused on preserving the two-phase flow regime transitions. However, a recent NRC analysis performed by Bessette and di Marzo suggests that preserving the PZR draining behavior is more important to the outcome of SBLOCA transients.⁷ Based on a thorough review of the NRC analysis, the PZR surge line will be modified to properly simulate the AP1000 PZR draining behavior.

Bessette and di Marzo expressed the governing momentum balance equation for the PZR surge line filling and draining process, in dimensionless form, as follows:

$$\dot{Z} \left| \dot{Z} \right| + AZ = B \quad (28)$$

where:

$$A = \frac{\frac{C}{\rho g} + 1}{\frac{\Phi_{LO}^2 \left(\frac{S_{PZR}}{S_{SL}} \right)^2 \left(f \frac{L}{D} + K \right)}{2}} \quad (29)$$

$$B = \frac{\frac{C}{\rho g} - \frac{P_{PZR}}{\rho g H_{PZR}} - (1 - \alpha) \frac{H_{SL}}{H_{PZR}}}{\frac{\Phi_{LO}^2 \left(\frac{S_{PZR}}{S_{SL}} \right)^2 \left(f \frac{L}{D} + K \right)}{2}} \quad (30)$$

and

$$C = \rho g \frac{S_{PZR}}{S_{SL}} \quad (31)$$

Integrating equation (28) yields the PZR surge line filling and draining period:

$$\tau_{SL} = 2 \left(\frac{H_{PZR}}{g} \right)^{1/2} \left[\left(\frac{B^{1/2}}{A} \right)_{\alpha=0} + \left(\frac{B^{1/2}}{A} \right)_{\alpha=0.8} \right] \quad (32)$$

For the APEX-1000, a 1:2 scale time period is required. Therefore preserving a one-half time scale PZR surge line filling and draining period requires that:

$$(H_{PZR})_R^{1/2} = \frac{1}{2} \quad (33)$$

and that:

$$\left(\frac{B^{1/2}}{A} \right)_R = 1 \tag{34}$$

The APEX-1000 PZR liquid height, H_{PZR} , is []^{a,b,c}. Therefore, the scaling criterion given by equation (33) is met.

Table 10 presents the results obtained for equation (34). The value is close to unity. It has been assumed that the ratio of the Martinelli-Nelson two-phase flow multiplier, Φ_{LR} is unity.

In addition to preserving the surge line drain and fill rates, it is desired that the pressure drop ratio in the surge line be []^{a,b,c}. That is:

$$\left[\quad \right]^{a,b,c} \tag{35}$$

This requires:

$$\left[\quad \right]^{a,b,c} \tag{36}$$

As shown in Table 10, for the line size selected, the friction factor ratio is []^{a,b,c} and the velocity ratio in the surge line is []^{a,b,c}. This yields the desired DP ratio of []^{a,b,c}.

Table 10 Results of Pressurizer Surge Line Scaling Analysis		
Parameter	AP1000	APEX
Roughness (in)		
ID (in)		
Relative Roughness		
Reynolds Number		
Friction Factor		
Calculated Pressure Drop Ratio =		
Friction Factor Ratio =		
(fL/d) Ratio =		
Pressurizer ID (in)		
$H_{PZR(ft)}$		
Head at 1 atm (ft)		
HsL (ft)		
A_R (Bessette & di Marzo)		
B_R (Bessette & di Marzo)		
$(B_R)^{1/2}/A =$		

a,b,c

5.0 REACTOR COOLANT SYSTEM DEPRESSURIZATION SCALING ANALYSIS

This section presents a revised depressurization scaling analysis for the APEX-1000 test facility. It represents a more comprehensive analysis than that presented in the original WCAP-14270. Figure 5 presents the scaling analysis flow diagram for primary system depressurization. First, the governing set of equations for the depressurization of a two-phase fluid system were developed. This resulted in obtaining a Depressurization Rate Equation. Next, a top-down system level scaling analysis was performed for the Reactor Coolant System (RCS) assuming multiple vent and injection paths. This included the development of scaling criteria for sizing the break and Automatic Depressurization System (ADS) flow areas. Last, a bottom-up analysis was performed to describe the scaling of local transport processes such as the critical flow through the breaks and ADS valves.

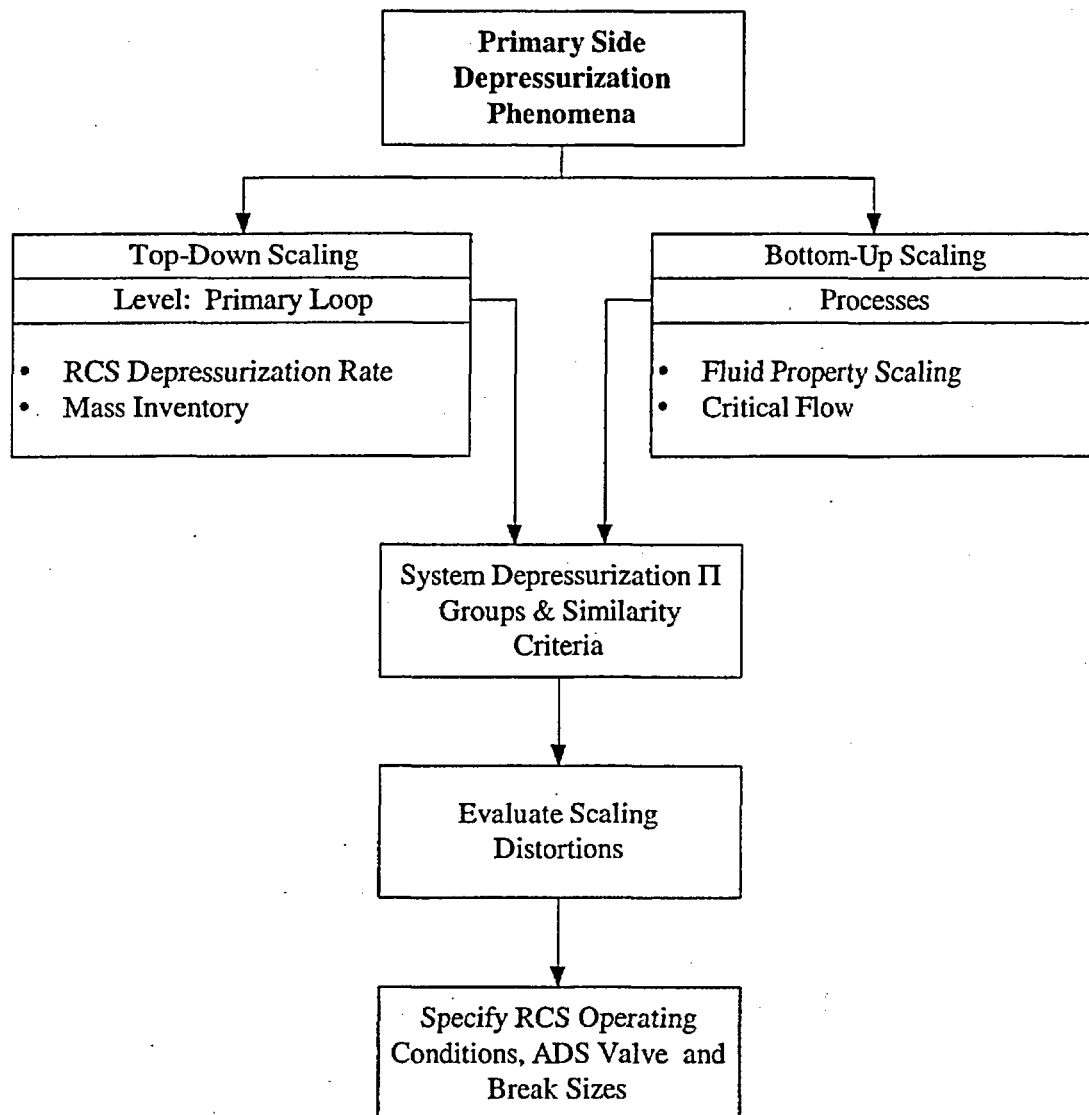


Figure 5 Flow Chart of the Primary Side Depressurization Scaling Analysis

5.1 Reference Pressure for LOCA Transients

A variety of primary loop blowdown tests will be performed in APEX. The integral system tests will be performed under pressure scaled conditions to observe all of the passive safety system functions. A series of *full pressure* tests shall also be performed to examine the transition from ADS-4 operation to IRWST injection.

Figure 6 presents typical trends for the reactor coolant system and steam generator pressures during a SBLOCA transient in APEX. The opening of a break is immediately followed by a period of subcooled blowdown during which the primary system depressurizes to a pressure equivalent to the steam generator PORV setpoint. Hence, the primary and secondary system pressures will meet at the onset of saturation conditions in the primary as shown in the figure. The AP600 scaling analysis was the first research to recognize that the onset of primary loop saturation offered a common reference point for the purpose of scaling. This fact, coupled with the concept that the depressurization of systems under phase equilibria conditions exhibits self-similarity, offered the possibility of performing pressure scaled testing.

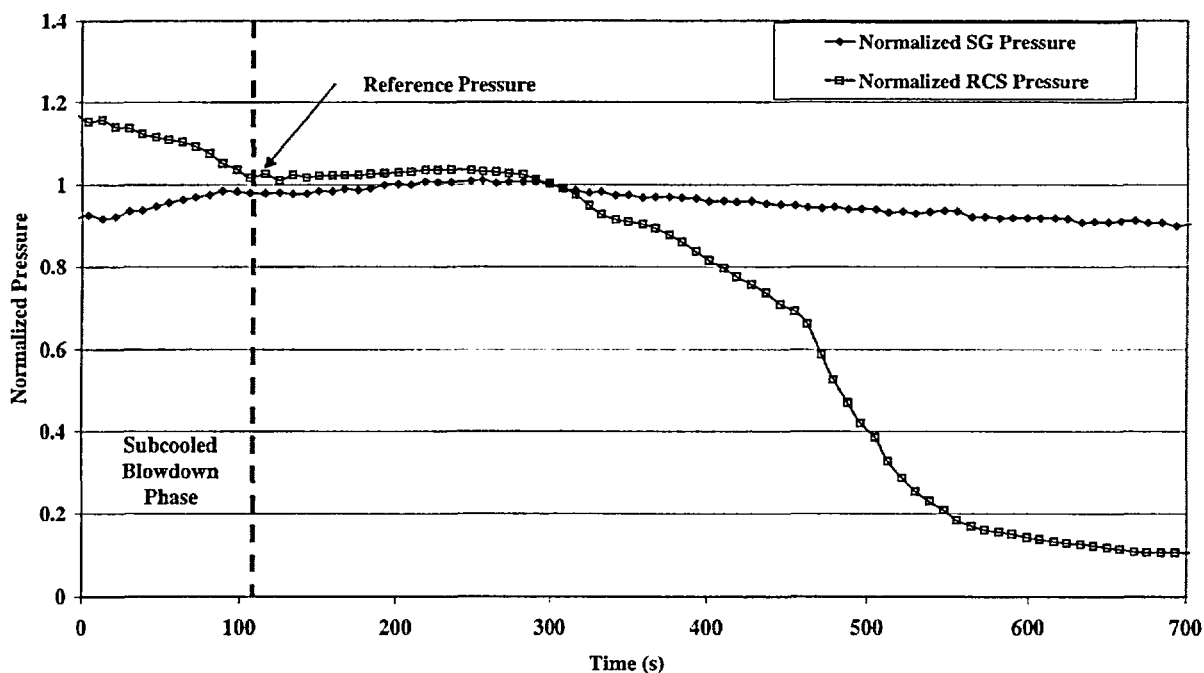


Figure 6 Primary and Secondary Side Pressures During a Typical 2-Inch Break LOCA in APEX

For the AP1000, the reference pressure for the onset of saturation conditions in the primary loop coincides with the Steam Generator PORV pressure setpoint of 1200 psia. For the APEX-1000, this value will be set at 345 psia. The goal of the pressure scaled testing is to provide the full range of passive safety system behavior for a given transient in the proper event sequence. This data can be used to benchmark the thermal hydraulic safety analysis codes. However, by scaling the break and ADS 1-3 flow areas relative to the saturation reference pressure, the timing of the subcooled blowdown portion of the

transient will not proceed at one-half time scale. For rapid blowdowns, such as the double-ended Direct Vessel Injection (DEDVI) line break, this effect is negligible. This was demonstrated by the excellent comparisons obtained between the APEX and the full pressure ROSA AP600 DEDVI tests.

The AP600 test program revealed that the transition from ADS-4 operation to the start of IRWST injection was important to core cooling. Therefore, this test program will include a series of full pressure ADS-4 blowdown tests to carefully examine the ADS-4 transition under prototypic fluid pressures and temperature.

5.2 Governing Equations for RCS Two-Phase Fluid Depressurization

The mass conservation equation for a RCS control volume undergoing a depressurization event is given by:

$$\frac{dM}{dt} = \sum \dot{m}_{in} - \sum \dot{m}_{out} \quad (37)$$

where M is the fluid mass within the RCS and \dot{m} represents the mass flow rate entering or leaving the reactor coolant system. The energy conservation equation for the RCS fluid is expressed as follows:

$$\frac{dU}{dt} = \sum (\dot{m}h)_{in} - \sum (\dot{m}h)_{out} + q_{SG} + q_{core} + q_{loss} - P \frac{dV}{dt} \quad (38)$$

where U is the bulk internal energy of the fluid within the RCS, h is the enthalpy of the fluid entering or leaving the RCS, q_{SG} , q_{core} and q_{loss} are the steam generator energy transfer rate, the core power and the heat loss respectively. P is the RCS pressure and V is the RCS volume. The specific internal energy and the specific volume are defined respectively as follows:

$$e = \frac{U}{M} \quad (39)$$

$$v = \frac{V}{M} \quad (40)$$

The total change in specific internal energy is written in terms of partial differentials with respect to pressure and specific volume as follows:

$$de = \left(\frac{\partial e}{\partial p} \right)_v dp + \left(\frac{\partial e}{\partial v} \right)_p dv \quad (41)$$

Substituting equation (39) into (38) yields:

$$\frac{dMe}{dt} = \sum (\dot{m}h)_{in} - \sum (\dot{m}h)_{out} + q_{SG} + q_{core} + q_{loss} - P \frac{dV}{dt} \quad (42)$$

Expanding the term on the LHS of equation (42), substituting equation (37) and rearranging yields:

$$M \frac{de}{dt} = (\sum \dot{m}_{in}) (h_{in} - e) - (\sum \dot{m}_{out}) (h_{out} - e) + q_{SG} + q_{core} + q_{loss} - P \frac{dV}{dt} \quad (43)$$

In equation (43), it has been assumed that h_{in} is the same for all the injection locations and h_{out} is the same for all the vent paths. Substituting equation (41) into (43), and rearranging yields:

$$\begin{aligned} M \left(\frac{\partial e}{\partial P} \right)_v \frac{dP}{dt} &= (\sum \dot{m}_{in}) (h_{in} - e) - (\sum \dot{m}_{out}) (h_{out} - e) \\ &+ q_{SG} + q_{core} + q_{loss} - P \frac{dV}{dt} - M \left(\frac{\partial e}{\partial v} \right)_p \frac{dv}{dt} \end{aligned} \quad (44)$$

Using equation (40), and the mass conservation equation, the last term on the RHS of equation (44) is written as:

$$M \left(\frac{\partial e}{\partial v} \right)_p \frac{dv}{dt} = \left(\frac{\partial e}{\partial v} \right)_p \frac{dV}{dt} - v \left(\frac{\partial e}{\partial v} \right)_p (\sum \dot{m}_{in} - \sum \dot{m}_{out}) \quad (45)$$

Substituting back into equation (44) yields:

$$\begin{aligned} M \left(\frac{\partial e}{\partial P} \right)_v \frac{dP}{dt} &= (\sum \dot{m}_{in}) \left[h_{in} - e + v \left(\frac{\partial e}{\partial v} \right)_p \right] \\ &- (\sum \dot{m}_{out}) \left[h_{out} - e + v \left(\frac{\partial e}{\partial v} \right)_p \right] \\ &+ q_{SG} + q_{core} + q_{loss} - \left[P + \left(\frac{\partial e}{\partial v} \right)_p \right] \frac{dV}{dt} \end{aligned} \quad (46)$$

which is the “depressurization rate equation.” For the RCS control volume, which has rigid boundaries, equation (46) becomes:

$$\begin{aligned} M \left(\frac{\partial e}{\partial P} \right)_v \frac{dP}{dt} &= (\sum \dot{m}_{in}) \left[h_{in} - e + v \left(\frac{\partial e}{\partial v} \right)_p \right] \\ &- (\sum \dot{m}_{out}) \left[h_{out} - e + v \left(\frac{\partial e}{\partial v} \right)_p \right] + q_{SG} + q_{core} + q_{loss} \end{aligned} \quad (47)$$

The net energy transfer rate is given as:

$$q_{\text{net}} = q_{\text{SG}} + q_{\text{core}} + q_{\text{loss}} \quad (48)$$

Equation (47) is the governing equation for depressurization behavior in the RCS.

5.3 Top-Down Reactor Coolant System Depressurization Scaling Analysis

The mass conservation equation, equation (37), is expressed in dimensionless form by dividing each term by its respective initial condition and further dividing by the mass flow rate of the fluid leaving the break. This results in the following dimensionless mass balance equation:

$$\tau_{\text{RCS}} \frac{dM^+}{dt} = \Pi_m \sum \dot{m}_{\text{DVI}}^+ - \sum \dot{m}_{\text{Brk}}^+ \quad (49)$$

where the superscript "+" indicates normalization with respect to initial conditions. The residence time constant, (τ_{RCS}), for the depressurization transient is given by:

$$\tau_{\text{RCS}} = \frac{M_o}{\sum \dot{m}_{\text{Brk},o}} \quad (50)$$

and the characteristic time ratio is given by:

$$\Pi_m = \frac{\sum \dot{m}_{\text{INJ},o}}{\sum \dot{m}_{\text{Brk},o}} \quad (51)$$

Π_m is the system mass flow rate ratio. For a constant injection flow rate, Π_m represents the total liquid mass injected into the RCS during the residence time (τ_{RCS}).

Equation (47) can be expressed in dimensionless form by dividing each term by its respective initial condition. The normalized terms are as follows:

$$M = M_o M^+ \quad (52)$$

$$P = P_o P^+ \quad (54)$$

$$q_{\text{net}} = q_{\text{net},o} q_{\text{net}}^+ \quad (53)$$

$$\sum \dot{m}_{\text{DVI}} = \sum \dot{m}_{\text{DVI},o} \sum \dot{m}_{\text{DVI}}^+ \quad (55)$$

$$\sum \dot{m}_{\text{Brk}} = \sum \dot{m}_{\text{Brk},o} \sum \dot{m}_{\text{Brk}}^+ \quad (56)$$

$$\left[h_{DVI} - e + v \left(\frac{\partial e}{\partial v} \right)_p \right] = \left[h_{DVI} - e + v \left(\frac{\partial e}{\partial v} \right)_p \right]_o \left[h_{DVI} - e + v \left(\frac{\partial e}{\partial v} \right)_p \right]^+ \quad (57)$$

$$\left[h_{Brk} - e + v \left(\frac{\partial e}{\partial v} \right)_p \right] = \left[h_{Brk} - e + v \left(\frac{\partial e}{\partial v} \right)_p \right]_o \left[h_{Brk} - e + v \left(\frac{\partial e}{\partial v} \right)_p \right]^+ \quad (58)$$

Substituting these equations into (47) and dividing through by $\dot{m}_{Brk,o} \left[h_{Brk} - e + v \left(\frac{\partial e}{\partial v} \right)_p \right]_o$ yields the dimensionless depressurization rate equation:

$$\begin{aligned} M^+ \left(\frac{\partial e}{\partial P} \right)_v^+ \tau_{RCS} \frac{\partial P^+}{\partial t} &= \frac{\Pi_h}{\Pi_-} \Sigma \dot{m}_{DVI}^+ \left[h_{DVI} - e + v \left(\frac{\partial e}{\partial v} \right)_p \right]^+ \\ &\quad - \frac{\Sigma \dot{m}_{Brk}^+}{\Pi_-} \left[h_{Brk} - e + v \left(\frac{\partial e}{\partial v} \right)_p \right]^+ \\ &\quad + \frac{\Pi_\Gamma}{\Pi_-} q_{net}^+ \end{aligned} \quad (59)$$

where the characteristic time ratios are given by:

$$\Pi_h = \frac{\Sigma \dot{m}_{DVI,o} \left[h_{DVI} - e + v \left(\frac{\partial e}{\partial v} \right)_p \right]_o}{\Sigma \dot{m}_{Brk,o} \left[h_{Brk} - e + v \left(\frac{\partial e}{\partial v} \right)_p \right]_o} \quad (60)$$

$$\Pi_\Gamma = \frac{q_{net,o}}{\Sigma \dot{m}_{Brk,o} \left[h_{Brk} - e + v \left(\frac{\partial e}{\partial v} \right)_p \right]_o} \quad (61)$$

$$\Pi_e = \varepsilon_o = \frac{p_o \left(\frac{\partial e}{\partial P} \right)_{v,o}}{\left[h_{Brk} - e + v \left(\frac{\partial e}{\partial v} \right)_p \right]_o} \quad (62)$$

Π_h is the energy flow rate ratio. It represents the ratio of the total energy change due to fluid injection to the energy change caused by the break flow. Π_r is the power ratio. It represents the ratio of the net heat into the system to the rate of fluid energy transport through the break. Π_e is the fluid mixture dilation property group.

Equation (62) reveals that the fluid dilation property group couples the system intensive energy change to the intensive energy at the break. For high pressure systems venting to the ambient, the fluid properties at the break are determined at critical flow conditions.

Evaluating the RCS time constant, τ_{RCS} , and the dimensionless groups Π_m , Π_b , Π_r , Π_e requires knowledge of the pressure scaled fluid properties and the critical mass flux. These parameters are evaluated in the bottom-up scaling analysis that follows.

5.3.1 Similarity of Pressure Trajectories in Dimensionless Phase Space

One of the goals of the test program is to operate the APEX facility such that the pressure trends that evolve in APEX for a given scenario would be the same for a similar scenario in AP1000 when the results are plotted in dimensionless phase space. That is, plotting scenario pressure histories as P/P_o versus t/τ_{RCS} , or P/P_o versus M/M_o , would yield overlaying curves for the two facilities. This condition can be achieved by satisfying the following requirements:

1. The scenarios are initiated from the same initial condition in dimensionless phase space. In this case P^* at $t^*=0$, is 1.
2. The rate of change, (i.e., slope), is preserved in dimensionless phase space. This imposes the following scaling criterion:

$$\left(\frac{dP^*}{dt^*} \right)_R = 1 \quad (63)$$

Satisfying the requirement given by equation (63) means preserving the dimensionless Π groups on the right hand side of equation (59). If the two requirements listed above are satisfied, then the following is true:

$$\left(\frac{P}{P_o} \right)_{\text{APEX}} = \left(\frac{P}{P_o} \right)_{\text{AP1000}} \quad (64)$$

This means that the dimensionless pressure at any point along the scenario trajectory will be the same in APEX and AP1000.

Figure 7 shows how the saturation pressures in APEX would relate to the saturation pressures in AP1000. In this figure, P_o for AP1000 is 8.27 MPa (1200 psia) and P_o for APEX is 2.36 MPa (342 psia). These pressures correspond to the turbine bypass pressure relief setpoints on the secondary side.

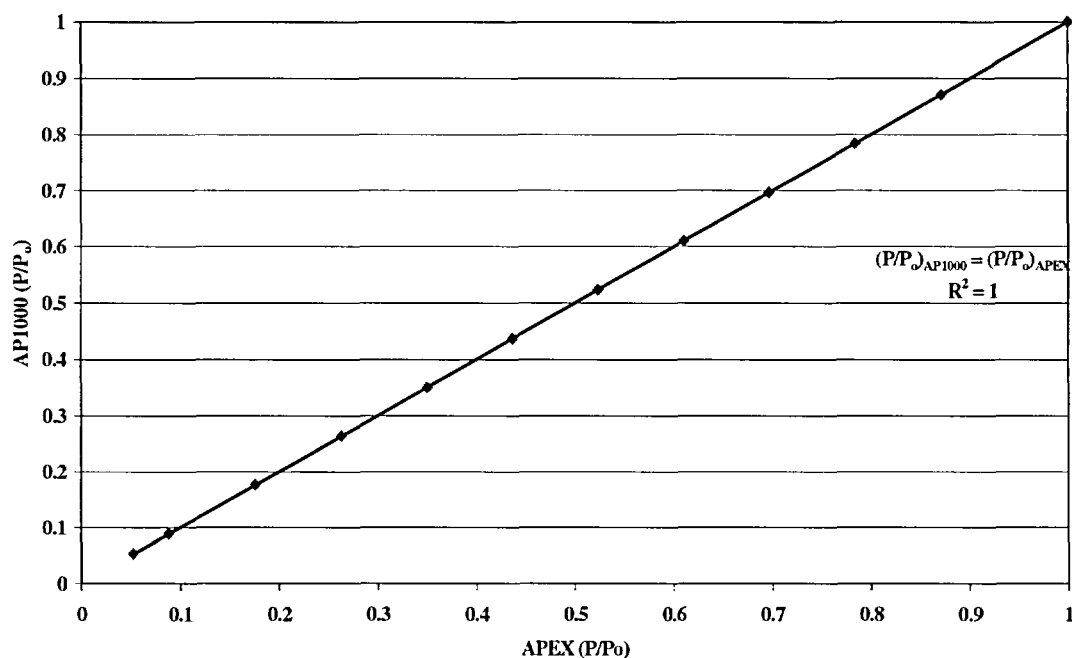


Figure 7 Scaling Relationship Between AP1000 and APEX Saturation Pressure

5.4 Bottom-Up Scaling Depressurization Scaling Analysis

The objective of the bottom-up scaling analysis was to obtain the closure relations needed to evaluate the scaling ratios developed through the top-down analysis. These closure relations are dependent on fluid properties. Therefore, the first step in the bottom-up analysis was the development of the method to relate fluid properties in AP1000 to those at reduced pressure in APEX.

5.4.1 Self-Similarity of Fluid Properties in Phase Equilibria (P_{sat} Scaling)

The equation of state for many of the important thermodynamic properties, $\psi(P)$, of the saturated fluid can be described by a simple power function as follows:

$$\psi = \psi_o \left(\frac{P}{P_o} \right)^\xi \quad (65)$$

where ψ_o can be evaluated at an arbitrary reference pressure, P_o , within the range of applicability of equation (65) and ξ is an empirically determined constant. For saturated water, having a pressure between atmospheric and approximately 15 MPa (2175 psia), the following thermodynamic properties are well correlated by equation (65) as demonstrated in Figures 8 through 11.

$$\frac{Pv_{fg}}{h_{fg}} = \left(\frac{Pv_{fg}}{h_{fg}} \right)_o \left(\frac{P}{P_o} \right)^{0.11} \quad (66)$$

$$s_f = s_{f,o} \left(\frac{P}{P_o} \right)^{0.20} \quad (67)$$

$$v_g = v_{g,o} \left(\frac{P}{P_o} \right)^{-1.02} \quad (68)$$

$$v_{fg} = v_{fg,o} \left(\frac{P}{P_o} \right)^{-1.06} \quad (69)$$

The form of equation (65) has the special property of being “invariant” with respect to a two-parameter transformation in scale. That is, rescaling the variables such that:

$$\psi = C_1 \psi^* \quad (70)$$

$$\psi_o = C_1 \psi_o^* \quad (71)$$

$$P = C_2 P^* \quad (72)$$

$$P_o = C_2 P_o^* \quad (73)$$

where C_1 and C_2 are constants, and substituting these rescaled variables into equation (65) yields:

$$\psi^* = \psi_o^* \left(\frac{P^*}{P_o^*} \right)^{\xi} \quad (74)$$

The form of the equation of state remains unchanged. This type of transformation is known as a “stretching” or “similarity” transformation. The special feature of invariance with scale implies that the points and slopes of any curves in the (ψ, P) phase space can be related to corresponding points and slopes in the (ψ^*, P^*) phase space. (Bluman, 1974).¹⁴ This type of scale invariance is known as “self-similarity.” Self-similarity can be defined as a repetition of detail at descending scales. If the dimensionless pressure ratios are preserved in the scale model, then self-similarity dictates that the dimensionless fluid properties (ψ/ψ_o) will also be preserved.

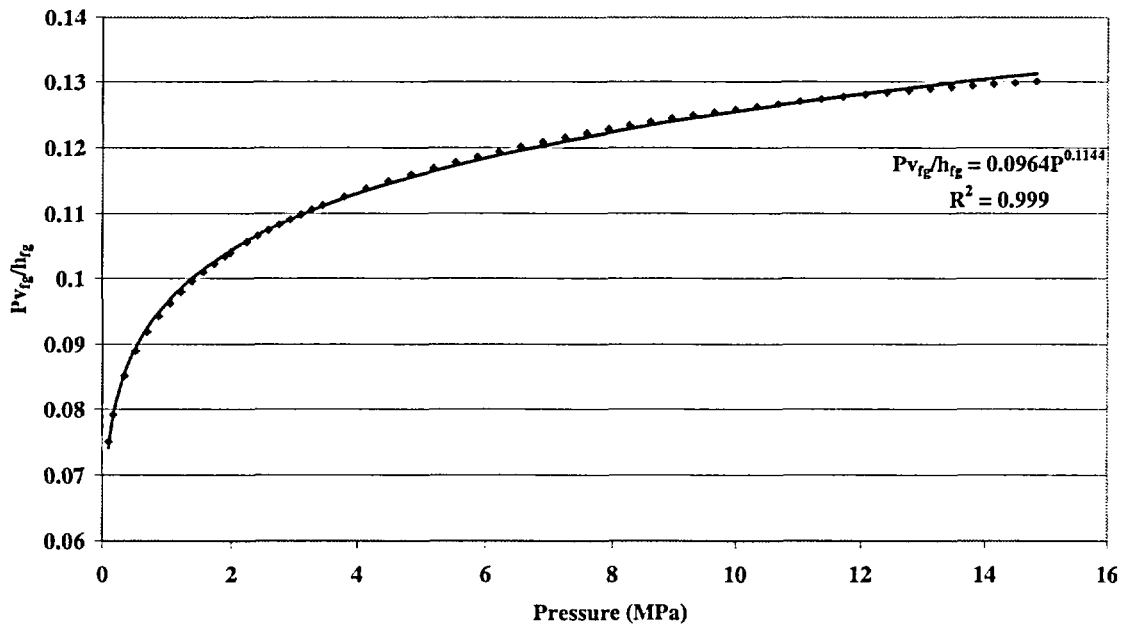


Figure 8 Power Law for Pv_{fg}/h_{fg} as a Function of Pressure

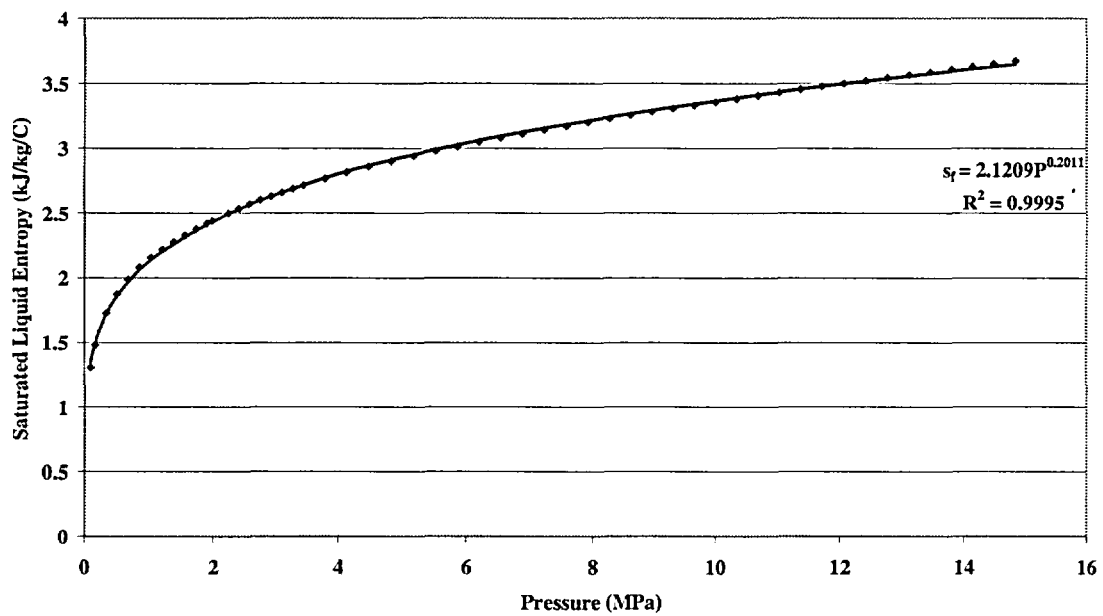


Figure 9 Power Law for s_f as a Function of Pressure

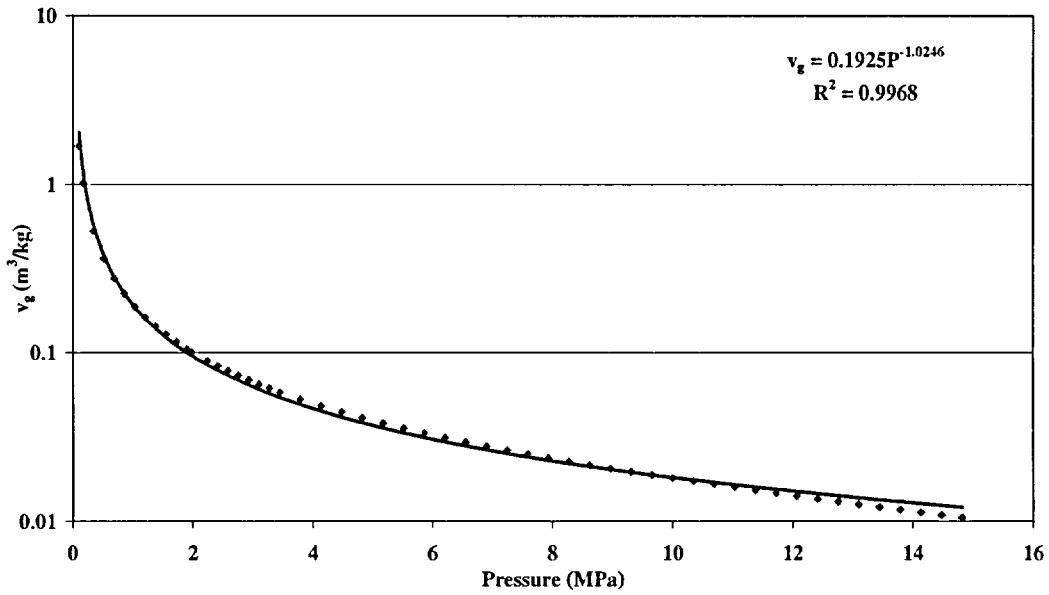


Figure 10 Power Law for v_g as a Function of Pressure

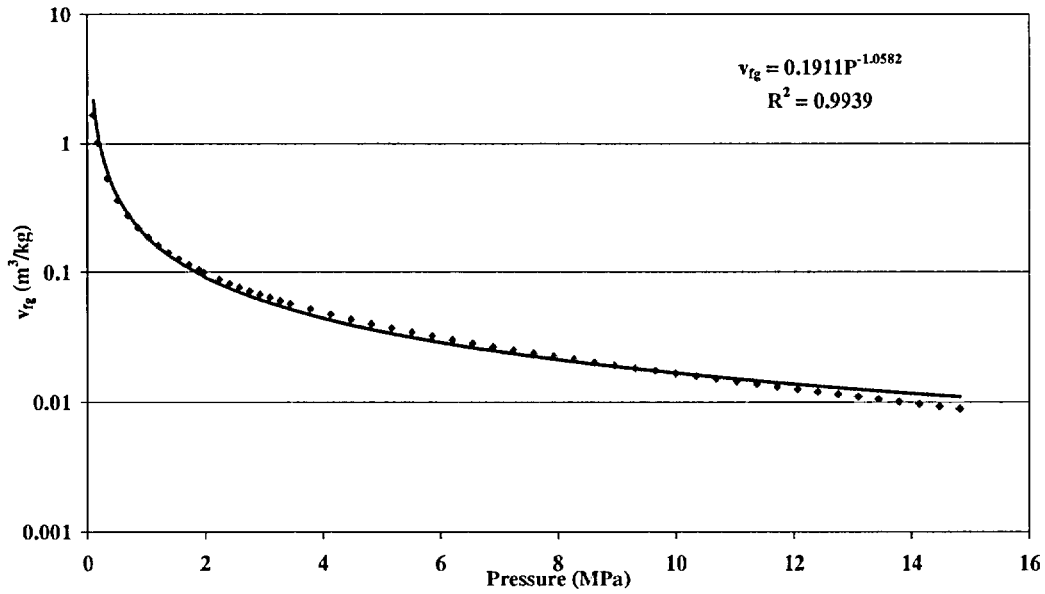


Figure 11 Power Law for v_{fg} as a Function of Pressure

5.4.2 Equations of State for Saturated Pressure and Temperature (T_{sat} Scaling)

The Clausius-Clapeyron equation is the classical differential equation that defines the slope dP/dT , for a phase equilibrium curve. It is derived assuming that the Gibb's free energies for the two-phases being considered are equal (Lay, 1990).¹⁵ Using the saturated definition for the Gibb's free energy and relating the change in entropy to the latent heat of vaporization and the saturation temperature yields the well-known Clausius-Clapeyron equation:

$$\frac{dP}{dT} = \frac{h_{fg}}{v_{fg} T} \quad (75)$$

An analytical expression for an equation of state relating saturation pressure to saturation temperature can be obtained as follows. Substituting equation (66) into (75), where ξ is 0.11 for water, and rearranging yields:

$$\left(\frac{P}{P_o}\right)^{\xi-1} dP = \left(\frac{h_{fg}}{v_{fg}}\right)_o \frac{1}{T} dT \quad (76)$$

Integrating from P_o to P_{sat} and from T_o to T_{sat} yields the desired relationship between P_{sat} and T_{sat} .

$$P_{\text{sat}}(T_{\text{sat}}) = P_o \left[1 + \xi \left(\frac{h_{fg}}{P v_{fg}}\right)_o \text{Ln} \left(\frac{T_{\text{sat}}}{T_o}\right)^{1/\xi} \right] \quad (77)$$

Figure 12 shows that equation (77) is quite accurate for the range of conditions examined.

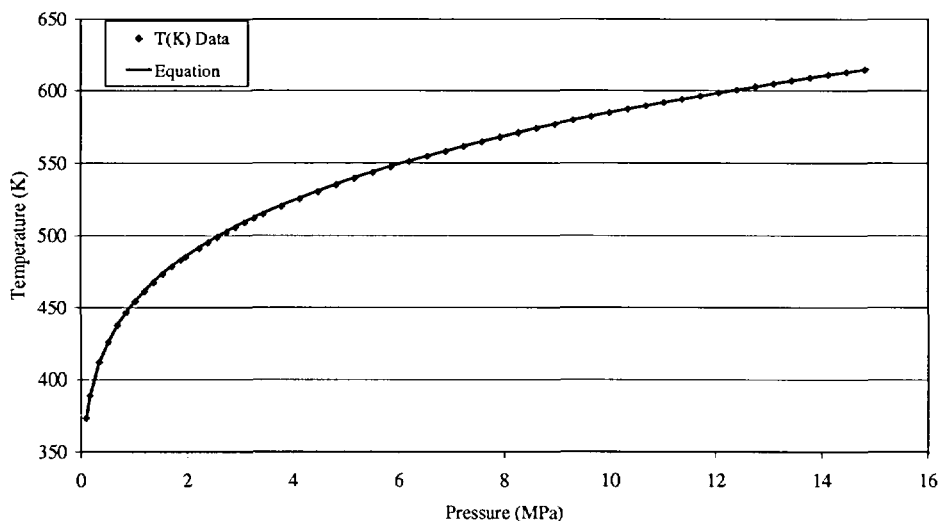


Figure 12 Comparison of Equation (77) to Steam Tables

Equation (77) can be rearranged to obtain saturation temperature in terms of saturation pressure. The result is:

$$T_{\text{sat}}(P_{\text{sat}}) = T_o \exp \left\{ -\frac{1}{\xi} \left(\frac{P v_{fg}}{h_{fg}} \right)_o \left[1 - \left(\frac{P_{\text{sat}}}{P_o} \right)^\xi \right] \right\} \quad (78)$$

This equation can be accurately approximated using the following identity:

$$\exp(\beta) \approx 1 + \beta \quad (79)$$

for $\beta \ll 1$ which is applicable to the current situation. Thus equation (78) is approximated by:

$$T_{\text{sat}} = T_o \left\{ 1 - \frac{1}{\xi} \left(\frac{P v_{fg}}{h_{fg}} \right)_o \left[1 - \left(\frac{P_{\text{sat}}}{P_o} \right)^\xi \right] \right\} \quad (80)$$

Rearranging equation (79) yields:

$$\left(\frac{h_{fg}}{P v_{fg}} \right)_o \left[1 - \left(\frac{T_{\text{sat}}}{T_o} \right) \right] = \frac{1}{\xi} \left[1 - \left(\frac{P_{\text{sat}}}{P_o} \right)^\xi \right] \quad (81)$$

This equation is valid for both APEX and AP1000 for the range of saturated conditions being examined. Writing this equation for APEX yields:

$$\left(\frac{h_{fg_o}}{P_o v_{fg_o}} \right)_{\text{APEX}} \left[1 - \left(\frac{T_{\text{sat}}}{T_o} \right)_{\text{APEX}} \right] = \frac{1}{\xi} \left[1 - \left(\frac{P_{\text{sat}}}{P_o} \right)_{\text{APEX}}^\xi \right] \quad (82)$$

and for AP1000:

$$\left(\frac{h_{fg_o}}{P_o v_{fg_o}} \right)_{\text{AP1000}} \left[1 - \left(\frac{T_{\text{sat}}}{T_o} \right)_{\text{AP1000}} \right] = \frac{1}{\xi} \left[1 - \left(\frac{P_{\text{sat}}}{P_o} \right)_{\text{AP1000}}^\xi \right] \quad (83)$$

Recalling that:

$$\left(\frac{P_{\text{sat}}}{P_o} \right)_{\text{APEX}} = \left(\frac{P_{\text{sat}}}{P_o} \right)_{\text{AP1000}} \quad (84)$$

it is recognized that the right hand side of equation (82) and (83) are identical. Therefore they can be set equal to obtain:

$$\left(\frac{h_{fgo}}{P_o v_{fgo}} \right)_{APEX} \left[1 - \left(\frac{T_{sat}}{T_o} \right)_{APEX} \right] = \left(\frac{h_{fgo}}{P_o v_{fgo}} \right)_{AP1000} \left[1 - \left(\frac{T_{sat}}{T_o} \right)_{AP1000} \right] \quad (85)$$

Rearranging this equation yields the desired saturation temperature scaling relation:

$$\left(\frac{T_{sat}}{T_o} \right)_{AP1000} = \left(\frac{h_{fgo}}{P_o v_{fgo}} \right)_R \left(\frac{T_{sat}}{T_o} \right)_{APEX} - \left[\left(\frac{h_{fgo}}{P_o v_{fgo}} \right)_R - 1 \right] \quad (86)$$

Equation (86) is linear as shown in Figure 13 for the APEX and AP1000 reference temperatures (i.e., the saturation temperatures for the corresponding APEX and AP1000 reference pressures). Figure 13 compares the approximate solution given by equation (86) to the exact result obtained using the steam tables.

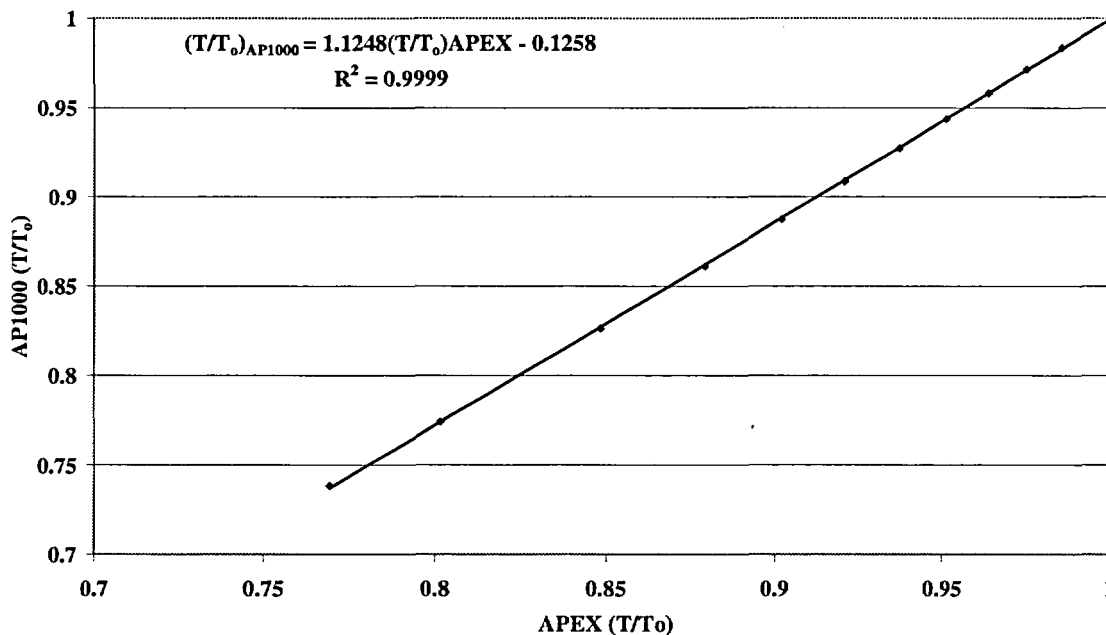


Figure 13 Scaling Relationship Between AP1000 and APEX Saturation Temperature

5.4.3 Dilation Property Group for Saturated Liquid-Vapor Blowdowns

This section demonstrates how the dilation property group, Π_ϵ , given by equation (62), is evaluated for different fluid conditions. For a two-phase fluid mixture in phase equilibrium, the following thermodynamic relations are applicable for the mixture specific internal energy and the mixture specific volume, respectively:

$$e = e_f + x e_{fg} \quad (87)$$

$$v = v_f + x v_{fg} \quad (88)$$

Eliminating the fluid mixture equilibrium quality, x , between equations (87) and (88) yields the following expression for the specific internal energy:

$$e = e_f + \frac{v - v_f}{v_{fg}} e_{fg} \quad (89)$$

The partial derivative of this equation with respect to specific volume, while holding pressure constant, yields:

$$\left(\frac{\partial e}{\partial v} \right)_P = \frac{e_{fg}}{v_{fg}} \quad (90)$$

Lastly, the latent heat of vaporization is given by:

$$h_{fg} = P v_{fg} + e_{fg} \quad (91)$$

Substituting equations (87) through (91) into equation (62) yields the following expression for the saturated mixture dilation property group:

$$\Pi_\epsilon = \frac{1}{[v_f + x_{Brk} v_{fg}]} \left(\frac{P v_{fg}}{h_{fg}} \right) \left(\frac{\partial e}{\partial P} \right)_v \quad (92)$$

where the equilibrium vapor quality at the break is given by x_{Brk} :

$$x_{Brk} = \frac{h_{Brk} - h_f}{h_{fg}} \quad (93)$$

Let us examine the pressure dependencies of the terms that comprise the fluid mixture dilation property group given by equation (92). The property group $(P v_{fg}/h_{fg})$ has already been evaluated as shown in Figure 8 and found to be described by equation (66), a power law that exhibits self-similarity for a wide range of saturation pressures.

The last term on the RHS of equation (92), $(\partial e/\partial P)_v$, is a partial derivative which requires examining the change in the fluid mixture internal energy with respect to pressure *while holding the mixture specific volume, v , constant*. It should not be confused with the total specific internal energy change with respect to pressure. An adequate model for this term can be obtained by developing an expression for the mixture internal energy as a function of pressure while at constant specific volume and taking the derivative with respect to pressure. Therefore, the term $(\partial e/\partial P)_v$ shall be evaluated assuming that the system expands along a trajectory which maintains the specific volume of the mixture at a constant value, v_o , which is the initial specific volume of the saturated mixture. That is,

$$e = e_f + e_{fg} \left(\frac{v_o - v_f}{v_{fg}} \right) \tag{94}$$

For the depressurization transients of interest to this analysis, the saturated mixture blowdown begins with the system nearly filled with saturated liquid with the exception of a small vapor volume located in the pressure vessel head. Since the density of the liquid phase is much greater than that of the vapor phase, the initial system vapor quality is very low and hence the initial fluid mixture specific volume is essentially the same as the saturated liquid phase specific volume. Thus the value of v_o , implemented in equation (94) is closely approximated by v_{fo} . Figure 14 shows how the mixture internal energy varies with pressure assuming a constant specific volume, $v_o = v_{fo}$, during the depressurization process. The plot has been made dimensionless to collapse the trends for a variety of initial pressures.

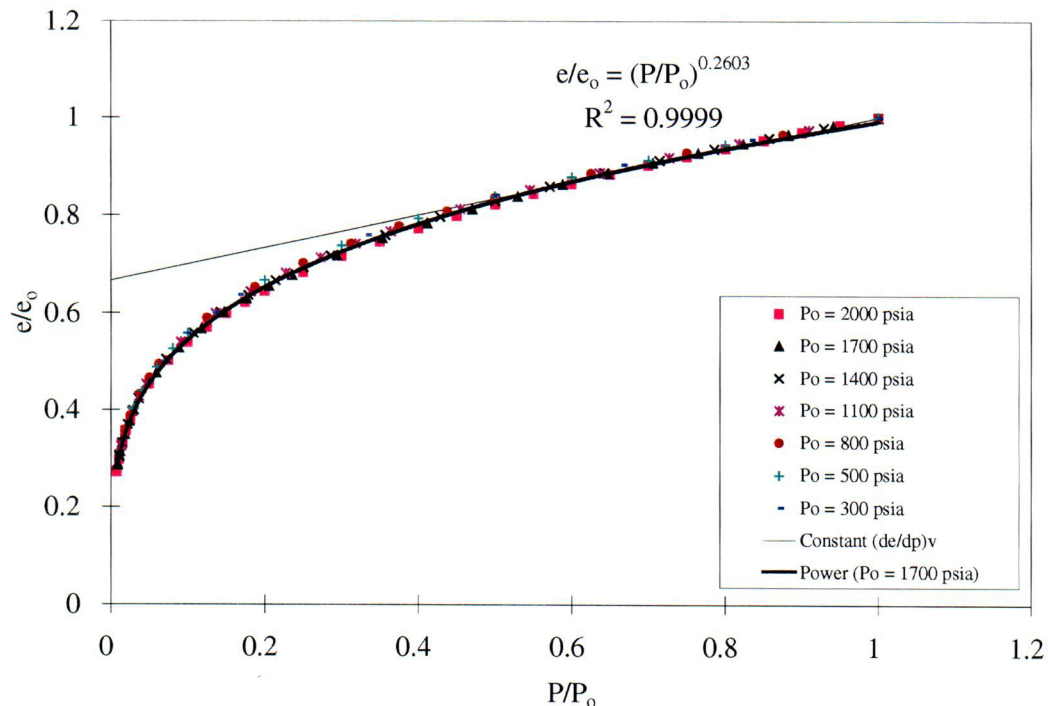


Figure 14 Plot of Dimensionless Mixture Specific Energy as a Function of Dimensionless Pressure

Note that for pressure ratios greater than ~0.5, the trend is linear; indicating that the slope, $(\partial e/\partial P)_v$, is a constant in this region. As shown in the figure, the following power law accurately ($R^2 = 0.9999$) describes the mixture specific internal energy ratio for a wide range of normalized pressures.

$$\left(\frac{e}{e_o}\right)_{v_{fo}} = \left(\frac{P}{P_o}\right)^{0.2603} \quad (95)$$

Taking the derivative of this equation with respect to pressure yields the expression for the desired partial derivative:

$$\left(\frac{\partial e}{\partial P}\right)_{v_{fo}} = 0.2603 \frac{e_{fo}}{P} \left(\frac{P}{P_o}\right)^{0.2603} \quad (96)$$

It should be noted that the numerical constants arising in equations (95) and (96) are particular to the case where the initial fluid mixture specific volume and specific energy are given by v_{fo} and e_{fo} respectively. Different constants are obtained at different initial vapor qualities for the saturated mixture.

Substituting equations (66) and (96) into (92) yields the following equation for the dilation property group.

$$\Pi_{\epsilon} = \frac{0.2603}{[v_f + x_{Brk} v_{fg}]} \left(\frac{e_f v_{fg}}{h_{fg}}\right)_o \left(\frac{P}{P_o}\right)^{-0.6257} \quad (97)$$

Equation (97) can be readily evaluated for two bounding cases, saturated liquid breaks and saturated vapor breaks.

The fluid conditions for breaks located at low points in the RCS can be approximated assuming saturated liquid at the break. For these conditions, x_{Brk} would be approximately zero, and equation (97) would become:

Saturated Liquid Breaks:

$$\Pi_{\epsilon_f} = 0.2603 \left(\frac{e_f v_{fg}}{v_f h_{fg}}\right)_o \left(\frac{P}{P_o}\right)^{-0.6257} \quad (98)$$

Here it has also been assumed that v_f does not change significantly over the range of pressure of interest.

The fluid conditions for breaks located at high points in the RCS (e.g., ADS 1-3) can be approximated assuming saturated vapor at the break. For these conditions, x_{Brk} would equal one and equation (97) would become:

Saturated Vapor Breaks:

$$\Pi_{\epsilon_g} = 0.2603 \left(\frac{\epsilon_f}{h_{fg}} \right)_o \left(\frac{P}{P_o} \right)^{0.4443} \quad (99)$$

To obtain this equation, use has been made of equation (68), the power law for the vapor specific volume. Equations (97) and (99) are written in terms of scaling ratios as follows:

$$\left(\Pi_{\epsilon_f} \right)_R = \left(\frac{\epsilon_f v_{fg}}{v_f h_{fg}} \right)_{o,R} \quad (100)$$

and

$$\left(\Pi_{\epsilon_g} \right)_R = \left(\frac{\epsilon_f}{h_{fg}} \right)_{o,R} \quad (101)$$

where equation (64) has been implemented to eliminate the pressure ratios.

5.4.4 Critical Flow Models

For the blowdown cases of interest to this study, all of the break flows are assumed to be choked. This section presents two critical flow models used to estimate the break mass flow rate; a saturated vapor model and a saturated liquid model.

In general, the break mass flow rate is expressed as:

$$\dot{m}_{Brk} = C_D G_c A_{Brk} \quad (102)$$

where C_D is the discharge coefficient, G_c is the critical mass flux and A_{Brk} is the break flow area.

5.4.4.1 Saturated Steam

This initial critical mass flow rate for saturated steam, approximated as a perfect gas, is given by: (Moody, 1990)¹⁶

$$\dot{m}_{Brk,o} = C_D A_{Brk} \left(\frac{2}{\gamma + 1} \right)^{\frac{\gamma+1}{2(\gamma-1)}} \left[\gamma P_{go} P_o \right]^{1/2} \quad (103)$$

where C_D is the discharge coefficient, A_{Brk} is the break flow area and γ is the ratio of specific heats, which is approximately 1.33 for steam.

The transient, pressure dependent, critical mass flow rate for the steam would be:

$$\dot{m}_{Brk} = \dot{m}_{Brk,o} \left(\frac{P}{P_o} \right)^{\frac{1+\gamma}{2\gamma}} \quad (104)$$

Once again we find a power law, self-similar in pressure.

5.4.4.2 Saturated Liquid

The models typically implemented for the case of saturated liquid choke flow are the Homogeneous Equilibrium Model or the Henry-Fauske Model.¹⁷ An earlier study of APEX data indicated that the Henry-Fauske Model at saturated liquid conditions best fit the APEX data (Pimentel, 1996).¹⁸

The Henry-Fauske critical flow model for saturated liquid is given by the following set of equations:

$$G_c = \left[\left\{ (v_g)_{Brk} - v_f \right\} \frac{x_{Brk}}{(0.14)(s_{fg})_{Brk}} \left(\frac{ds_f}{dP} \right)_{Brk} \right]^{-1/2} \quad (105)$$

and

$$\frac{P_{Brk}}{P} = 1 - \frac{v_f G_c^2}{2P} \quad (106)$$

In these equations, the parameters with the subscript "Brk" are evaluated at the break plane. All other parameters are evaluated at the system conditions. Thus, P_{Brk} is commonly known as the throat pressure and P would be the stagnation pressure. A typical value of equilibrium quality for the saturated liquid breaks observed in APEX was x_{Brk} equal to 0.03.

The saturated liquid entropy derivative on the right-hand side of equation (105) was obtained by taking the derivative of equation (67) with respect to pressure. This yielded the following expression for (ds_f/dP) :

$$\frac{ds_f}{dP} = 0.2 \frac{s_{f,o}}{P} \left(\frac{P}{P_o} \right)^{0.2} \quad (107)$$

Equations (105) and (106) were solved iteratively to obtain the critical flow rates for saturated liquid breaks in APEX and AP1000. Figure 15 presents the result of this analysis. Furthermore, it indicates that the critical flow model also obeys a power law that is self-similar in pressure. That is:

$$G_c \approx G_{co} \left(\frac{P}{P_o} \right)^{0.7063} \quad (108)$$

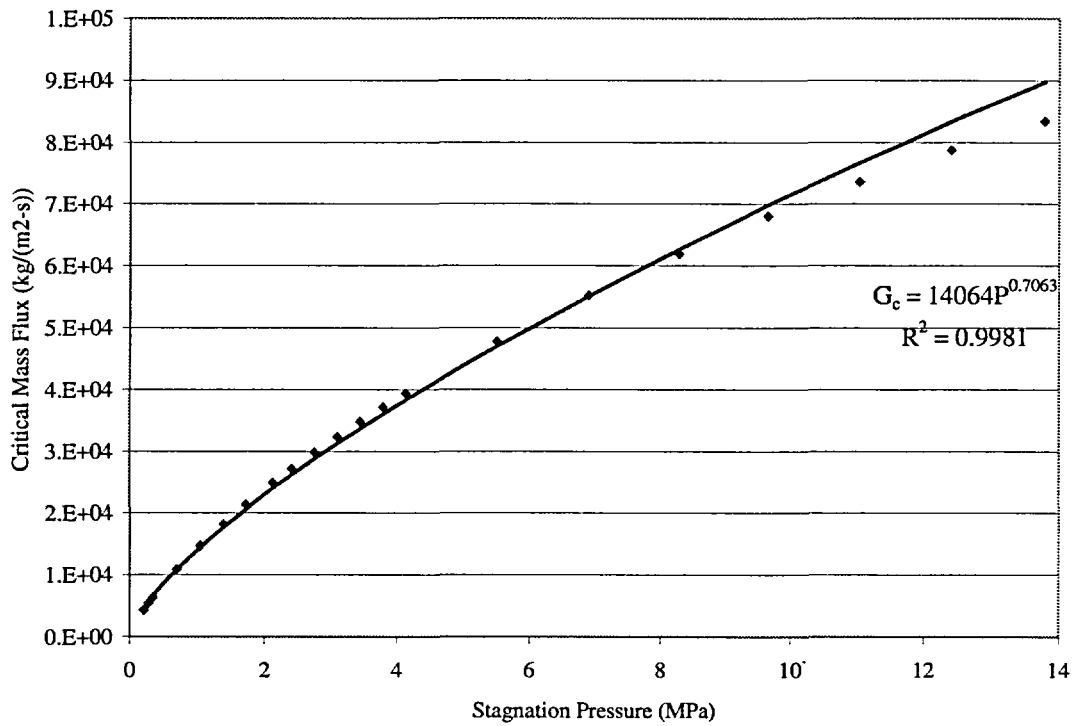


Figure 15 Critical Mass Flux for Saturated Liquid Breaks as Predicted by the Henry-Fauske Model ($x_{Brk} = 0.03$)

Using equation (102), the mass flow rate for saturated liquid breaks can be expressed as:

$$\dot{m}_{Brk} \approx \dot{m}_{Brk,o} \left(\frac{P}{P_o} \right)^{0.7063} \quad (109)$$

Equations (104) and (109) served as the closure relations for the top-down scaling dimensionless groups, Π_m , Π_h , Π_r , and the time constant τ_{RCS} .

5.5 RCS depressurization and Inventory Scaling Criteria

It is desired that APEX-1000 depressurization rate and the rate at which the RCS mass inventory changes be preserved in dimensionless phase space, (P^+, M^+) . That is, the following similarity criteria shall be imposed:

$$\left(\tau_{RCS} \frac{dM^+}{dt} \right)_R = 1 \quad (110)$$

$$\left(\tau_{RCS} \frac{dP^+}{dt} \right)_R = 1 \quad (111)$$

where:

$$\tau_{RCS,R} = \left[\frac{M_{RCS}}{\dot{m}_{Brk}} \right]_{o,R} \quad (112)$$

and the one-half time scale requirement has been set. That is,

If these criteria are preserved and the same initial conditions, $(P^+, M^+)_o$ are imposed in APEX-1000, the

$$(\tau_{RCS})_R = \frac{1}{2} \quad (113)$$

same process trajectory will result when plotted in dimensionless phase space. Applying these conditions to the dimensionless balance equations given by equations (49) and (59) means that the following scaling criteria must be on the order of unity.

$$\Pi_{m,R} = \left(\frac{\dot{m}_{INJ,o}}{\dot{m}_{Brk,o}} \right)_R \quad (114)$$

$$\left(\frac{\Pi_b}{\Pi_-} \right)_R = \left[\frac{\Sigma \dot{m}_{DVI,o} \left[h_{DVI} - e + v \left(\frac{\partial e}{\partial v} \right)_{P,o} \right]}{\dot{m}_{Brk,o} P_o \left(\frac{\partial e}{\partial P} \right)_{v,o}} \right]_R \quad (115)$$

$$\left(\frac{\Pi_\Gamma}{\Pi_-} \right)_R = \left[\frac{q_{net,o}}{\dot{m}_{Brk,o} P_o \left(\frac{\partial e}{\partial P} \right)_{v,o}} \right]_R \quad (116)$$

$$(\Pi_-)_R = \left[\frac{P_o \left(\frac{\partial e}{\partial P} \right)_{v,o}}{\left[h_{Brk} - e + v \left(\frac{\partial e}{\partial v} \right)_{P,o} \right]} \right]_R \quad (117)$$

The SBLOCA cases considered in the analysis are the case of saturated vapor at the ADS 1-3 location and saturated liquid at the break and ADS 4 locations.

5.5.1 Saturated Vapor Break Flow Areas

$$h_{Brk} = h_g$$

For saturated vapor breaks, the following would be applicable:

$$h_{Brk} = h_g \quad (118)$$

Thus implementing equations (89) through (91) yields:

$$\left[h_{Brk} - e + v \left(\frac{\partial e}{\partial v} \right)_{p,o} \right] = \frac{v_g h_{fg}}{v_{fg}} \quad (119)$$

Similarly:

$$\left[h_{DVI} - e + v \left(\frac{\partial e}{\partial v} \right)_{p,o} \right] = \left[\frac{h_{fg} v_f}{v_{fg}} - \Delta h_{sub} \right] \quad (120)$$

The injected liquid subcooling is defined as $h_f - h_{DVI}$. Using these fluid property relations, it is now possible to evaluate equations (113) through (117). Substituting the critical flow equation for saturated vapor, equation (103), and the RCS time constant ratio given by equation (110) into (111) yields.

$$\left[\frac{M_{RCS}}{A_{Brk} [\rho_{go} P_o]^{1/2}} \right]_R = \frac{1}{2} \quad (121)$$

The M_{RCS} ratio shall be set such that:

$$M_{RCS,R} = \frac{1}{192} \quad (122)$$

Substituting this condition into equation (120) and solving for the break area ratio yields:

$$(A_{Brk})_R = \frac{1}{96} \left(\frac{1}{[\rho_{go} P_o]^{1/2}} \right)_R \quad (123)$$

5.5.2 Saturated Liquid Break Flow Areas

For saturated liquid breaks, the following would be applicable:

$$h_{Brk} = h_f \quad (124)$$

Thus implementing equations (89) through (91) results in:

$$\left[h_{Brk} - e + v \left(\frac{\partial e}{\partial v} \right)_P \right]_0 = \frac{v_f h_{fg}}{v_{fg}} \quad (125)$$

Substituting the critical flow equation for saturated liquid, equation (109), and the RCS time constant ratio given by equation (110), into (111) yields:

$$\left[\frac{M_{RCS}}{C_D A_{Brk} P_o^{0.7063}} \right]_R = \frac{1}{2} \quad (126)$$

Assuming similar discharge coefficients, substituting equation (122) and rearranging, yields the break flow area ratio:

$$(A_{Brk})_R = \frac{1}{96} \left(\frac{1}{P_o^{0.7063}} \right)_R \quad (127)$$

Equations (123) and (127) become identical for the case of fluid property similitude. That is:

$$(A_{Brk})_R = \frac{1}{96} \quad (128)$$

5.5.3 ADS Valve Flow Area Scaling Ratios

Operation of the ADS system is initiated when the CMT liquid level drops below a prescribed setpoint. This typically occurs subsequent to pressurizer draining. Therefore most of the flow is single phase steam. As a result, the ADS 1 and ADS 2 valves will be scaled in accordance with equation (123). That is:

$$(A_{ADS1,2})_R = \frac{1}{96} \left(\frac{1}{[\rho_{go} P_o]^{1/2}} \right)_R \quad (129)$$

The opening of the ADS 3 valve shall be used to transition to fluid property similitude conditions. This procedure was first implemented in the NRC AP600 test program to allow actuation of the ADS 4 valves at higher operating pressures. The flow area for the APEX ADS 3 valve was designed such that:

$$(A_{ADS-3})_{APEX} = \frac{1}{96} \Sigma (A_{ADS1,2,3})_{AP} 1000 \quad (130)$$

The procedure was such that ADS 1 and ADS 2 would open sequentially as specified by the safety logic. Then ADS 1 and ADS 2 would be closed and APEX ADS 3, representing the sum of flow areas for all three stages, would be opened. Thus the ADS 1-3 train would be configured for fluid property similitude and long term cooling.

The ADS 4 valve flow area was sized based on fluid property similitude as follows:

$$(A_{ADS4})_R = \frac{1}{96} \tag{131}$$

5.5.4 DVI Mass Flow Rate Scaling Ratio

All of the injection flow rates will be scaled as follows for the one-half time scale. This is done by preserving the line resistance and relative elevation in the IRWST, CMT and Accumulators. Thus:

$$(\dot{m}_{DVI,o})_R = \frac{1}{96} \tag{132}$$

5.5.5 Net Power Scaling Ratio

Substituting equation (96) into (116) and setting the result equal to one yields the net power scaling ratio: Use has been made of the fact that $(P/P_o)_R$ is unity. The core decay power scaling has already been set in Chapter 3 to be 1/96.

$$(q_{net,o})_R = [\dot{m}_{Brk} e_{fo}]_R \tag{133}$$

5.6 Initial Conditions and Flow Areas

Tables 11 presents the initial conditions for the APEX test facility for a LOCA transient. These parameters will be modified for other transients such as the station blackout.

Table 11 APEX-1000 LOCA Initial Conditions			
Parameters	AP1000	APEX	Units
Decay Power (2.8%)			
RCS Pressure			
Steam Generator Operating Pressure			
Cold Leg Temperature			
Steam Generator Operating Pressure			
Steam Generator PORV Setpoint (Reference Pressure)			
Steam Generator Shell Side Liquid Level			
Steam Generator Shell Side Liquid Mass			
Steam Generator Shell Side Vapor Mass			
Pressurizer Liquid Volume			
Accumulator Gas Pressure			

a,b,c

Table 12 presents the flow areas required for the ADS valves as used for LOCA transients. Table 13 presents the ADS 1 and 2 flow areas for the special case of a transient initiated by the inadvertent opening of the ADS 1 valve. Table 14 presents the scaled break sizes and Table 15 presents the numerical values for the RCS time constant and P ratios.

Table 12 Summary of APEX-1000 ADS 1-4 Valve Flow Areas for LOCA							
ADS 1-2 Flow Areas for LOCA (Saturated Steam)							
	Scaling Ratio	AP1000	APEX	Units	AP1000	APEX	Units
ADS 1 Single Valve Effective Flow Area (min)							
ADS 1 Single Valve Effective Throat I.D.							
ADS 1 Two Valves Effective Flow Area (combined)							
ADS 1 Two Valves Effective Throat I.D. (combined)							
ADS 2 Single Valve Effective Flow Area (min)							
ADS 2 Single Valve Effective Throat I.D.							
ADS 2 Two Valves Effective Flow Area (combined)							
ADS 2 Two Valves Effective Throat I.D. combined							
ADS 1-3 Flow Areas Combined (Fluid Property Similitude)							
ADS 1,2,3 Single Train Effective Flow Area (min)							
ADS 1,2,3 Single Train Effective Throat I.D.							
ADS 1,2,3 Two Trains Effective Flow Area (combined)							
ADS 1,2,3 Two Trains Effective Throat I.D. (combined)							
ADS 4 Flow Areas Per Hot Leg (Fluid Property Similitude)							
ADS 4 Single Train (50% Effective Flow Area)							
ADS 4 Single Train Effective Throat I.D.							
ADS 4 Two Trains (100% Effective Flow Area)							
ADS 4 Two Trains Effective Throat I.D. (combined)							

a,b,c

Table 13 Summary of APEX-1000 ADS 1-2 Valve Flow Areas for Inadvertent Opening of ADS							
ADS 1-2 Flow Areas for Inadvertent ADDS O Pen in Transient (Saturated Liquid)							
	Scaling Ratio	AP1000	APEX	Units	AP1000	APEX	Units
ADS 1 Single Valve Effective Flow Area (mini)							
ADS 1 Single Valve Effective Throat I.D.							
ADS 1 Two Valves Effective Flow Area (combined)							
ADS 1 Two Valves Effective Throat I.D. (combined)							
ADS 2 Single Valve Effective Flow Area (min)							
ADS 2 Single Valve Effective Throat I.D.							
ADS 2 Two Valves Effective Flow Area (combined)							
ADS 2 Two Valves Effective Throat I.D. (combined)							

a,b,c

Table 14 APEX-1000 Break and Steam Generator PORV Sizes				
LOCA Flow Areas (Pressure Scaled Two Phase Fluid)				
	Scaling Ratio	AP1000	APEX	Units
2" Cold Leg Break				
Flow area				
Diameter				
Double-Ended DVI Line Break				
DVI Nozzle Flow Area				
Diameter				
Steam Generator PORV Flow Area (Single-Phase Steam)				
*PORV Equivalent Flow Area				
PORV Equivalent Throat Diameter				

a,b,c

*Based on 1.02×10^6 lbm/hr at 1200 psia for AP1000

Table 15 Time Constants and Π Groups for APEX Pressure Scaled LOCAs

	Saturated Vapor Breaks	Saturated Liquid Breaks
$(t/\tau_{RCS})_R$		
$\Pi_{m,R}$		
$\left(\frac{\Pi_h}{\Pi_\epsilon}\right)_R$		
$\left(\frac{\Pi_\Gamma}{\Pi_\epsilon}\right)_R$		
$(\Pi_\epsilon)_R$		

a,b,c

5.7 Summary and Conclusions

This chapter presents the results of the SBLOCA scaling analysis. The goal was to scale the APEX initial conditions and break flow areas such that the RCS depressurization rate and corresponding cooldown rate would be preserved in dimensionless phase space. Two types of break conditions were considered; all saturated vapor at the break, such as the stuck-open ADS 1-3 and an all saturated liquid break, which was the assumed condition for the hot leg break.

The scaling analysis provided the RCS initial conditions and the break flow areas. All of the Π groups, as shown in Table 14, were found to have values on the order of one with the exception of the fluid property group under pressure scaled conditions.

An examination of the Π groups ratios indicates that for saturated vapor breaks (i.e., stuck-open ADS 1-3) the depressurization and cooldown rate will be reasonably simulated in APEX. Some distortion may occur in simulating the hot leg break because conditions at the break will likely be two-phase rather than saturated liquid as assumed in the analysis. The validity of this assumption will depend on whether the injection flows keep the break conditions near the saturated liquid state.

For the conditions of fluid property similitude, all of the P group ratios listed in Table 14 will be one. Thus the full pressure tests that will be performed in APEX to assess the transition from ADS-4 operation to IRWST injection are expected to yield depressurization behavior that is similar to the AP1000. The next chapter presents the scaling analysis for the full pressure ADS-4 blowdown phenomena.

6.0 SCALING ANALYSIS OF THE FULL PRESSURE ADS 4 BLOWDOWN TO IRWST INJECTION TRANSITION PERIOD

The APEX-1000 test facility will be modified to conduct full pressure studies of the thermal hydraulic phenomena that arise during the transition from ADS-4 blowdown to the onset of IRWST injection. This transition period was previously studied under full pressure conditions in the SPES and ROSA-AP600 test facilities. This period was deemed to be very important by analysts because there is a limited amount of liquid available for core cooling while the system depressurizes to the IRWST injection setpoint. Operating the APEX facility under reduced pressure conditions during this phase of a transient results in distorting the conditions at which the IRWST begins to drain.

In the AP1000, IRWST injection would initiate when the primary system pressure drops below ~ 0.198 MPa (28.7 psia), based on the minimum initial IRWST liquid level. At this pressure, the flow at the ADS-4 valves would be still be choked (i.e., essentially single-phase vapor flow) and independent of the ADS-4 line resistance. However, for the 1/4 height IRWST in APEX, the onset of flow would not begin until the primary system pressure dropped below ~ 0.125 MPa (18.2 psia). At this pressure, the ADS-4 flow would be unchoked and therefore the ADS-4 flow rate would be dependent on ADS-4 line resistance.

In an effort to eliminate the ADS-4 flow distortions in APEX during this transition period, a series of full pressure ADS-4 blowdown tests will be performed. This will require configuring APEX to provide pressure control for ADS-4 blowdowns initiating from steady-state conditions, pressuring the IRWST to simulate full height conditions and adjusting the IRWST line resistance to achieve properly scaled injection flow rates under full height IRWST conditions. This section presents the scaling analysis performed to design the ADS-4 blowdown to IRWST injection transition tests.

6.1 Description of the ADS-4 Blowdown to IRWST Injection Thermal Hydraulic Phenomena

Figure 16 presents an overview of the thermal hydraulic phenomena that arises during a typical ADS-4 blowdown. This figure characterizes the phenomena in terms of reactor pressure vessel mixture level (or liquid mass) versus the system pressure. The ADS-4 valves open when the liquid volume in either of the two CMTs drops below 20% of its initial volume. At P_{ADS4} , the pressure at which the ADS-4 valves open, two-phase fluid choke flow will exist at the ADS-4 valves. All of the liquid located above the top of the hot legs, (i.e. the entrance to the ADS-4 line), will eventually be swept out of the ADS-4 valves. The amount of liquid located above the hot legs is dependent on the amount of level swell in the core. When the fluid mixture level drops below the top of the hot legs, the flow out of the ADS-4 valves can be best described as a high quality vapor choke flow. Liquid boil-off in the core, liquid flashing to vapor and liquid carryover from the upper plenum will act to reduce the liquid inventory in the reactor pressure vessel. Because there are no other sources of liquid during this phase of the transient, primary system pressure must drop below the IRWST liquid level head pressure, P_{IRWST} , before the RPV mixture level reaches the top of the core. When the primary system pressure drops below P_{IRWST} , less some small check valve cracking pressure, IRWST will liquid flow will act to reflood the RPV.

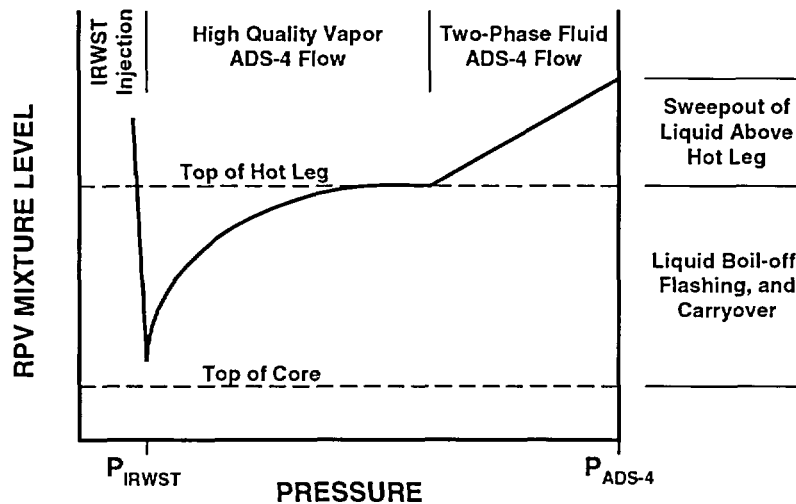


Figure 16 Description of the Transition from ADS-4 Blowdown to the Onset of IRWST Injection

Figure 17 shows how the thermal hydraulic phenomena described in this section have been addressed in the top-down and bottom-up scaling analyses. First a top-down scaling analysis was performed to obtain a single governing equation in terms of dP^*/dM^* . Next, a bottom-up scaling analysis was performed to describe the local thermal hydraulic processes, including critical flow, core fluid boil-off, and core mixture level swell.

6.2 Top-Down RCS Depressurization and Mass Inventory Scaling Analysis (Pressure Similitude)

The mass balance equation and the depressurization rate equation developed in Chapter 5 are directly applicable to this analysis. However, the initial conditions and the processes to be examined are specific to the transition period from ADS-4 blowdown to IRWST injection under full pressure conditions. The objective of this analysis is to develop the criteria for preserving the AP1000 depressurization and mass inventory behavior for the transition period as described in dimensionless phase space (M^* , P^*).

The following mass balance equation was developed for the RCS in section 5.2.

$$\frac{dM}{dt} = \sum \dot{m}_{in} - \sum \dot{m}_{out} \quad (134)$$

During the ADS-4/IRWST transition period, there will be no sources of liquid injection, therefore, the first term on the RHS of equation (134) can be deleted. Furthermore, the only vent paths to be considered in this analysis shall be the ADS-4 valves.

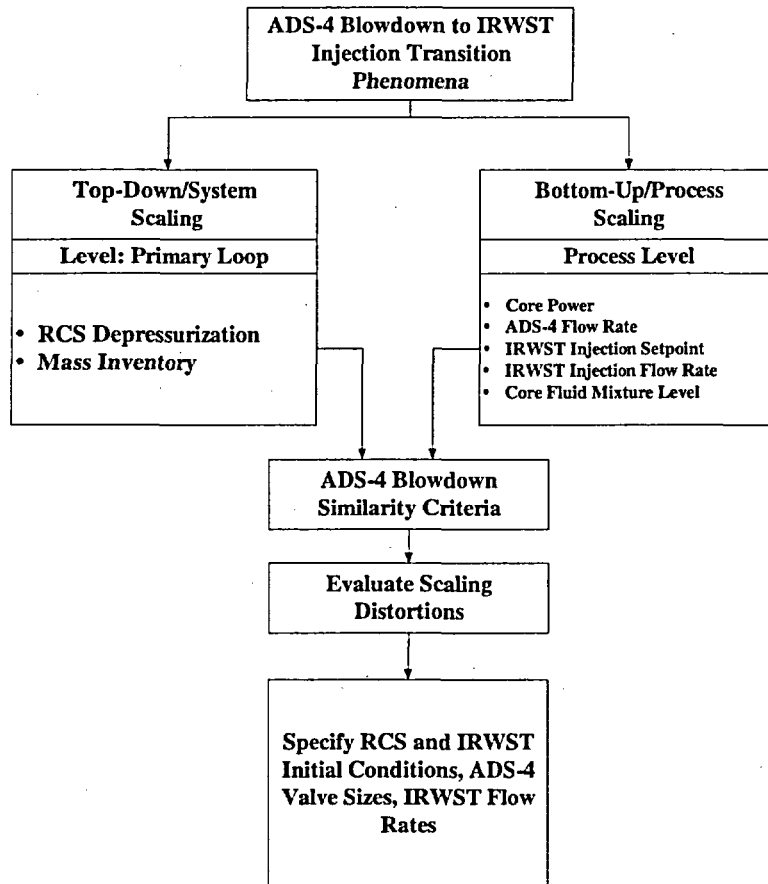


Figure 17 Scaling Analysis Flow Chart for the Full Pressure ADS-4 Blowdown Experiments

Applying these assumptions results in the following equation:

$$\frac{dM}{dt} = - \dot{m}_{ADS4} \quad (135)$$

The following depressurization rate equation was also developed for the RCS in section 5.2.

$$M \left(\frac{\partial e}{\partial P} \right)_v \frac{dP}{dt} = (\sum \dot{m}_{in}) \left[h_{in} - e + v \left(\frac{\partial e}{\partial v} \right)_p \right] - (\sum \dot{m}_{out}) \left[h_{out} - e + v \left(\frac{\partial e}{\partial v} \right)_p \right] + q_{SG} + q_{core} + q_{loss} \quad (136)$$

During the ADS-4/IRWST transition period, the steam generators will be isolated. Therefore, the q_{SG} term can be deleted. The heat loss will be negligible compared to the core decay heat. Therefore, the q_{loss} term can also be neglected. Applying these assumptions and those for the mass balance equation yields:

$$M \left(\frac{\partial e}{\partial P} \right)_v \frac{dP}{dt} = - \dot{m}_{ADS4} \left[h_{ADS4} - e + v \left(\frac{\partial e}{\partial v} \right)_p \right] + q_{core} \quad (137)$$

It is noted that the key behavior of interest to the transition period can be described in terms of system pressure versus RCS mass inventory (or RPV mixture level) as shown in Figure 20. The process could also be described in terms of two time scales. The first is the time required for the RCS to depressurize from P_{ADS4} to P_{IRWST} . The second is the time required to deplete the RCS mass inventory from its initial condition $M_{RCS,o}$ to its final mass inventory state which may or may not be sufficient to keep the core covered. However, rather than working with time scales, a departure from previous analyses, the present analysis was simplified by developing a single governing equation in terms of RCS mass and pressure. This was done by dividing equation (137) by the mass balance equation (135). The result is:

$$M \left(\frac{\partial e}{\partial P} \right)_v \frac{dP}{dM} = \left[h_{ADS4} - e + v \left(\frac{\partial e}{\partial v} \right)_p \right] - \frac{q_{core}}{\dot{m}_{ADS4}} \quad (138)$$

This equation can be expressed in non-dimensional form by dividing each term by its respective initial conditions. The normalized terms are as follows:

$$M = M_{RCS,o} M^+ \quad (139)$$

$$P = P_{RCS,o} P^+ \quad (140)$$

$$q_{core} = q_{core,o} q_{core}^+ \quad (141)$$

$$\dot{m}_{ADS4} = \dot{m}_{ADS4,o} \dot{m}_{ADS4}^+ \quad (142)$$

$$\left(\frac{\partial e}{\partial P} \right)_v = \left(\frac{\partial e}{\partial P} \right)_{v,o} \left(\frac{\partial e}{\partial P} \right)_v^+ \quad (143)$$

$$\left[h_{ADS4} - e + v \left(\frac{\partial e}{\partial v} \right)_p \right] = \left[h_{ADS4} - e + v \left(\frac{\partial e}{\partial v} \right)_p \right]_o \left[h_{ADS4} - e + v \left(\frac{\partial e}{\partial v} \right)_p \right]^+ \quad (144)$$

Substituting these dimensionless initial conditions into (138) and dividing through by $P_o \left(\frac{\partial e}{\partial P} \right)_{v,o}$ yields the non-dimensional governing equation:

$$\left(\frac{\partial e}{\partial P} \right)_v^+ \frac{dP^+}{dM^+} = \frac{1}{\Pi_\epsilon} \left[h_{\text{ADS4}} - e + v \left(\frac{\partial e}{\partial v} \right)_P \right]_o - \frac{\Pi_\Gamma}{\Pi_\epsilon} \left(\frac{q_{\text{core}}}{\dot{m}_{\text{ADS4}}} \right)_o \quad (145)$$

where the dimensionless property group Π_ϵ is given as in the previous chapter as:

$$\Pi_\epsilon = \frac{P_o \left(\frac{\partial e}{\partial P} \right)_{v,o}}{\left[h_{\text{ADS4}} - e + v \left(\frac{\partial e}{\partial v} \right)_P \right]_o} \quad (146)$$

and the power to energy flow rate ratio is:

$$\Pi_\Gamma = \frac{q_{\text{core},o}}{\dot{m}_{\text{ADS4},o} \left[h_{\text{ADS4}} - e + v \left(\frac{\partial e}{\partial v} \right)_P \right]_o} \quad (147)$$

Hence to simulate the transition behavior in APEX-1000, the dimensionless groups defined in equations (146) and (147) must be preserved. For the full pressure conditions proposed for the ADS4 blowdown test series, fluid property similitude reduces the ratio of these groups to:

$$\Pi_{\epsilon,R} = 1 \quad (148)$$

and

$$\Pi_{\Gamma,R} = \left(\frac{q_{\text{core},o}}{\dot{m}_{\text{ADS4},o}} \right)_R \quad (149)$$

The property group, Π_ϵ in AP1000 and APEX-1000 are identical and therefore the similarity criterion is automatically satisfied.

6.3 Bottom-Up Scaling Analysis

This section describes the scaling analyses performed for the ADS-4 Blowdown/IRWST transition phenomena. The core power and the ADS-4 choked flow rate behavior have already been assessed in Chapter 5. The core power has been scaled as 1:96. Similarly, when fluid property similitude exists, the choked flow conditions at the ADS-4 valves are preserved and the mass flow rate is scaled at 1:96 because the ADS-4 flow areas have been scaled by 1:96. Thus, equation (149) becomes:

$$\Pi_{\Gamma,R} = 1 \quad (150)$$

which indicates that this dimensionless group will also be preserved in APEX-1000.

6.3.1 Flashing and Liquid Boil-off Rate

The flashing phenomena is automatically preserved by establishing the initial pressure and subcooling conditions in APEX as those in the AP1000 for the ADS-4 blowdown phase.

The liquid mass boil-off rate in the core, under steady-state conditions is described as follows:

$$\dot{m}_{\text{Boil-off}} = \frac{q_{\text{core}}}{h_{fg} + h_{\text{subcooled}}} \quad (151)$$

For fluid property similitude, the ratio of this equation (i.e., APEX to AP1000) becomes:

$$\dot{m}_{\text{Boil-off,R}} = q_{\text{core,R}} = \frac{1}{96} \quad (152)$$

which is the required value to preserve the one-half time scale requirement. However, it is noted that the volume of the APEX downcomer is large on a scaled basis. Of particular interest to the full pressure ADS-4 blowdown tests is the downcomer volume between the bottom of the cold leg and the top of the heated fuel elevation. This region represents a source of liquid that resides in the downcomer at an elevation above the top of the heated fuel. For APEX, this region has a length of 0.5 m (1.64 ft) and a corresponding volume of 0.057 m³ (2.02 ft³). For AP1000, this region has a length of 2.0 m (6.53 ft) and a volume of 5.73 m³ (202.2 ft³). The length scale ratio is 1:4 as desired. However, the volume scale ratio is 1:100 which is approximately 2 times the desired value of 1:192.

At a system pressure of 0.69 MPa (100 psia), the amount of saturated liquid mass that could be contained in this region for AP1000 would be 5172 kg (11,402 lbm). For the similar region in APEX, this corresponds to 51.6 kg (113.7 lbm).

During the transition period of the ADS-4 blowdown, the primary source of water will be the 20% liquid volume remaining in the CMT. For the fluid conditions stated earlier, this corresponds to a volume of 14.2 m³ (500 ft³) in AP1000 and 0.0742 m³ (2.62 ft³) in APEX-1000. It is desired that a 1:2 boil-off time scale be simulated. Therefore the following scaling criterion must be preserved:

$$\tau_{\text{Boil-off,R}} = \left(\frac{\rho_f (V_{\text{CMT}} + V_{\text{DC}})(h_{fg} + h_{\text{subcooled}})}{q_{\text{core}}} \right)_R = 0.5 \quad (153)$$

For the case of fluid property similitude and a fixed core power ratio, this criterion becomes:

$$(V_{\text{CMT}} + V_{\text{DC}})_R = \frac{1}{192} \quad (154)$$

Because the downcomer volume in APEX is oversized, this criterion can be satisfied by initiating the ADS-4 blowdown in APEX with a reduced liquid inventory in the CMT. Starting the ADS-4 blowdown with a 12.5% volume rather than a 20% volume would satisfy this requirement.

6.3.2 IRWST Full Height Liquid Head and Injection Flow Rate

Simulating the full pressure ADS-4 blowdown transition in APEX will require a full height liquid head in the IRWST. This will be achieved by pressurizing the APEX IRWST to a pressure of ~10.8 psig to simulate full height AP1000 conditions. Similarly, the IRWST line resistance shall be increased such that the initial IRWST mass flow rate at the simulated full height conditions is 1:96. Flow tests shall be performed to fine tune the IRWST line resistance.

6.3.3 Core Fluid Mixture Level Swell

The initial liquid mass distribution in the RCS will determine the conditions at which the hot leg uncovers. As shown in Figure 20, when the hot leg uncovers, the ADS-4 flow transitions from two-phase choked flow to essentially single-phase vapor choked flow. This choked flow transition is important because the RCS depressurization rate will depend on the type of choked flow conditions at the ADS-4 valves.

Properly modeling the initial RCS liquid mass distribution requires preserving the core fluid mixture level swell. The equation for level swell is given by:

$$H_{\text{mix}} = \frac{H_{\text{collapsed}}}{1 - \langle \alpha_c \rangle} \quad (155)$$

where H_{mix} is the fluid mixture level, $H_{\text{collapsed}}$ is the collapsed liquid level and $\langle \alpha_c \rangle$ is the average core void fraction. To preserve the level swell in the core, the following similarity criterion must be preserved:

$$\left(\frac{H_{\text{collapsed}}}{H_{\text{mix}}} \right)_R = (1 - \langle \alpha_c \rangle)_R \quad (156)$$

which implies that the average core void fraction ratio must also be preserved. That is;

$$\langle \alpha_c \rangle_R = 1 \quad (157)$$

The void fraction as a function of position in the core was obtained using the drift-flux relationship.¹⁸ :

$$\alpha(z) = \frac{j_g(z)}{C_o j(z) + V_{gj}} \quad (158)$$

At stagnant loop conditions, j_c is zero, so equation (158) becomes:

$$\alpha(z) = \left[C_o + \frac{V_{gj}}{j_g(z)} \right]^{-1} \quad (159)$$

The volumetric vapor flux, j_g , was found using the following relation:

$$j_g(z) = \frac{1}{\rho_g a_c h_{fg} L_{NB}} \int_{L_{NB}}^z q'(z) dz \quad (160)$$

where L_{NB} is the non-boiling height. The core averaged void fraction, $\langle \alpha_c \rangle$, was obtained by integration as follows:

$$\langle \alpha_c \rangle = \frac{1}{L_c} \int_{L_{NB}}^{L_c} \alpha(z) dz \quad (161)$$

APEX-1000 will implement a constant axial power profile. Therefore equation (158) is given by:

$$j_g(z) = \frac{q_{core} (z - L_{NB})}{\rho_g a_c h_{fg} L_c} \quad (162)$$

Substituting equations (157) and (160) into (159) yields the core averaged void fraction for constant axial power:

$$\langle \alpha_c \rangle = \frac{1}{C_o} \left[1 - \frac{L_2}{C_o \Pi_z (L_c - L_{NB})} \text{Ln} \left(1 + \frac{C_o \Pi_z (L_c - L_{NB})}{L_c} \right) \right] \quad (163)$$

where Π_{zuber} is the Zuber number, rearranged as:

$$\Pi_{zuber} = \frac{q_{core}}{\rho_g v_{gj} a_c h_{fg}} \quad (164)$$

The AP1000 is assumed to have a chopped cosine shape axial power profile defined as follows.

$$q(z) = \int_{-L_c/2}^z q'_c \cos\left(\frac{\pi z}{L_c}\right) dz \tag{165}$$

Integrating equation (163) yields:

$$q(z) = q'_c \frac{L_c}{\pi} \left[1 + \sin\left(\frac{\pi z}{L_c}\right) \right] \tag{166}$$

Substituting equation (164) into equations (158) yields:

$$j_g(z) = \frac{q'_c L_c}{\pi \rho_g a_c h_{fg}} \left[1 + \sin\left(\frac{\pi z}{L_c}\right) \right] \tag{167}$$

Equation (165) was substituted into (159) and numerically integrated to obtain the core averaged void fraction for the AP1000. The churn-turbulent drift-flux correlation was used to assess equation (157) for both APEX and AP1000. That is,

$$v_{gj} = 1.53 \left[\frac{\sigma g \Delta \rho}{\rho_{\text{liquid}}^2} \right]^{1/4} \tag{168}$$

Table 16 presents the data used to calculate the core average void fraction for the case of an ADS-4 blowdown from 0.69 MPa (100 psia) and a decay heat of 2.08%. The core averaged void fraction was found to be 57% for APEX and 60% for AP1000.

Parameter	AP1000	APEX-1000	Units
Core Flow Area (a_c)			
Core Heated Length			
Power (2.1% Decay)			
Average Linear Power at Decay Heat			
Pressure			
ρ_g			
P_l			
σ			
H_g			
H_L			
$C_o =$			
$v_{gi} =$			
$\langle \alpha_c \rangle =$			

Figure 18 compares the axial void fraction profiles in AP1000 and APEX-1000 for an average subchannel for this ADS-4 blowdown case. The difference in void fraction profiles arises because the power profiles have different shapes. The core exit void fractions were calculated to be 73% and 71% for AP1000 and APEX respectively.

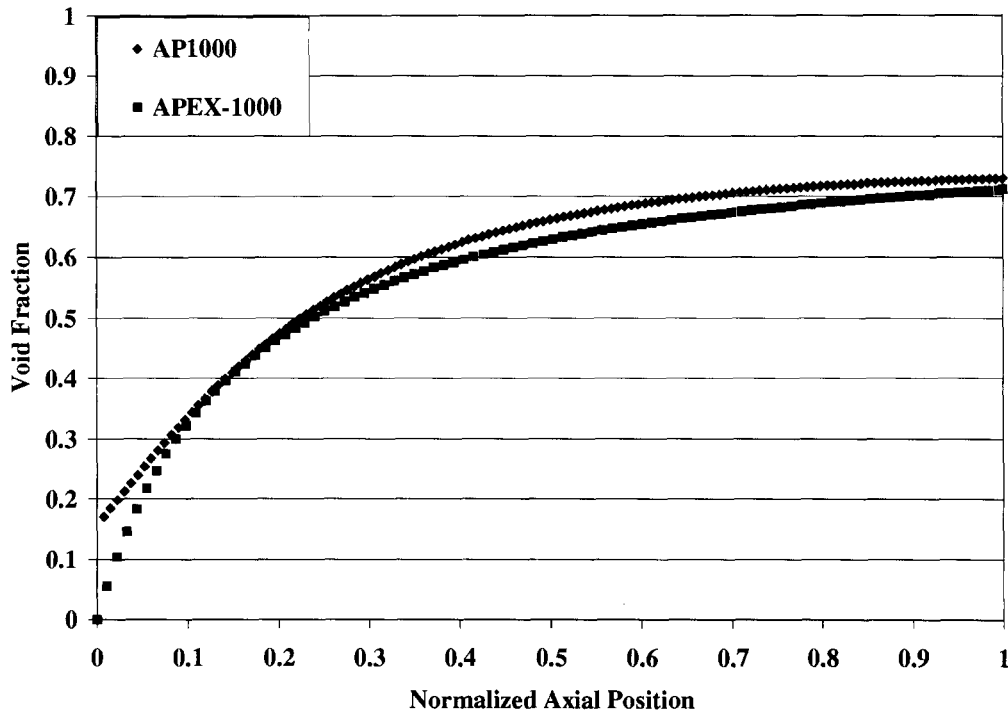


Figure 18 Comparison of AP1000 and APEX Axial Void Fraction Profiles for an Average Subchannel

6.3.4 Initial Conditions for the Full Pressure ADS-4 Blowdown Tests

The following table presents the initial conditions for a full pressure ADS-4 test in APEX-1000. The test shall be initiated from steady-state conditions. The decay power and system pressure was selected based on the results of Chapter 15 of the AP1000 Safety Analysis Report. The highest decay power observed while actuating ADS-4 was ~2.0% for the DEDVI case. The typical pressure at which ADS-4 actuates is 0.69 MPa (100 psia).

Table 17 Proposed Initial Conditions for a Full Pressure ADS-4 Blowdown Test In APEX-1000

Parameter	AP1000	APEX-1000	Units
RCS Pressure			
2% Core Decay Power			
Initial CMT Volume			
ADS-4 Flow Areas – 100%			
ADS-4 Flow Areas – 50%			
IRWST Nominal Liquid Level			
IRWST Head Pressure			

a,b,c

7.0 UPPER PLENUM ENTRAINMENT SCALING ANALYSIS

Top-down component level and bottom-up process level scaling analyses have been performed to establish the upper plenum geometry and flow conditions that should be modeled in the APEX-1000 integral system test facility. Figure 19 describes the scaling analysis process.

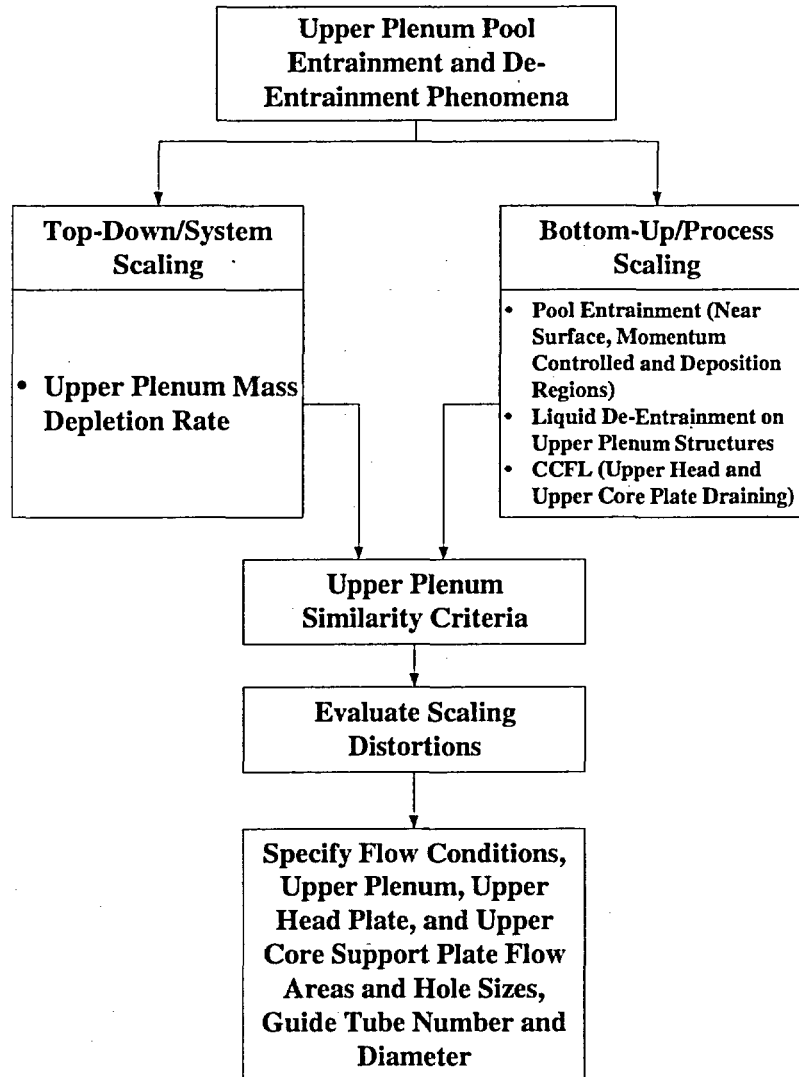


Figure 19 Upper Plenum Scaling Analysis Flow Chart

The main objective of the analysis was to obtain the scaling ratios that would preserve, on a scaled basis, the rate at which the liquid level in the upper plenum decreases during pool boiling. The top-down scaling analysis resulted in a non-dimensional mass balance equation for the upper plenum control volume. The bottom-up scaling analysis provided the closure relationships for the top-down analysis. In particular, pool boiling entrainment was examined for the near-surface, momentum dominated and deposition regions of the upper plenum.

7.1 Top-Down Scaling Analysis

The control volume shown in Figure 20 was defined for the Upper Plenum for the purpose of writing the mass balance equation.

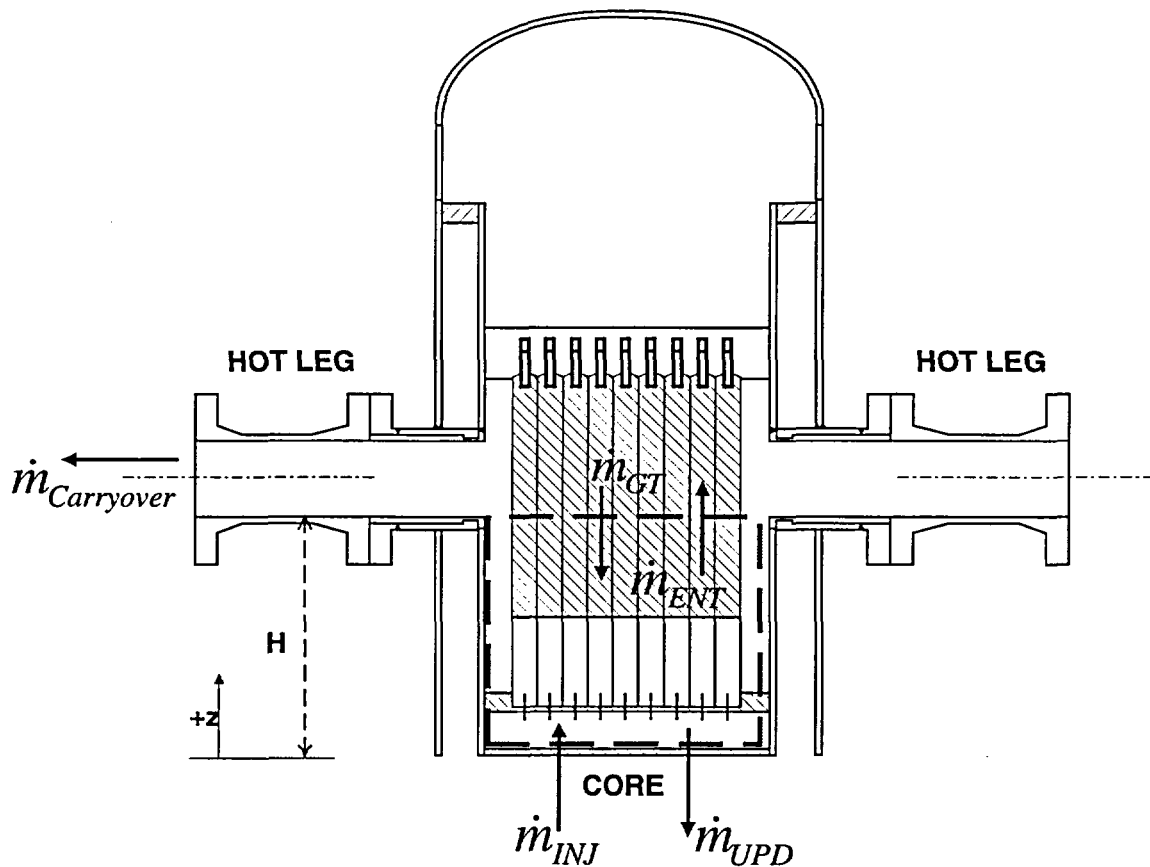


Figure 20 Upper Plenum Control Volume Located Below the Hot Legs

The liquid mass conservation equation for the upper plenum is written as follows:

$$\frac{dM_{UP}}{dt} = \dot{m}_{IN} - \dot{m}_{OUT} \quad (169)$$

The Upper Plenum flow cross-sectional area, a_{UP} , is constant inside the control volume and the liquid is assumed to be incompressible, therefore liquid density ρ_L is uniform and constant. The vertical upward direction is defined as the z -coordinate. Thus, removing the constants from the derivative on the left hand side of equation (169) yields:

$$a_{UP}\rho_L \frac{dz}{dt} = \dot{m}_{IN} - \dot{m}_{OUT} \quad (170)$$

One source of liquid to the control volume is liquid mass flow from the core region due to safety injection. During the later part of ADS-4 operation, IRWST injection would be supplying liquid to the core. A second source of liquid to the upper plenum is de-entrainment on the vertical guide tubes. A third source of liquid mass into the control volume is draining from the upper head through the upper support plate.

The primary path of liquid mass loss from the upper plenum is through the hot leg. When the liquid level is below the bottom of the hot leg, pool entrainment results, causing liquid droplets to be carried with the steam out the hot leg to the ADS 4 line. Another source of mass loss is due to draining from the upper plenum through the upper core plate back into the core. Loss of upper plenum liquid mass due to flashing or boiling due to stored energy release from upper plenum structures are not considered applicable during this phase of the transient. Equations for the liquid mass loss and injection terms are presented in the bottom-up scaling analysis.

Expanding equation (170) to include the individual liquid mass source and sink terms yields:

$$a_{UP} \rho_L \frac{dz}{dt} = \dot{m}_{INJ} + \dot{m}_{GT} - \dot{m}_{ENT} - \dot{m}_{UPD} \quad (171)$$

The first term on the RHS represents the sum of the DVI injection flows that tend to fill the upper plenum via the downcomer (i.e., CMT, Accumulator, IRWST, and Sump flows). It is the mass flow rate of liquid entering the control volume through the core. The second term on the RHS represents the guide tube de-entrainment rate. It is the mass flow rate of liquid that is de-entrained by the upper plenum structure and that eventually drains as a liquid film into the control volume. The third term on the right hand side is the liquid entrainment rate. It is the mass flow rate of liquid produced by the vapor interaction with the liquid (i.e., near surface, momentum controlled or deposition pool entrainment). This liquid is carried out of the control volume where a portion is de-entrained by the guide tubes and the remainder is carried out to the hot leg. The last term on the RHS represents mass flow rate of liquid that drains out of the control volume by gravity through the upper core plate back into the core region.

7.1.1 Dimensionless Liquid Mass Balance

Equation (171) can be made dimensionless using the following initial and boundary conditions:

$$z_{INJ}^+ = \frac{z}{H} \quad (172)$$

where H is the vertical length between the top of the core and the bottom of the Hot Leg. The dimensionless injection mass flow rate is given as:

$$\dot{m}_{INJ}^+ = \frac{\dot{m}_{INJ}}{\dot{m}_{INJ,0}} \quad (173)$$

The dimensionless guide tube de-entrainment rate is given as:

$$\dot{m}_{GT}^+ = \frac{\dot{m}_{GT}}{\dot{m}_{GT,O}} \quad (174)$$

The dimensionless liquid entrainment rate is given as:

$$\dot{m}_{ENT}^+ = \frac{\dot{m}_{ENT}}{\dot{m}_{ENT,O}} \quad (175)$$

The dimensionless upper plenum draining rate is given as:

$$\dot{m}_{UPD}^+ = \frac{\dot{m}_{UPD}}{\dot{m}_{UPD,O}} \quad (176)$$

Substituting these ratios into equation (171) and dividing both sides of the equation by the initial entrainment mass flow rate yields the dimensionless mass balance equation for the upper plenum liquid.

$$\tau_{ENT} \frac{dz^+}{dt} = \Pi_{INJ} \dot{m}_{INJ}^+ + \Pi_{GT} \dot{m}_{GT}^+ - \dot{m}_{ENT}^+ - \Pi_{UPD} \dot{m}_{UPD}^+ \quad (177)$$

In this equation, the liquid entrainment reference time scale has been defined as:

$$\tau_{ENT} = \frac{a_{UP} \rho_L H}{\dot{m}_{ENT,O}} \quad (178)$$

Thus the dimensionless time coordinate for upper plenum emptying due to liquid entrainment is given by:

$$t^+ = \frac{t}{\tau_{ENT}} \quad (179)$$

All of the remaining filling and draining processes are therefore expressed in terms of the liquid entrainment process. That is, the dimensionless P groups of equation (177) are written as:

$$\Pi_{INJ} = \frac{\dot{m}_{INJ,O}}{\dot{m}_{ENT,O}} \quad (180)$$

$$\Pi_{GT} = \frac{\dot{m}_{GT,O}}{\dot{m}_{ENT,O}} \quad (181)$$

$$\Pi_{UPD} = \frac{\dot{m}_{UPD,O}}{\dot{m}_{ENT,O}} \quad (182)$$

Equations (178) through (182) will be evaluated in the bottom-up scaling analysis.

7.1.2 Preserving the Upper Plenum Draining Rate During Integral System Testing

The desired outcome of this scaling analysis is to establish the geometry and flow conditions in APEX that would preserve the upper plenum draining rate when plotted in dimensionless phase space. That is, plotting the upper plenum liquid level history in terms of the dimensionless spatial coordinate, z^+ , and the dimensionless time coordinate t^+ would yield overlaying curves for the model and the prototype. This condition can be achieved by satisfying the following requirements:

1. The scenarios are initiated from the same initial condition in dimensionless phase space. In this case, z^+ at $t^+ = 0$ is 1.
2. The rate of change (i.e., slope) is preserved in dimensionless phase space. This imposes the following scaling criterion:

$$\left(\frac{dz^+}{dt^+} \right)_R = 1 \quad (183)$$

Note that $(z^+)_R$ and $(t^+)_R$ are unity. Satisfying the requirement given by equation (183) can only be accomplished by preserving the ratios of the individual P groups on the right hand side of equation (177). The APEX facility transient response was originally designed to operate at one-half time scale ($t_R = 0.5$) which means that the reference time scale ratio, τ_R , must also be one-half to keep $(t^+)_R$ at unity. Because the APEX facility height is fixed at one-fourth scale, and the flow area is roughly fixed at 1:48 certain physical limitations have already been established. Nonetheless, minor modifications to the upper plenum structures are possible. To preserve the one-half scale timing of integral system transient behavior, it is desired that:

$$\left(\frac{dz}{dt} \right)_R = \frac{1}{2} \quad (184)$$

Substituting equations (172) and (179) into (184) yields:

$$\left(\frac{H}{\tau_{ENT}} \right)_R \left(\frac{dz^+}{dt^+} \right)_R = \frac{1}{2} \quad (185)$$

Imposing the requirement given by equation (183) yields:

$$\left(\frac{H}{\tau_{ENT}} \right)_R = \frac{1}{2} \quad (186)$$

This is a direct result of the one-half time scale requirement. Substituting equation (178), assuming fluid property similitude and rearranging yields the following simple scaling criterion for the upper plenum:

$$\left(\frac{\dot{m}_{ENT,O}}{a_{UP}} \right)_R = \frac{1}{2} \quad (187)$$

For the case where liquid entrainment is the dominant mechanism (i.e., the largest mass transfer term on the right hand side of the balance equation) then equation (187) coupled with a correlation for liquid entrainment represents the governing scaling criterion. The next section presents the bottom-up scaling analysis and includes liquid entrainment equations that can be used to provide closure to equation (187).

7.2 Bottom-up Scaling Analysis

This section examines the various upper plenum filling and draining mechanisms. This includes:

- Pool Entrainment
- Guide Tube De-entrainment
- The effects of Counter-Current Flow Limitations (CCFL) on Upper Plenum Draining

The phenomenon of interest to this study is upper plenum pool entrainment. The following section presents a review of the phenomenon and the existing predictive models.

7.2.1 Pool Entrainment

The basic equations of pool entrainment will be derived to provide a theoretical context for their application to the scaling analysis. Here the discussion will consist of a brief derivation of Ishii's pool entrainment equations. Following this derivation, certain questions regarding the application of these equations in scaling the AP1000 experiments will be addressed. In particular, it will be necessary to examine the vertical extent of various entrainment regions, the flow regime in the pool, the question of flooding, the phenomena of re-entrainment from a falling film, and the issue of enhanced deposition due to the lateral motion of the flow.

In Ishii's pool entrainment model, the entrainment is defined as the ratio of the droplet to vapor mass flux, and represented phenomenologically by the following equation:⁸

$$E_{fg}(h, j_g) = \frac{\rho_f j_f}{\rho_g j_g} = \frac{\dot{\epsilon}(j_g)}{\rho_g j_g} \int_0^{D_{max}} f_D(D, j_g) \int_{v_n}^{\infty} g(v_i, D, j_g) dv_i dD \quad (188)$$

Here $\dot{\epsilon}$ is the mass flux of droplets at the liquid surface which is a function of the vapor superficial velocity j_g . As the droplets generated at the surface vary in size from zero to some maximum diameter, a distribution function for the droplet diameters is employed. This function f_D gives the fraction of droplets within any given range dD and is itself a function of j_g . Obviously, since all the droplets must fall within the range $0 \leq D \leq D_{max}$,

$$\int_0^{D_{max}} f_D(D, j_g) dD = 1 \quad (189)$$

Furthermore, the droplets so generated will have an initial velocity v_i which depends upon both the superficial velocity j_g and the droplet diameter D . Hence, a distribution function g is needed for the initial velocity such that:

$$\int_0^{\infty} g(v_i, D, j_g) dv_i = 1 \quad (190)$$

As written, equation (189) depends upon the maximum droplet diameter to define an upper limit of integration. By using the pool entrainment data to determine various experimental constants, Ishii found the best agreement for

$$D_{\max}^* = 7.24 j_g^{*-1} \quad (191)$$

In this equation the asterisk denotes a dimensionless variable such that

$$D^* = \frac{D}{\sqrt{\frac{\sigma}{g \Delta \rho}}} \quad (192)$$

and

$$j_g^* = \frac{j_g}{\left[\frac{\sigma g \Delta \rho}{\rho_g^2} \right]^{1/4}} \quad (193)$$

With regard to the second integral in equation (188), the lower limit v_h is the minimum initial velocity required for a droplet of diameter D to reach height h . With regard to its dependence on the droplet diameter, $v_h = 0$ for droplets in the range $0 \leq D \leq D_c$, where the critical diameter D_c is the diameter of the largest droplet which can be suspended by vapor drag. Thus the droplets within this range can reach height h by virtue of drag alone and hence need no initial velocity. On the other hand, droplets in the range $D_c < D \leq D_{\max}$ are too large to be suspended by vapor drag and hence fall back into the pool after losing their initial momentum. Consequently, these droplets must possess a minimal initial velocity v_h to reach the height in question.

With regard to these calculations, the critical droplet diameter D_c is first obtained by balancing the weight of the droplet with the vapor drag

$$g \Delta \rho \pi \frac{D_c^3}{6} = \pi \frac{D_c^2}{4} C_D \frac{1}{2} \rho_g j_g^2 \quad (194)$$

where

$$C_D = \frac{10.76}{Re^{1/2}} \quad (195)$$

Solving equation (194) for the critical diameter subject to the drag relation given by equation (195) yields

$$D_c^* = 4 j_g^* (N_{\mu_g})^{1/3} \quad (196)$$

where the viscosity number is given by:

$$N_{\mu_g} = \frac{\mu_g}{(\rho_g \sigma \sqrt{\sigma/g \Delta \rho})^{1/2}} \quad (197)$$

As mentioned above $v_h = 0$ for diameters within the range $0 \leq D \leq D_c$. For diameters within the range $D_c < D \leq D_{max}$, v_h is determined by neglecting drag compared to gravity and calculating the velocity needed to reach height h .

$$v_h = \sqrt{2gh \frac{\Delta \rho}{\rho_f}}; \text{ for } D_c < D \leq D_{max} \quad (198)$$

Thus, in terms of dimensionless parameters

$$v_h^* = 0; \text{ for } 0 \leq D^* \leq D_c^* \quad (199)$$

and

$$v_h^* = \sqrt{2h^*} \left[\frac{\rho_g}{\rho_f} \right]^{1/2}; \text{ for } D_c^* < D^* \leq D_{max}^* \quad (200)$$

Having discussed the basic equation and the limits of integration, it remains to determine expressions for the surface mass flux $\dot{\epsilon}$, the diameter distribution function f_D , and the velocity distribution function g . To this end observe first of all that near the water surface v_h goes to zero for all droplet diameters in accordance with equations (199) and (200). Hence, by virtue of equations (188), (189), and (190)

$$E_{fg}(0, j_g) = \frac{\dot{\epsilon}(j_g)}{\rho_g j_g} \int_0^{D_{max}^*} f_D(D, j_g) \int_0^\infty g(v_i, D, j_g) dv_i dD = \frac{\dot{\epsilon}(j_g)}{\rho_g j_g} \quad (201)$$

Using the limited data available for near surface entrainment, Ishii determined that⁸

$$E_{fg}(0, j_g) = \frac{\dot{\epsilon}(j_g)}{\rho_g j_g} = 4.84 \times 10^{-3} \left[\frac{\rho_g}{\Delta \rho} \right]^{-1.0} \quad (202)$$

Thus

$$\dot{\epsilon}(j_g) = 4.84 \times 10^{-3} \rho_g j_g \left[\frac{\rho_g}{\Delta \rho} \right]^{-1.0} \quad (203)$$

To determine the distribution function f_D , observe that after the droplets in the supercritical range have fallen back into the pool, one is left with droplets in the subcritical range. Since these droplets are sufficiently small to be suspended by vapor drag, they do not fall back into the pool. Consequently, the entrainment above a certain height remains constant except for the phenomenon of deposition on solid surfaces. Moreover, since these droplets are in the range $0 \leq D \leq D_c$, $v_b = 0$ by virtue of equation (199), and equation (188) can be integrated for a subrange of droplet sizes subject to equation (190) to yield:

$$\frac{\dot{\epsilon}(j_g)}{\rho_g j_g} \int_0^D f_D(D, j_g) \int_0^\infty g(v_i, D, j_g) dv_i dD = \frac{\dot{\epsilon}(j_g)}{\rho_g j_g} \int_0^D f_D(D, j_g) dD \quad (204)$$

Now on the basis of experimental data, it has been determined that

$$\frac{\dot{\epsilon}(j_g)}{\rho_g j_g} \int_0^D f_D(D, j_g) dD = C(D^*)^{1.5} (j_g^*)^{1.5} \quad (205)$$

By differentiating this equation with respect to D , one obtains

$$\frac{\dot{\epsilon}(j_g)}{\rho_g j_g} f_D(D, j_g) = \frac{1.5C}{\sqrt{\sigma/g \Delta \rho}} (D^*)^{0.5} (j_g^*)^{1.5} \quad (206)$$

By comparing to the experimental data, and utilizing equation (203), Ishii obtained

$$f_D(D, j_g) = \frac{0.077}{\sqrt{\sigma/g \Delta \rho}} (D^*)^{0.5} (j_g^*)^{1.5} \quad (207)$$

To obtain the velocity distribution function, Ishii first made a rough model based on the breakup of liquid ligaments to determine the initial velocity of a droplet of diameter D in a vapor stream of superficial velocity j_g . Such a breakup mechanism is consistent only with churn flow in the pool and is therefore inapplicable for pools in the bubbly or annular flow regimes. Accordingly, Ishii's entire model is limited to situations where there is churn flow in the pool because the initial velocity distribution derived from this assumption impacts all the subsequent correlations. With respect to this initial velocity, Ishii set up a rough equation based on the above mechanism and utilized experimental data to obtain:⁸

$$v_i^* = 75.17 j_g^{*1/4} N_{\rho_g}^{1/4} D^{*-1/4} \left[\frac{\rho_g}{\rho_f} \right]^{1/2} D_H^{*0.21} \left[\frac{\rho_g}{\Delta \rho} \right]^{0.115} \quad (208)$$

Moreover, since no information was available on the distribution of initial velocities, Ishii assumed that a single initial velocity characterizes a droplet of a given size D such that the distribution reduces to a delta function.

$$g(v_i, D, j_g) = \delta \left(v_i - 75.17 j_g^*{}^{1/4} N_{\mu_g}^{1/4} D^{-1/4} \left[\frac{\rho_g}{\rho_f} \right]^{1/2} D_H^{*0.21} \left[\frac{\rho_g}{\Delta\rho} \right]^{0.115} \right) \quad (209)$$

Having determined expressions for all parameters in equation (188), the entrainment as a function of height can now be determined. To this end, observe from equation (208) that the initial velocity of a given droplet decreases with increasing size. Nevertheless, since there is a maximum droplet size, even the heaviest droplets will possess a minimal initial velocity and thus will rise a definite height before falling back into the pool. Thus, there will be no fall out before a minimum height is attained so that there will be a near surface region where the entrainment is constant. Above this height entrainment will decrease as first the heavier and then the lighter droplets within the supercritical range fall back into the pool. This second region is therefore called the momentum controlled region because the entrainment at any given height is dependent upon the droplets having sufficient initial momentum to reach the height in question. Finally, after all the supercritical droplets have fallen out of the flow, the entrainment will consist only of those droplets small enough to be suspended by the vapor drag. Thus, above a certain height the droplets quit falling back into the pool and are taken out of the flow entirely as a result of deposition on solid surfaces. For this reason the third region is referred to as the deposition controlled region.

The extent of the near surface region can be determined by setting the initial velocity of the largest droplets equal to the initial velocity v_h needed to attain a particular height h , and then solving for this height. The velocity of the largest droplets can be obtained by substituting the maximum diameter from equation (50) into equation (208). As usual, v_h is given by equation (200).

$$\sqrt{2h^*} \left[\frac{\rho_g}{\rho_f} \right]^{1/2} = 75.17 j_g^*{}^{1/4} N_{\mu_g}^{1/4} \left[7.24 j_g^*{}^{-1} \right]^{-1/4} \left[\frac{\rho_g}{\rho_f} \right]^{1/2} D_H^{*0.21} \left[\frac{\rho_g}{\Delta\rho} \right]^{0.115} \quad (210)$$

From this relation the near surface region can be shown to extend from

$$0 \leq h^* \leq 1.038 \times 10^3 j_g^* N_{\mu_g}^{1/2} D_H^{*0.42} \left[\frac{\rho_g}{\Delta\rho} \right]^{0.23} \quad (211)$$

where the upper limit on h^* is obtained by solving equation (210). Within this region v_h is effectively zero since $v_h < v_i$ for all droplet sizes. Thus, using equations (188) and (202), the entrainment becomes

$$E_{fg}(h, j_g) = \frac{\dot{\epsilon}(j_g)}{\rho_g j_g} \int_0^{D_{\max}} f_D(D, j_g) \int_{v_h}^{\infty} g(v_i, D, j_g) dv_i dD = \frac{\dot{\epsilon}(j_g)}{\rho_g j_g} = 4.84 \times 10^{-3} \left[\frac{\rho_g}{\Delta\rho} \right]^{-1.0} \quad (212)$$

Above the near surface region is the momentum controlled region where the heavier droplets within the supercritical range progressively fall back into the pool. The lower limit for this region is given by the right hand side of equation (211). The upper limit is determined by the point at which all the supercritical droplets have fallen out of the stream so that only subcritical droplets remain. To determine this limit it is first necessary to substitute equation (196) into equation (208) to get the initial velocity of a critically sized droplet and then to set the resulting expression equal to the initial velocity v_h given by equation (200). When these steps are performed, the following expression is obtained:

$$\sqrt{2h^*} \left[\frac{\rho_g}{\rho_f} \right]^{1/2} = 75.17 j_g^*{}^{1/4} N_{\mu_t}^{1/4} \left[4 j_g^* (N_{\mu_t})^{1/3} \right]^{-1/4} \left[\frac{\rho_g}{\rho_f} \right]^{1/2} D_H^{*0.21} \left[\frac{\rho_g}{\Delta\rho} \right]^{0.115} \quad (213)$$

On the basis of this relation and equation (196), the momentum controlled region can be shown to extend from

$$1.038 \times 10^3 j_g^* N_{\mu_t}^{1/2} D_H^{*0.42} \left[\frac{\rho_g}{\Delta\rho} \right]^{0.23} \text{LE} h^* \text{LE} 1.413 \times 10^3 N_{\mu_t}^{1/3} D_H^{*0.42} \left[\frac{\rho_g}{\Delta\rho} \right]^{0.23} \quad (214)$$

To determine the entrainment as a function of height within these limits, it is first necessary to determine the diameter of the largest supercritical droplet having the initial velocity needed to reach the point in question. Denoting this diameter D_h , substituting the variable D_h into equation (208), and setting the result equal to equation (200), yields the following expression:

$$\sqrt{2h^*} \left[\frac{\rho_g}{\rho_f} \right]^{1/2} = 75.17 j_g^*{}^{1/4} N_{\mu_t}^{1/4} [D_h^*]^{-1/4} \left[\frac{\rho_g}{\rho_f} \right]^{1/2} D_H^{*0.21} \left[\frac{\rho_g}{\Delta\rho} \right]^{0.115} \quad (215)$$

In this expression D_h should not be confused with the hydraulic diameter D_H . If equation (215) is solved for D_h , one obtains.

$$D_h^* = \frac{(75.17)^4 j_g^*}{2^2 h^{*2} N_{\mu_t}} D_H^{*0.84} \left[\frac{\rho_g}{\Delta\rho} \right]^{0.46} \quad (216)$$

Now since all droplets within the range $D_h < D \leq D_{\max}$ lack sufficient initial momentum to reach height h , only diameters within the range $0 \leq D \leq D_h$ remain within the flow. Moreover, since all droplets remaining within the flow have initial velocities greater than or equal to v_h , v_h is effectively zero for these droplets. Hence the entrainment at height h is given by

$$E_{fg}(h, j_g) = \frac{\dot{\epsilon}(j_g)}{\rho_g j_g} \int_0^{D_h} f_D(D, j_g) \int_{v_h}^{\infty} g(v_i, D, j_g) dv_i dD = \frac{\dot{\epsilon}(j_g)}{\rho_g j_g} \int_0^{D_h} f_D(D, j_g) dD \quad (217)$$

Utilizing equations (202) and (207), and switching to dimensionless coordinates yields

$$E_{fg}(h, j_g) = 4.84 \times 10^{-3} \left[\frac{\rho_g}{\Delta\rho} \right]^{-1.0} \int_0^{D_h^*} 0.077(D^*)^{0.5} (j_g^*)^{1.5} dD^* \quad (218)$$

Finally, integrating this equation subject to the expression for D_h given by equation (216) yields the entrainment as a function of height in the momentum controlled region.

$$E_{fg}(h, j_g) = 5.603 \times 10^6 \frac{j_g^{*3}}{h^{*3}} N_{\mu_e}^{1.5} D_H^{*1.25} \left[\frac{\rho_g}{\Delta\rho} \right]^{-0.31} \quad (219)$$

Above the momentum controlled region lies the deposition controlled region which only droplets within the subcritical diameter range can reach. Since these droplets can be suspended entirely by vapor drag, $v_h = 0$ for these droplets in accordance with equation (191). Hence, the entrainment is given by

$$E_{fg}(h, j_g) = \frac{\dot{e}(j_g)}{\rho_g j_g} \int_0^{D_c} f_D(D, j_g) \int_{v_h}^{\infty} g(v_i, D, j_g) dv_i dD = \frac{\dot{e}(j_g)}{\rho_g j_g} \int_0^{D_c} f_D(D, j_g) dD \quad (220)$$

where D_c is the diameter of a critically sized droplet. Utilizing equations (202) and (207), and switching to dimensionless coordinates yields

$$E_{fg}(h, j_g) = 4.84 \times 10^{-3} \left[\frac{\rho_g}{\Delta\rho} \right]^{-1.0} \int_0^{D_c^*} 0.077(D^*)^{0.5} (j_g^*)^{1.5} dD^* \quad (221)$$

Integrating this equation subject to the expression for D_c given by equation (196) gives the entrainment in the deposition controlled region.

$$E_{fg}(h, j_g) = 1.988 \times 10^{-3} j_g^{*3} N_{\mu_e}^{1/2} \left[\frac{\rho_g}{\Delta\rho} \right]^{-1.0} \quad (222)$$

As written, equation (222) predicts that entrainment remains constant with height. However, due to deposition on solid surfaces, the entrainment will decrease. Ishii makes the case that the deposition rate should be proportional to the entrainment itself so that the entrainment decreases exponentially with height. On the basis of experimental data, Ishii determines an exponential attenuation term and adjusts the leading constant to yield.

$$E_{fg}(h, j_g) = 7.13 \times 10^{-4} j_g^{*3} N_{\mu_e}^{1/2} \left[\frac{\rho_g}{\Delta\rho} \right]^{-1.0} \exp(-0.205 (h/D_H)) \quad (223)$$

Then, to ensure a smooth transition at the boundary and hence consistency among his equations, Ishii sets equation (223) for the deposition controlled region equal to equation (219) for the momentum controlled region to obtain the following equation for the transition height:⁸

$$h^* \exp(-0.068 (h^*/D_H^*)) = 1.97 \times 10^3 N_{\mu_g}^{1/3} D_H^{*0.42} \left[\frac{\rho_g}{\Delta\rho} \right]^{0.23} \quad (224)$$

When the deposition term is small the equation can be approximated as

$$h^* = 1.97 \times 10^3 N_{\mu_g}^{1/3} D_H^{*0.42} \left[\frac{\rho_g}{\Delta\rho} \right]^{0.23} \quad (225)$$

The entrainment correlations, E_{fg} , listed above can be expressed in terms of mass flow rate using the following definition:

$$E_{fg} = \frac{\rho_f j_f}{\rho_g j_g} \quad (226)$$

and the liquid mass continuity equation:

$$\dot{m}_{ENT} = \rho_f j_f a_{up} \quad (227)$$

Substituting equation (226) into (227) yields:

$$\dot{m}_{ENT} = \rho_g j_g E_{fg} a_{up} \quad (228)$$

This places the entrainment equations in the form needed to evaluate the dimensionless groups obtained in the top-down scaling analysis.

In summary, based on Ishii's pool entrainment model, the following entrainment relations are predicted:⁸

Near Surface Region:

$$0 \leq h^* \leq 1.038 \times 10^3 j_g^* N_{\mu_g}^{1/2} D_H^{*0.42} \left[\frac{\rho_g}{\Delta\rho} \right]^{0.23} \quad (229)$$

$$E_{fg}(h, j_g) = 4.84 \times 10^{-3} \left[\frac{\rho_g}{\Delta\rho} \right]^{-1.0} \quad (230)$$

$$\dot{m}_{ENT} = 4.84 \times 10^{-3} \Delta\rho j_g a_{up} \quad (231)$$

Momentum Controlled Region:

$$1.038 \times 10^3 j_g^* N_{\mu_t}^{1/2} D_H^{*0.42} \left[\frac{\rho_g}{\Delta\rho} \right]^{0.23} LE h^* LE 1.97 \times 10^3 N_{\mu_t}^{1/3} D_H^{*0.42} \left[\frac{\rho_g}{\Delta\rho} \right]^{0.23} \quad (232)$$

$$E_{fg}(h, j_g) = 5.603 \times 10^6 \frac{j_g^{*3}}{h^{*3}} N_{\mu_t}^{1.5} D_H^{*1.25} \left[\frac{\rho_g}{\Delta\rho} \right]^{-0.31} \quad (233)$$

$$\dot{m}_{ENT} = 5.603 \times 10^6 \rho_g a_{UP} \frac{j_g^{*4}}{h^{*3}} \left[\frac{\sigma g \Delta\rho}{\rho_g^2} \right]^{.25} N_{\mu_t}^{1.5} D_H^{*1.25} \left[\frac{\rho_g}{\Delta\rho} \right]^{-0.31} \quad (234)$$

Deposition Controlled Region:

$$1.97 \times 10^3 N_{\mu_t}^{1/3} D_H^{*0.42} \left[\frac{\rho_g}{\Delta\rho} \right]^{0.23} LE h^* \quad (235)$$

$$E_{fg}(h, j_g) = 7.13 \times 10^{-4} j_g^{*3} N_{\mu_t}^{1/2} \left[\frac{\rho_g}{\Delta\rho} \right]^{-1.0} \exp(-0.205 (h/D_H)) \quad (236)$$

$$\dot{m}_{ENT} = 7.13 \times 10^{-4} \rho_g a_{UP} j_g^{*4} \left[\frac{\sigma g \Delta\rho}{\rho_g^2} \right]^{.25} N_{\mu_t}^{1/2} \left[\frac{\rho_g}{\Delta\rho} \right]^{-1.0} \exp(-0.205 (h/D_H)) \quad (237)$$

As mentioned above, these equations are built upon a particular entrainment mechanism under the assumed conditions of churn flow in the pool. Thus, the validity of these equations hinges upon the satisfaction of this initial assumption.

7.2.2 Upper Plenum Liquid Entrainment Rate Scaling Criteria

The upper plenum geometry and flow conditions can be determined by substituting the entrainment correlations into the scaling criterion given by equation (187).

Near Surface Region:

Substituting equation (231) into (187) and assuming fluid property similitude, yields the following relation:

$$j_{g,R} = \frac{1}{2} \quad (238)$$

This ratio is established by controlling the core power and fixing the upper plenum flow area. Performing a simple steady-state energy balance for the core yields:

$$\rho_g j_g a_{UP} (h_{fg} - \Delta h_{SC}) = \dot{q} \quad (239)$$

where Dh_{SC} is the core subcooling and q is the core power. Rearranging and substituting into equation (238) yields:

$$\left(\frac{\dot{q}}{a_{UP}} \right)_R = \frac{1}{2} \quad (240)$$

Currently the APEX upper plenum flow area, a_{UP} , ratio is approximately equal to 1:48. Thus the core power scaling ratio becomes:

$$\dot{q}_R = \frac{1}{96} \quad (241)$$

The requirements for liquid entrainment in the near surface region can be easily met.

Momentum Controlled Region:

Substituting equation (234) into equation (187) and assuming fluid property similitude yields:

$$\left(\frac{j_g^4 D_H^{1.25}}{h^3} \right)_R = \frac{1}{2} \quad (242)$$

Fixing $j_{g,R}$ to 1:2 and h_R to 1:4 yields the following scaling ratio for the hydraulic diameter of the upper plenum:

$$D_{H,R} = \left(\frac{1}{8} \right)^{0.8} = 0.1895 \quad (243)$$

This new scaling criterion shall be applied in the upper plenum design section.

Deposition Controlled Region:

Substituting equation (237) into equation (187) and assuming fluid property similitude yields:

$$\left[j_g^4 \exp\left(-.205 \frac{h}{D_H}\right) \right]_R = \frac{1}{2} \quad (244)$$

The form of this criterion requires that it be assessed numerically for the model and the prototype.

7.2.3 Scaling Criterion for Lateral De-entrainment

A study of droplet de-entrainment on vertical tubes in droplet cross flow was performed by Dallman and Kirchner at Los Alamo Scientific Laboratory in 1980.⁹ The study included both analytical and experimental research. Droplets of a known size were sprayed perpendicular to vertical conduits situated in a draft induced wind tunnel. The two geometries examined were square channels (76.2 mm square) and cylindrical tubes (25.4 mm, 63.5 mm, and 101.6 mm diameters). The air velocities were varied from 0 m/s to 14 m/s and the liquid droplet velocities were varied from 10 m/s to 15 m/s. It was found that the de-entrainment efficiency for a single tube was only weakly dependent on the tube diameter, air velocity, droplet mean velocity and total liquid flow rates for air velocities below 14 m/s. And droplet mass flux rates greater than 2 kg/(m²-s). In fact, the de-entrainment rate was nearly a constant value of 0.19 for cylinders and 0.27 for square tubes for this range. That is:

$$\eta_l = 0.19 \text{ (For Cylinders)} \quad (245)$$

and

$$\eta_l = 0.27 \text{ (For a 76.2 mm Square Tube)} \quad (246)$$

The authors cited the work of Chen,¹⁰ as providing a method of extrapolating the single tube data to an array of tubes. Namely, the de-entrainment efficiency for horizontal droplet flow through “k” rows of identical vertical tubes with a constant diameter to pitch ratio is :

$$\eta_k = A[1 - C(1 - \eta_l(1 + 4.5(D/P)^2)^k)] \quad (247)$$

where C is a geometric factor dependent on pitch to diameter ratios. The constant “A” is unity for a staggered array with no line of sight through the array. Equation (247) indicates that preserving the upper plenum guide tube de-entrainment efficiency requires preserving the guide tube diameter to pitch ratio and the number of guide tube rows. Therefore, the first criterion can be written as:

$$(D/P)_R = 1 \quad (248)$$

For the diameter to pitch ratios in this study, very high entrainment efficiencies (i.e., greater than 90%) are achieved with just 3 staggered rows of guide tubes. Therefore the number of guide tube rows beyond three does not contribute much to the de-entrainment process. Furthermore, an examination of the AP1000 upper plenum structure geometry reveals the following:^{11,12,13}

1. The upper core plate includes a significant number of holes at its periphery. De-entrainment of liquid from the peripheral holes will occur on the core barrel walls since there are no guide tubes to impede the flow.
2. There are several (~6.0 inch) diameter flow holes located adjacent to each hot leg. No de-entrainment will occur at those sites. Thus the entrainment efficiency at those sites is zero. Modeling of those flow holes in the APEX test facility will be important.

3. Liquid from the central internal flow holes will be de-entrained at a relatively high de-entrainment efficiency (i.e. on the guide tubes). Thus the flow through the peripheral flow holes will dominate the behavior.
4. The flow path of least resistance for the fluid is radially outward toward the periphery of the upper internals.

The upper plenum can be effectively divided into two zones, a peripheral zone that exhibits no de-entrainment and an internal guide tube zone with a relatively high de-entrainment efficiency. Rather than preserving the row numbers, the scaling approach shall be to preserve the flow area averaged de-entrainment efficiency for the internal guide tube zone. That is, the following scaling criterion will be applied:

$$\eta_{\text{eff,R}} = 1 \quad (249)$$

Effective De-entrainment Efficiency

For purpose of this analysis, the AP1000 guide tube bundle has been divided into five flow zones, from $I = 4$ at the center of the upper plenum to $i = 0$ at the periphery of the upper plenum. The total liquid mass flow rate entering the flow zones through the upper core plate and traveling to the periphery of the guide tube bundle is given by:

$$\dot{m}_{\text{Periphery}} = \sum \dot{m}_i (1 - \eta_k)_i \quad (250)$$

where k represents the number of guide tube rows between a flow zone and the guide tube bundle periphery. For the AP1000, the upper plenum flow zones have been selected such that $k = i$. Dividing by the total liquid mass flow rate through the upper core plate, yields the fraction of entrained liquid reaching the periphery. One minus this value yields the equation for the desired effective de-entrainment efficiency. That is,

$$\eta_{\text{eff}} = 1 - \frac{\sum \dot{m}_i (1 - \eta_k)_i}{\dot{m}_{\text{UCP}}} \quad (251)$$

Substituting equation (247) into (251) yields:

$$\eta_{\text{eff}} = 1 - \sum \left(\frac{\dot{m}_i}{\dot{m}_{\text{UCP}}} \right) [1 - A(1 - C\Phi^k)]_i \quad (252)$$

where:

$$\Phi = 1 - \eta_l [1 + 4.5(D/P)^2] \quad (253)$$

Furthermore, for the case of a constant inlet mass flux, ρv , equation (253) becomes a flow area averaged de-entrainment efficiency:

$$\eta_{\text{eff}} = 1 - \sum \left(\frac{a_i}{a_{\text{UCP}}} \right) [1 - A(1 - C\Phi^k)]_i \quad (254)$$

For the case of A and C equal to one, and $i = k$, this equation reduces to:

$$\eta_{\text{eff}} = 1 - \sum \left(\frac{a_i}{a_{\text{UCP}}} \right) \Phi^i \quad (255)$$

Equations (247) and (249) shall be used to help scale the lateral de-entrainment phenomenon.

7.2.4 Scaling Criterion for the Upper Core Plate

The two key phenomenon to be preserved by scaling the upper core plate flow holes are:

- Upper plenum flow distribution
- Counter-current flooding limitation (CCFL) at the core upper support plate holes.

Flow through the upper core plate at the guide tube bundle periphery will dominate the entrainment behavior in the upper plenum. In particular, the flow area directly adjacent to the hot legs has unimpeded access to the hot legs. Thus preserving the flow distribution in the upper core plate will be essential to the proper simulation of the entrainment behavior in the upper plenum. The following scaling criterion will be implemented:

$$\left(\frac{a_{\text{Periphery}}}{a_{\text{UCP}}} \right)_R = 1 \quad (256)$$

Similarly, the upper core plate flow area at the entrance to the hot legs shall also be preserved as follows:

$$\left(\frac{a_{\text{HL}}}{a_{\text{UCP}}} \right)_R = 1 \quad (257)$$

Preserving the counter current flooding behavior in the upper core plate requires that the Kutateladze Number flooding limit, defined in terms of j_g^* in this analysis, be preserved in APEX. That is,

$$\frac{j_g}{\left[\frac{\sigma g \Delta \rho}{\rho_g^2} \right]^{1/4}} = 4 \quad (258)$$

For the condition of fluid property similitude, properly matching the Kutateladze number requires that j_g in APEX match that in AP1000. That is,

$$(j_{g,UCP})_R = 1 \quad (259)$$

Thus the flow area of the APEX upper core plate must be scaled as 1:96 as follows:

$$(a_{UCP})_R = \frac{1}{96} \quad (260)$$

Furthermore, the minimum upper core plate hole diameter must be greater than ~ 2.0 inches so that the onset of the flooding behavior is not dependent on the hole diameter.

7.2.5 Scaling Criterion for the Upper Support Plate

The upper support plate separates the upper plenum from the reactor vessel head. The plate provides support for the control rod guide tubes and includes twelve 3.32 inch diameter holes that permit the upper head to drain into the upper plenum. During the pool entrainment process, it is expected that the upper head will be empty of liquid. Nonetheless, it has been included to document the scaling basis for this component.

Because the flow area represented by the drain holes is quite small, the flooding behavior and the flow distribution cannot both be simultaneously preserved. Since the upper head is essentially a dead-ended volume (there is a small bypass flow path from the upper head to the upper downcomer), flooding behavior will not be as important as the flow distribution. That is, CCFL is not expected to occur in the plate. The dominant phenomenon will be the pressurized draining of the upper head due to the flashing of liquid during a depressurization event. As a result, the drain hole number and distribution will be preserved and the flow area will be scaled as follows:

$$(a_{USP})_R = \frac{1}{48} \quad (261)$$

7.2.6 Design of APEX Upper Plenum Guide Tube Bundle, Upper Core Plate and Upper Support Plate

Based on the Top-Down and Bottom-Up scaling analyses presented in the previous sections, the following scaling approach for the Upper Plenum Guide Tubes, the Upper Core Plate and the Upper Support Plate was adopted:

- Preserve the upper plenum hydraulic diameter ratio using equation (243)
- Preserve the local upper plenum subchannel hydraulic diameter ratio using equation (243)
- Preserve the total upper plenum flow area based on 1:48 flow area scaling
- Preserve the guide tube diameter to pitch ratio using equation (248)
- Preserve the effective de-entrainment efficiency for the guide tube bundle using equation (249)
- Preserve the upper core plate flow area distribution using equations (256) and (257)

- Preserve the vapor volumetric flux, j_g , in the upper core plate holes using equation (260)
- Preserve the upper support plate flow distribution and flow area using equation (261)

With regard to the scaling basis for the upper plenum guide tube bundle, the momentum controlled entrainment scaling criterion given by equation (243) has been selected to guide the modification to the APEX upper internals. The basis for this selection is as follows. The near surface entrainment rates can be properly simulated in APEX solely by maintaining j_{gR} at a constant value of 0.5. In that sense, no modification to the facility would be needed. However, the momentum controlled entrainment rates can only be matched by preserving both the j_{gR} and the hydraulic diameter ratios. It will be shown that the deposition controlled region is both unimportant and not achievable in the 1/4 length scale APEX facility.

Figure 21 depicts the upper core plate geometry. There are a total of thirteen (13) flow holes. The six holes on the periphery are 1.91 inch in diameter and represent approximately 37% of the total upper core plate flow area as compared to 38% in the AP1000. The flow holes at the entrance of each hot leg represent 6.2% of the total flow area as in the AP1000.

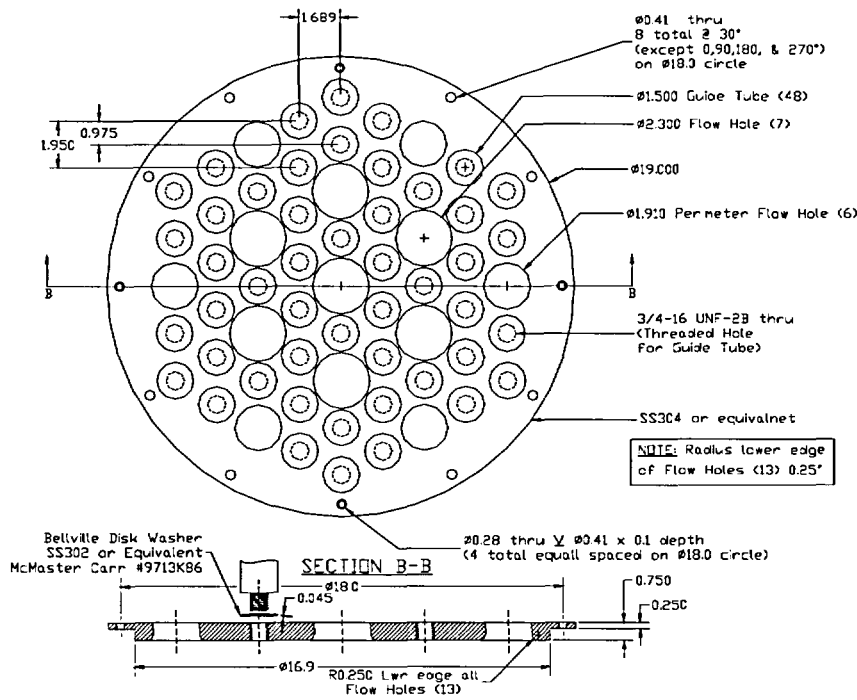


Figure 21 APEX Upper Core Plate Geometry

Figure 22 illustrates the APEX upper core plate guide tube pitch and diameter. Figure 23 presents the APEX Upper Support Plate flow hole location. Table 18 presents the revised upper plenum geometry design based on matching the scaling criteria given above.

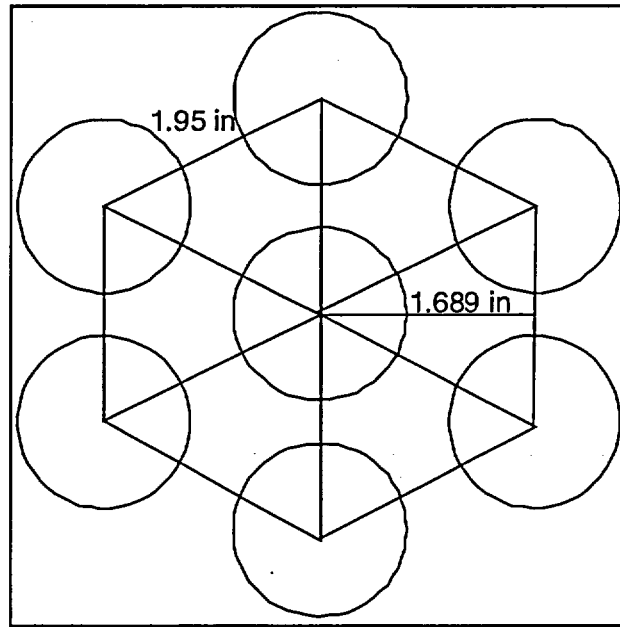


Figure 22 APEX Upper Plenum Guide Tube Pitch and Diameter

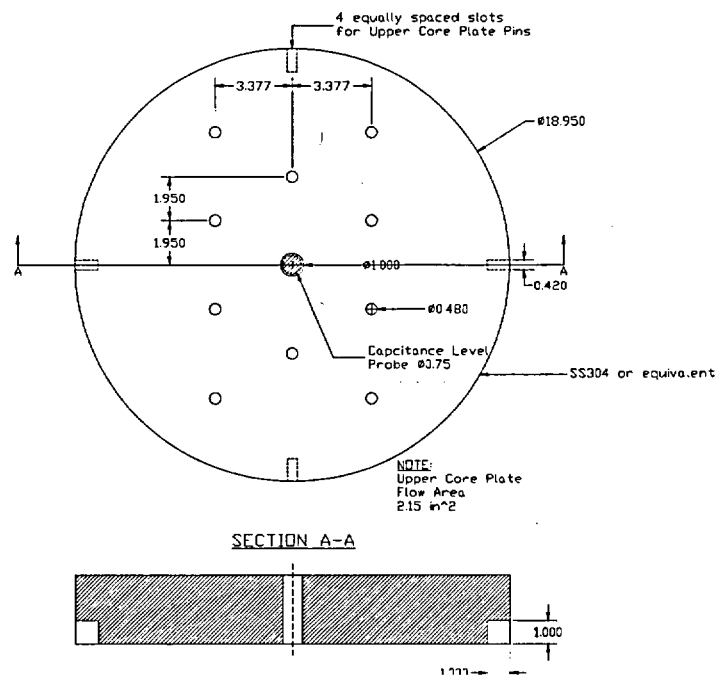


Figure 23 APEX Upper Support Plate Flow Hole Locations

Table 18 Comparison of the APEX and AP1000 Upper Plenum Geometries			
	AP1000	APEX	Units
Upper Plenum			
Core Barrel Inside Diameter			
Length*			
Flow Area with Internals			
Total Wetted Perimeter			
Total Hydraulic Diameter			
Support Columns			
Number			
Diameter			
Guide Tubes			
Number			
Pitch			
Equivalent Diameter			
Pitch to Diameter Ratio			
Subchannel Flow Area			
Subchannel Wetted Perimeter			
Subchannel Hydraulic Diameter			
Upper Core Plate			
Number of Large Thru Holes			
Total Thru Hole Flow Area			
Number of Guide Tube Flow Holes			
Total Guide Tube Flow Area			
Number of Support Column Flow Holes			
Total Support Column Flow Area			
Total Upper Core Plate Flow Area			
Peripheral Flow Area			
Ratio of Peripheral Flow Area to Total Area			
Hot Leg Entrance Flow Area			
Ratio of Hot Leg Entrance Flow Area to Total Area			
Upper Support Plate			
Number of Holes			
Hole Diameter			
Total Flow Area			

a,b,c

*Bottom of Hot Leg to Top of Active Fuel

7.2.7 Assessment of Pool Entrainment Limiting Conditions

This section examines the limiting conditions for the APEX entrainment tests. A core power of 1 MW in APEX, represents a 2.8% decay power in the AP1000. The greatest vapor generation rates would be achieved at saturation conditions at 1 atmosphere. These conditions would produce an upper plenum vapor volumetric flux, j_g , of 11.2 m/s and 5.7 m/s in AP1000 and APEX respectively. Applying these conditions to the entrainment transition and rate correlations presented in the previous section results in Figure 24.

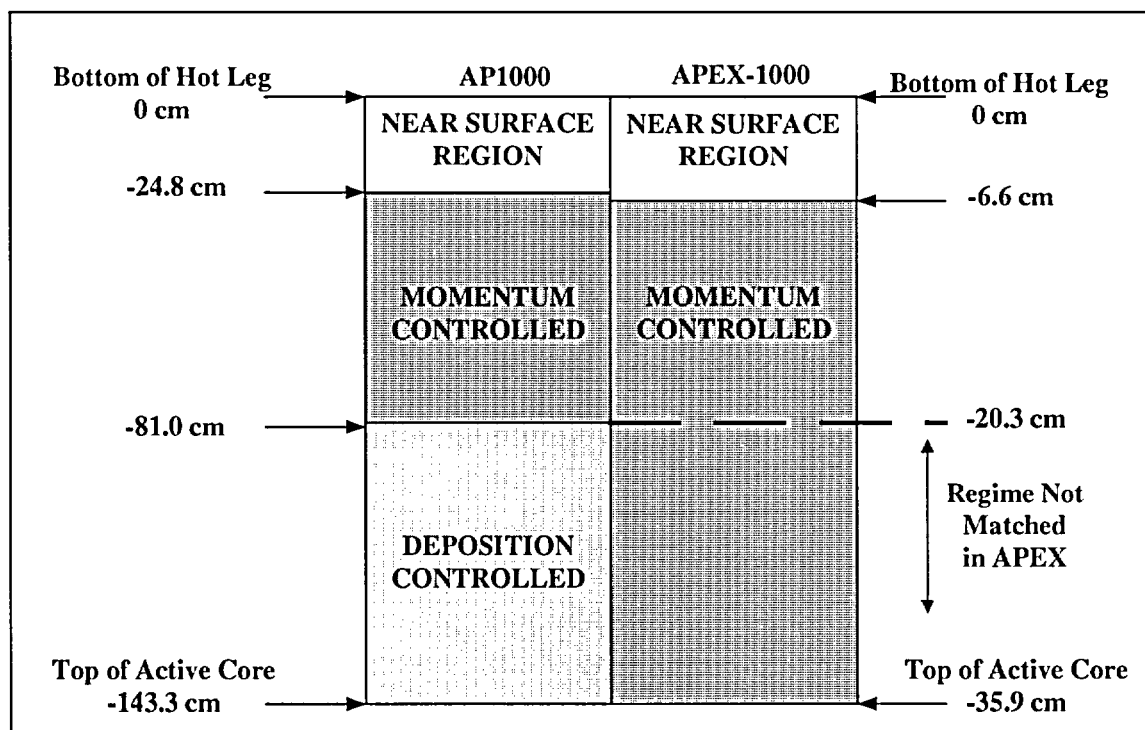


Figure 24 Assessment of AP1000 and APEX Upper Plenum Pool Entrainment Regimes for a 2.8% Core Decay Power at Atmospheric Pressure

This figure shows how the different pool entrainment regions would exist in the upper plenums for the prescribed set of conditions. As the level drops below the hot leg, both the AP1000 and APEX upper plenums would exhibit entrainment characteristic of the near surface region. The entrainment rates that would be observed in APEX in this region are well scaled and the transition to the momentum controlled region is also well scaled. *It is very important to note that the entrainment rates in the near surface region are a factor of 150 times greater than the entrainment rates generated in the momentum controlled region.*

The figure shows that well-scaled entrainment behavior in APEX is expected to a depth of about 18.9 cm below the hot leg. Below this depth, APEX is in the momentum controlled region whereas AP1000

would be in the deposition controlled region at the equivalent scaled depth. *It is also important to note that the entrainment rates in the momentum controlled region are a factor of 4-6 times greater than the entrainment rates generated in the deposition controlled region.*

With regard to the test facility scaling, the entrainment rate is well-scaled for depths to approximately the middle of the upper plenum. Below this depth, the APEX entrainment rates will range from 4 to 16 times greater, on a scaled basis, than what would be expected in the AP1000. Thus the APEX facility will conservatively simulate the entrainment behavior when the level is below the midpoint of the upper plenum.

In general, relative to the near surface region and momentum controlled region entrainment rates, the deposition controlled region entrainment rates are quite small.

On the basis of the conditions prescribed earlier, some preliminary calculations can be made to narrow down the flow conditions in the problem. First, since it is imperative that churn flow exists in the pool, it is necessary to determine if the flow is between the limits of bubbly and annular flow. For bubbly flow Ishii gives the limit as⁹

$$j_g^* = 0.325 \left[\frac{\rho_g}{\rho_f} \right]^{1/2} = 0.008 \quad (262)$$

where the previous density values have been substituted into Ishii's formula to give the numerical result. For annular flow, the criterion is given by⁹

$$j_g^* = 3.1 \quad (263)$$

For these conditions, the value of j_g^* for AP1000 was found to be 1.75. For APEX it was found to be 0.89. Thus, the j_g^* values fall between these limits for both the model and the prototype. Thus, churn flow exists in the pool for both systems over the full range of operating conditions, making Ishii's equations applicable to the analysis.

The next issue to be resolved is whether the flooding criterion is exceeded. After all, if the flooding criterion is exceeded, all of the liquid will be quickly expelled from the pool as a rising film, making the entrainment of droplets irrelevant. As is well known, the flooding criterion depends upon the diameter of the channel. For diameters in the range $3 \leq D_H^* \leq 20$, Ishii restates the Wallis criterion in the following form⁹

$$\frac{j_g^*}{\sqrt{D_H^*}} = 0.5 \quad (264)$$

Furthermore, for diameters within the range $D_H^* \geq 30$, Ishii gives the Kutateladze criterion as⁹

$$j_g^* = 4 \quad (265)$$

The dimensionless hydraulic diameters, D_H^* , for AP1000 and APEX were for these conditions were found to be 135 and 29 respectively. Using equation (248) for APEX and AP1000 or equation (247) for APEX, the criterion indicates that flooding in the upper plenum will not occur for the 2.8% power conditions described.

The next question to be addressed is whether the deposition on the wall is sufficiently large that one must consider re-entrainment from a falling film back into the vapor. In addressing this question, observe that only a fraction of the droplets are taken out of the flow by deposition. Furthermore, only a fraction of this fraction is re-entrained from the film back into the flowing vapor. Consequently, since only a fraction of the liquid removed by deposition is re-entrained back into the flow, it would seem that conservative results could be obtained by ignoring deposition in the first place. The only objection to this conservatism would be if deposition removes large droplets from the flow which are replaced by smaller droplets as a result of re-entrainment. Since this effect could shift the droplet distribution to subcritical diameters which are more easily carried by the vapor, the entrainment might be increased at large heights. However, a second and quite convincing argument is as follows. Since the data used by Ishii was based on flow in tubes, the phenomena of deposition and re-entrainment was necessarily present in the experiments themselves and therefore already included in the correlations. Given this fact, the equations may be used straightforwardly without having to account for this added effect.

7.3 Evaluation of Scale Distortion

Properly simulating the upper plenum pool entrainment process requires that the following ratios be on the order of unity:

$$t_R^+ = \left(\frac{\dot{m}_{ENT,O} t}{a_{UP} \rho_L H} \right)_R \quad (266)$$

$$\Pi_{INJ,R} = \left(\frac{\dot{m}_{INJ,O}}{\dot{m}_{ENT,O}} \right)_R \quad (267)$$

$$\Pi_{GT,R} = \left(\frac{\dot{m}_{GT,O}}{\dot{m}_{ENT,O}} \right)_R \quad (268)$$

$$\Pi_{UPD,R} = \left(\frac{\dot{m}_{UPD,O}}{\dot{m}_{ENT,O}} \right)_R \quad (269)$$

The numerical values for each of the non-dimensional ratios are presented in Table 17 for the near surface entrainment and momentum controlled entrainment regions. The data obtained from the assessment of limiting conditions presented in the previous section were used in the evaluation. The desired timescale ratio, t_R , of 0.5 was used to assess equation (266). All of the injection flow rates have been scaled to 1:96. Furthermore, equation (269) can be interpreted as the ratio of effective de-entrainment efficiencies. That is,

$$\Pi_{GT,R} = \eta_{eff,R} \quad (270)$$

The facility has been scaled to match the onset of upper plenum draining behavior when CCFL conditions are present at the upper core plate flow holes.

The ratio of the gravity driven draining rates for the APEX and AP1000 upper plenums is given by:

$$(\dot{m}_{UPD,O})_R = [a_{UCP} (H_{UP} - h)^{1/2}]_R \quad (271)$$

Table 19 indicates that the APEX-1000 upper plenum geometry and long term cooling operating conditions match the pool entrainment scaling criterion very well with the exception of $P_{UPD,R}$.

Non-Dimensional Ratio	Near Surface	Momentum Controlled
$(t^+)_R$		
$P_{inj,R}$		
$P_{GT,R}$		
$P_{UPD,R}$		
$(j_g^+)_R$		

a,b,c

7.3.1 Impact of Reduced Flow Area in the Upper Core Plate

The greatest source of distortion will be the upper plenum draining rate with a P ratio of 0.5. This distortion arises because matching the flooding behavior at the upper core plate required reducing the upper core plate flow area such that the Kutateladze number was identically preserved. This delayed draining effect is conservative relative to core cooling. In addition, the vapor jetting behavior at the upper core plate produces a local vapor volumetric flux j_g equivalent to what would be observed in the AP1000. Preserving a 1:1 vapor velocity in a 1:4 length upper plenum will produce conservative results. It is expected that the proposed set of upper internals will overestimate the amount of entrained liquid on a scaled basis. This is a conservative feature of the experiment.

8.0 SUMMARY AND CONCLUSIONS

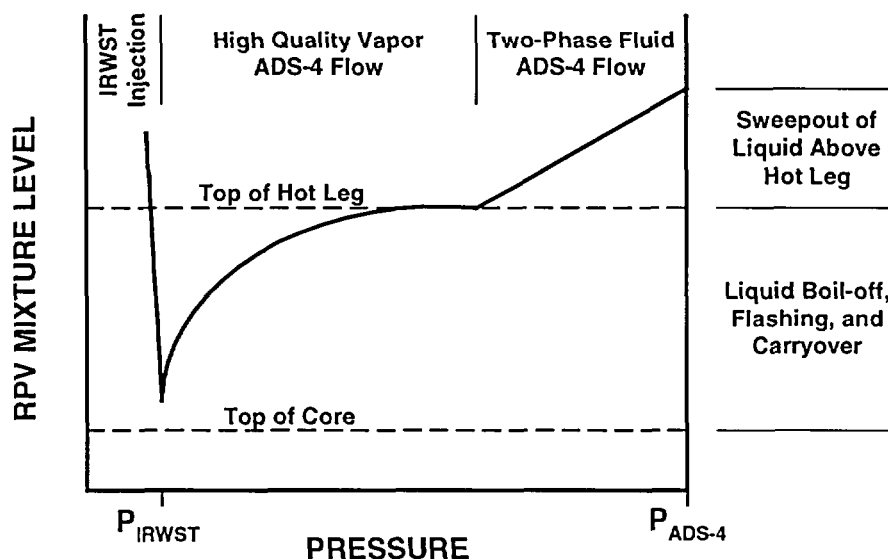
This document presents the scaling analysis performed to guide the OSU APEX-1000 test facility modifications. The purpose of the test program is to provide high quality benchmark data for the reactor safety analysis codes. Previous testing in APEX has demonstrated that all of the thermal hydraulic phenomena observed in the large scale AP600 facilities such as ROSA-AP600 or SPES was also observed in APEX- thereby providing a broad data base for code assessment. However, the most faithful representation of the AP600 phenomena was for the very long term cooling phase which occurs at low system pressure. The APEX-1000 test program will be modified to include full pressure ADS-4 blowdown tests to investigate the transition period that leads to the onset of IRWST injection. This scaling analysis provides the basis for the following plant modifications:

Component	Modification to APEX
Reactor Power	Increase core power by 67%. (Maximum of 1MW)
Pressurizer	Increase Pressurizer volume. Reduce Pressurizer Surge Line Diameter.
Core Makeup Tanks	Increase Core Makeup Tank (CMT) volumes by 25%. Reduce line resistance to 64% of original value.
IRWST	Increase IRWST liquid level.
Automatic Depressurization Stage 4	Increase ADS-4 flow area by 76%. Reduce line resistance to 28% of original value.
Passive Residual Heat Removal (PRHR) Heat Exchanger	Increase PRHR flow capacity by 74% by reducing line resistance. No change in surface area/tube number required for testing.
Containment Sump Flood-Up Elevation	Change flood-up elevation in primary sump tank.

The following paragraphs briefly summarize the results of the study.

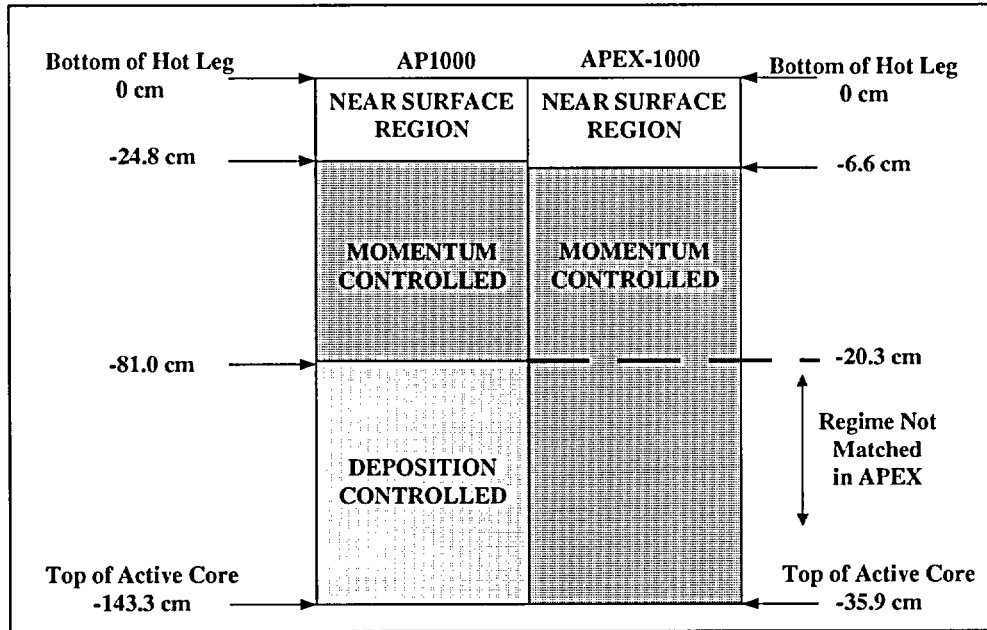
1. The original AP600 Scaling Analysis, WCAP-14270, that was performed in support of the design of the existing Advanced Plant Experiment (APEX) at Oregon State University was found to be applicable to the APEX-1000 design for two reasons. First, the thermal hydraulic phenomena to be studied fell within the purview of the original AP600 test program with the exception of upper plenum behavior. Second, the AP1000 is geometrically similar to AP600. As a result, all of the tank volumes, flow areas, and line resistance scaling ratios found in WCAP-14270 were used in the present study.
2. An NRC pressurizer surge line study by DiMarzo and Bessette was used to guide the modifications to the APEX-1000 PZR surge line. The reduced line diameter is expected to produce a better simulation of the PZR draining behavior.

3. The Reactor Coolant System depressurization scaling analysis represents a more comprehensive approach than that implemented in the original AP600 study. Nonetheless, the similarity criteria derived in this report resulted in scaling ratios that were identical to the original study. It was found that the characteristic time ratios for AP1000 would be well matched in APEX-1000. The greatest distortion (a factor of 2) was the result of pressure scaled fluid properties.
4. A scaling analysis has been performed to design the APEX-1000 to simulate the important phenomena that occurs during the transition from ADS-4 blowdown to the onset of IRWST injection. The key phenomena have been identified, described and the scaling analysis indicates that full pressure ADS-4 blowdown tests can be performed using the modified APEX-1000 test facility. Chapter 15 of the Westinghouse AP1000 Safety Analysis Report indicates that ADS-4 actuation typically occurs near 100 psia. The maximum decay power, $\sim 2.0\%$, at the time of ADS-4 valve opening was calculated for the DEDVI break. These initial conditions will be examined as part of the testing. The AP1000 core axial void fraction profile and the core averaged void fraction were shown to be preserved in APEX-1000.



5. A detailed Pool Entrainment Scaling Analysis has been performed to design the upper plenum components in APEX-1000. The analysis indicates that well-scaled entrainment behavior in APEX is expected to a depth of about 18.9 cm below the hot leg. Below this depth, APEX is in the momentum controlled region whereas AP1000 would be in the deposition controlled region at the equivalent scaled depth. It was found that the entrainment rates in the near surface region are a factor of 150 times greater than the entrainment rates generated in the momentum controlled region. The figure shows that well-scaled entrainment behavior in APEX is expected to a depth of about 18.9 cm below the hot leg. Below this depth, APEX is in the momentum controlled region whereas AP1000 would be in the deposition controlled region at the equivalent scaled depth. It was also found that the entrainment rates in the momentum controlled region are a factor of 4-6 times greater than the entrainment rates generated in the deposition controlled region. Thus the APEX facility

will conservatively simulate the entrainment behavior when the level is below the midpoint of the upper plenum. In addition, the vapor volumetric flow rate ratio, ($j_{g,R}$) at the upper core plate holes has been set to unity to preserve the Kutateladze Number. This adds an additional conservatism to the pool entrainment process because the local vapor jets at the upper core plate holes will extend into the upper plenum increasing liquid entrainment.



9.0 REFERENCES

1. Reyes, J.N. and L.E. Hochreiter, AP600 Low-Pressure Integral Systems Test at Oregon State University- Facility Scaling Report, WCAP-14270, January 1995.
2. Weisman, D.A., Westinghouse Electric Company LLC, *AP1000 Plant Parameters*, APP-GW-G0-002, Revision 1, July 18, 2002.
3. Bessette, D and Marino di Marzo, "Transition from depressurization to long term cooling in AP600 scaled integral test facilities," *Nuclear Engineering and Design* 188, Elsevier, pp 331-344, 1999.
4. Westinghouse. AP1000 PIRT and Scaling Assessment, WCAP-15613, February 2001.
5. Zuber, N., 1991. Appendix D: a hierarchical, two-tiered scaling analysis, an integrated structure and scaling methodology for sever accident technical issue resolution. US Nuclear Regulatory Commission, Washington, DC 20555, NUREG/CR-5809, November 1991.
6. Conway, L. E., Effective Core Flow Area, Westinghouse Electric Corporation, Electronic Mail, June 9, 2002.
7. American National Standard for Decay Heat Power in Light Water Reactyors, 1979. American Nuclear Society, La Grange, IL, ANSI/ANS-5.1.24.
8. Kataoka, I. and M. Ishii. Mechanistic Modeling and Correlations for Pool-Entrainment Phenomenon, Prepared for the U.S. Nuclear Regulatory Commission, NUREG/CR-3304, April 1983.
9. Dallman, J.C. and W.L. Kirchner, "De-Entrainment Phenomena on Vertical Tubes in Droplet Cross Flow," NUREG/CR-1421, U.S. Nuclear Regulatory Commission, April 1980.
10. Chen, C.Y., "Filtration of Aerosols by Fibrous Media," *Chem. Rev.* 55, 595, (1955).
11. Westinghouse Electric Company, LLC, AP1000 Reactor General Assembly, Drawing Number APP-RXS-V2-003, Rev 0., 10/5/01
12. Westinghouse Electric Company, LLC, AP1000 Reactor Internals Critical Interface Features, Drawing Number APP-MI01-M8-102, Rev 0., 10/5/01
13. Westinghouse Electric Company, LLC, AP1000 Reactor, Drawing Number APP-RXS-V2-002 Rev 0.
14. Bluman, G.W., and J.D. Cole. *Similarity Methods for Differential Equations*, Applied Mathematical Sciences 13, Springer-Verlag, New York, 1974.
15. Lay, J.F., 1990. *Statistical mechanics and thermodynamics od matter*. Harper and Row Publishers, New York, pp. 453-456.

9.0 REFERENCES

1. Reyes, J.N. and L.E. Hochreiter, AP600 Low-Pressure Integral Systems Test at Oregon State University- Facility Scaling Report, WCAP-14270, January 1995.
2. Weisman, D.A., Westinghouse Electric Company LLC, *AP1000 Plant Parameters*, APP-GW-G0-002, Revision 1, July 18, 2002.
3. Bessette, D and Marino di Marzo, "Transition from depressurization to long term cooling in AP600 scaled integral test facilities," *Nuclear Engineering and Design* 188, Elsevier, pp 331-344, 1999.
4. Westinghouse. AP1000 PIRT and Scaling Assessment, WCAP-15613, February 2001.
5. Zuber, N., 1991. Appendix D: a hierarchical, two-tiered scaling analysis, an integrated structure and scaling methodology for sever accident technical issue resolution. US Nuclear Regulatory Commission, Washington, DC 20555, NUREG/CR-5809, November 1991.
6. Conway, L. E., Effective Core Flow Area, Westinghouse Electric Corporation, Electronic Mail, June 9, 2002.
7. American National Standard for Decay Heat Power in Light Water Reactyors, 1979. American Nuclear Society, La Grange, IL, ANSI/ANS-5.1.24.
8. Kataoka, I. and M. Ishii. Mechanistic Modeling and Correlations for Pool-Entrainment Phenomenon, Prepared for the U.S. Nuclear Regulatory Commission, NUREG/CR-3304, April 1983.
9. Dallman, J.C. and W.L. Kirchner, "De-Entrainment Phenomena on Vertical Tubes in Droplet Cross Flow," NUREG/CR-1421, U.S. Nuclear Regulatory Commission, April 1980.
10. Chen, C.Y., "Filtration of Aerosols by Fibrous Media," *Chem. Rev.* 55, 595, (1955).
11. Westinghouse Electric Company, LLC, AP1000 Reactor General Assembly, Drawing Number APP-RXS-V2-003, Rev 0., 10/5/01
12. Westinghouse Electric Company, LLC, AP1000 Reactor Internals Critical Interface Features, Drawing Number APP-MI01-M8-102, Rev 0., 10/5/01
13. Westinghouse Electric Company, LLC, AP1000 Reactor, Drawing Number APP-RXS-V2-002 Rev 0.
14. Bluman, G.W., and J.D. Cole. *Similarity Methods for Differential Equations*, Applied Mathematical Sciences 13, Springer-Verlag, New York, 1974.
15. Lay, J.F., 1990. *Statistical mechanics and thermodynamics od matter*. Harper and Row Publishers, New York, pp. 453-456.

-
16. Moody, Frederick J., *Introduction to Unsteady Thermofluid Mechanics*, A Wiley -Interscience Publication, New York, 1990, p.60.
 17. Henry, F.E., and H.K. Fauske., 1971. The two-phase critical flow of one component mixtures in nozzles, orifices and short tubes. *Journal of Heat Transfer, ASMAE Transactions*, 93 (2), 179-187.
 18. Pimentel, D., *Two-Phase Fluid Break Flow Measurements and Scaling in the Advanced Plant Experiment (APEX)*, Master's Thesis, Oregon State University, May 1996.